CANADIAN JOURNAL OF RESEARCH

VOLUME 26 NOVEMBER, 1948 NUMBER 6

— SECTION A —

PHYSICAL SCIENCES

Contents

	Page
Theoretical Study of Ram-jet Propulsion—*Boleslaw Szczeniowski*	327
Remarks on the Excitation of Hydrogen and Helium in the Upper Atmosphere—*William Petrie*	359
Gamma Rays from the Disintegration of Boron by Slow Neutrons—*B. Rose*	366
Search for a 3.20 Mev. γ-Ray in the Disintegration of Thorium C″—*R. E. Bell and L. G. Elliott*	379
Attempt to Detect an $(n,2n)$ Reaction in Deuterium —*L. G. Elliott, E. P. Hincks, and A. N. May*	386
The Emission of *L* Radiation Following Internal Conversion of γ-Radiation in Heavy Elements—*B. B. Kinsey*	404
The Emission of *L* Radiation in the Disintegration of ThC and RaD—*B. B. Kinsey*	421

NATIONAL RESEARCH COUNCIL
OTTAWA, CANADA

CANADIAN JOURNAL OF RESEARCH

The *Canadian Journal of Research* is issued in six sections, as follows:

A. Physical Sciences	D. Zoological Sciences
B. Chemical Sciences	E. Medical Sciences
C. Botanical Sciences	F. Technology

For the present, Sections A, C, D, and E are to be issued six times annually, and Sections B and F, twelve times annually, each under separate cover. with separate pagination.

The *Canadian Journal of Research* is published by the National Research Council of Canada under authority of the Chairman of the Committee of the Privy Council on Scientific and Industrial Research. The *Canadian Journal of Research* is edited by a joint Editorial Board consisting of members of the National Research Council of Canada, the Royal Society of Canada, and the Chemical Institute of Canada.

Sections B and F of the *Canadian Journal of Research* have been chosen by the Chemical Institute of Canada as its medium of publication for scientific papers.

EDITORIAL BOARD

Representing National Research Council	*Representing* Royal Society of Canada	
Dr. G. H. Henderson, (*Chairman*), Professor of Mathematical Physics, Dalhousie University, Halifax.	Dr. A. Norman Shaw, Chairman, Department of Physics, McGill University, Montreal.	Section III
Dr. A. R. Gordon, Head, Department of Chemistry, University of Toronto, Toronto.	Dr. J. W. T. Spinks, Department of Chemistry, University of Saskatchewan Saskatoon.	
Dr. Robert Newton, President, University of Alberta, Edmonton, Alta.	Dr. H. S. Jackson, Head, Department of Botany, University of Toronto, Toronto.	Section V
Dr. C. H. Best, The Banting and Best Department of Medical Research, University of Toronto, Toronto.	Dr. E. Horne Craigie, Department of Zoology, University of Toronto, Toronto.	

Ex officio	*Representing* The Chemical Institute of Canada
Dr. Léo Marion, Editor-in-Chief, Division of Chemistry, National Research Laboratories, Ottawa.	Dr. H. G. Thode, Department of Chemistry, McMaster University, Hamilton.
Dr. H. H. Saunderson, Director, Division of Information Services, National Research Council, Ottawa.	

Editorial Committee

Editor-in-Chief,	Dr. Léo Marion	Editor, Section D,	Dr. E. Horne Craigie
Editor, Section A,	Dr. A. Norman Shaw	Editor, Section E,	Dr. J. B. Collip
Editor, Section B,	Dr. J. W. T. Spinks; Dr. H. G. Thode	Editor, Section F,	Dr. J. A. Anderson; Dr. A. Norman Shaw; Dr. H. G. Thode
Editor, Section C,	Dr. H. S. Jackson		

Manuscripts should be addressed:

Editor-in-Chief,
Canadian Journal of Research,
National Research Council, Ottawa, Canada.

Canadian Journal of Research

Issued by THE NATIONAL RESEARCH COUNCIL OF CANADA

VOL. 26, SEC. A. NOVEMBER, 1948 NUMBER 6

THEORETICAL STUDY OF RAM-JET PROPULSION[1]

BY BOLESLAW SZCZENIOWSKI

Abstract

In ram-jet propulsion, artificial compression before combustion does not exist. Therefore, the only factors which may influence the increase in momentum, i.e., the thrust, are:

(1) The degree of initial dynamic compression by a diffuser;
(2) The shape of the combustion chamber;
(3) The variations of the rate of heat release along the tube;
(4) Air excess coefficient;
(5) Kind of fuel;
(6) Velocity of flight;
(7) Aerodynamic and heat losses.

This paper deals almost exclusively with the first four factors, i.e., with the theoretical case of an ideal gas and a perfect flow, with no heat or aerodynamic losses involved. The possible appearance of shock waves is disregarded. Neither are boundary layer phenomena discussed in this paper. The external fairing and the relation between the internal and external shape, as well as the influence of this relation on the actually obtainable thrust and efficiency, are also considered to be beyond the scope of the paper. General conclusions are drawn as to the optimum shape of the ideal engine from the standpoint of efficiency. It is found that air should be submitted initially to as high a dynamic compression as possible, i.e., using all kinetic energy available, after which a combustion chamber of constant cross section is used—and finally a nozzle. Another conclusion is that it is impossible to obtain a positive thrust with a combustion chamber of constant cross section, if no dynamic compression, by a diffuser, is initially applied. Special attention is drawn in the paper to the representation and interpretation of the ideal ram-jet cycle on the entropy diagram, this giving a clear picture of the relations between the energy released and the efficiency and thrust obtainable. The fact that in the flow through a tube of constant cross section with heat release (e.g., by combustion), the pressure may decrease even if ideal gas and perfect flow (with no losses involved) are concerned, is emphasized throughout the paper, as it seems that generally this fact is rather overlooked.

1. Denotations

Absolute pressure	P, lb. per sq. ft.
Absolute temperature	T, °Rankine
Specific volume	v, cu. ft. per lb.
Specific weight	$\gamma = 1/v$, lb. per cu. ft.
Velocity	c, ft. per sec.

[1] *Manuscript received in original form June 12, 1947, and, as revised May 26, 1948. Contribution from École Polytechnique, Université de Montréal, Montréal, P.Q.*

Duct cross section area — A, sq. ft.

Air weight output — G_a, lb. per sec.

Fuel weight output — G_f, lb. per sec.

Mixture weight output — $G_m = (G_a + G_f)$, lb. per sec.

Work done per unit of time (power) — W, ft-lb. per sec.

Theoretical heat exchanged by 1 lb. of working medium (heat brought to the medium is assumed to be positive) — Q, B.t.u. per lb.

Specific heat at P = Const. — c_p, B.t.u. per lb., °F.

Entropy — Φ, B.t.u. per lb., °F.

Gas constant of air — R_a, ft. per °Rankine

Gas constant of burning mixture — R_m, ft. per °Rankine

Isentropic exponent — $\kappa = c_p/c_v$

Thrust — (Th), lb.

Specific thrust — $\zeta = (Th)/G_a$

Unit thrust — $\epsilon = (Th)/A$, lb. per sq. ft.

Distance between cross-sections A and A_0 — x, ft.

Diffuser efficiency — η_d

Nozzle efficiency — η_n

External (propulsive) efficiency — η_{ex}

Internal (thermal) efficiency — η_{th}

Over-all efficiency — $\eta_0 = \eta_{ex}\eta_{th}$

Pressure efficiency — η_p

Efficiency expressing heat loss by conduction — η_h

Efficiency of pumping fuel — η_p

Air excess coefficient:

$$\lambda = \frac{\text{Actual mass of air involved for 1 lb. of fuel}}{\text{Mass of air necessary to burn completely 1 lb. of fuel}}$$

Weight of air theoretically necessary to burn completely 1 lb. of fuel — α, lb. per lb.

Lower heat value of 1 lb. of chemically correct air–fuel mixture — H_{m_0}, B.t.u. per lb.

Mechanical heat equivalent — $J = 778$ ft-lb. per B.t.u.

Terrestrial acceleration — $g = 32.174$ ft. per sec.^{2}

Standard conditions at sea level:

$P_{st} = 14.72$ lb. per sq. in. $= 29.92$ in. of mercury $= 2120$ lb. per sq. ft.

$T_{st} = 459.4 + 59 = 518.4$ °Rankine

Subscripts:

0 — for surroundings

1 — at the exit of a perfect theoretical cycle

2 — after dynamic compression by a diffuser

3 — after combustion

4 — at the nozzle exit

Dimensionless coefficients:

for pressure $\pi = P/P_0$

for temperature $\tau = T/T_0$

for specific volume $\nu = v/v_0$

for velocity $\sigma = c/c_0$

for cross section $\psi = A/A_0$

for theoretical heat $\varphi = \dfrac{(\kappa - 1)JQ}{\kappa RT_0}$

for lower heat value of burning mixture $\beta = \dfrac{(\kappa - 1)}{\kappa RT_0} H_{m_0}$

for entropy $\rho = \Phi/c_p = \dfrac{(\kappa - 1)J\Phi}{\kappa R}$

Mach number $M = \dfrac{c}{\sqrt{g\kappa RT}}$

Abbreviations:

$$\frac{\alpha\lambda + 1}{\alpha\lambda} = \delta$$

$$1 + \frac{(\kappa - 1)}{2} M^2 = \mu$$

2. Flow of Gas Through a Duct of Variable Cross Section with Heat Release

The theoretical study of jet propulsion of any kind will not be entirely exact until a study has been made of the problem of flow through a duct of variable cross section with heat exchange (or, what has theoretically the same meaning, with heat release). Solving this problem and deriving hereafter special instances which may be useful in our case will provide the tools necessary to a further development of the jet propulsion theory. Such attempts have already been made and published (1, 7, 10); the paper by Dr. Samaras seems to be the most complete and adequate study to date.

Assume the general case of flow of an ideal gas, with no hydraulic or heat losses involved, through a tube of a cross section arbitrarily variable with the tube length (Fig. 1), in which heat is released (i.e., "introduced") at a rate likewise arbitrarily variable along the channel.

The initial values at the channel inlet are assumed to be A_0, P_0, T_0, c_0. At a certain distance x these values become A, P, T, c and they are functions of x, the movement being assumed to be steady, i.e., independent directly of time.

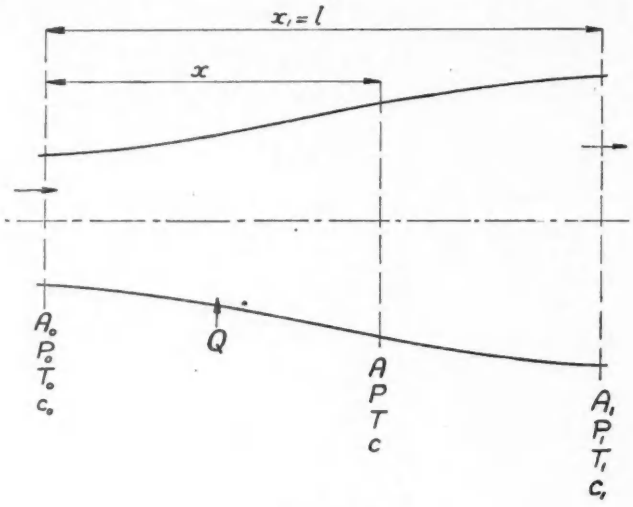

FIG. 1.

The form of duct is arbitrarily given as function of x:

$$\frac{A}{A_0} = \psi(x). \tag{1}$$

On the other hand, the amount of heat brought to the section $(0 - x)$ of the duct during the unit of time is also arbitrarily given in function of x:

$$GQ = F(x) \text{ B.t.u. per sec.} \tag{2}$$

The equation of state being:

$$P_0 v_0 = RT_0, \tag{3}$$

the output becomes:

$$G = \frac{A_0 c_0}{v_0} = \frac{A_0 c_0 P_0}{RT_0}. \tag{4}$$

In order to make clearer the significance of the function $F(x)$ assume that a certain amount of heat GQ_1 has been released along the distance $(0 - x)$ of the duct. If the rate of heat release were constant, i.e., the same on any element dx of the duct length, the form of function $F(x)$ would be

$$GQ = GQ_1 \frac{x}{x_1}.$$

As is known, three laws of conservation govern the flow of gas with heat exchange:

(1) Principle of conservation of mass, the mathematical expression of which for a steady flow is

$$\frac{AcP}{T} = \text{Const.} = \frac{A_0 c_0 P_0}{T_0} = RG; \tag{5}$$

(2) Principle of conservation of momentum, which may be represented by the equation of motion:

$$gRT\frac{dP}{P} + cdc = 0; \tag{6}$$

(3) Principle of conservation of energy, the mathematical expression of which is the first equation of thermodynamics:

$$dQ = c_p dT - \frac{1}{J} v\, dP,$$

which, if bound with the equation of motion, gives the so-called equation of aerothermodynamics which may be expressed in the integral form:

$$Q = \frac{\kappa R}{(\kappa - 1)J}(T - T_0) + \frac{1}{2gJ}(c^2 - c_0^2), \tag{7}$$

where $\frac{\kappa R}{(\kappa - 1)J}$ is the specific heat c_p.

Eliminating Q and G from (2), (4), and (7), and introducing dimensionless coefficients, Equation (7) becomes:

$$\tau = \mu_0 + \varphi(x) - (\mu_0 - 1)\sigma^2. \tag{8}$$

Next, eliminating A and T from (1), (5), and (8), Equation (5) becomes:

$$\pi = \frac{\tau}{\sigma\psi(x)} = \frac{\mu_0 + \varphi(x) - (\mu_0 - 1)\sigma^2}{\sigma\psi(x)}. \tag{9}$$

At the same time Equation (6) becomes:

$$\tau\frac{d\pi}{\pi} + \kappa M_0^2 \sigma d\sigma = 0. \tag{10}$$

Equations (8), (9), and (10) determine pressure π, temperature τ, and velocity σ, provided that φ and ψ are given. For instance, τ and π may be eliminated, thus giving:

$$\left[\frac{(\kappa - 1)}{2} M_0^2\sigma^2 - (\varphi + \mu_0) + \frac{\varphi'\psi}{\psi'}\right]\frac{\psi'}{\psi}dx + \left[\frac{(\kappa + 1)}{2} M_0^2\sigma^2 - (\varphi + \mu_0)\right]\frac{d\sigma}{\sigma} = 0, \tag{11}$$

which defines the velocity in function of x, i.e., of Q, according to (2). The only difficulty is to find the integral form of Equation (11). As is seen, values of P, c, T depend both on the shape of the duct (ψ) and on variation of heat release (φ). Therefore these last two quantities as a whole—not only their initial and final values—*influence the obtainable thrust and efficiency of the ram jet engine.* This means that in a duct in which initial and final cross

sections, the total amount of heat released, and the initial values P_0, T_0, c_0 are given, the final values P, T, c may vary, according to the form of duct (ψ) and to the kind of variations of heat release (φ). As is seen, the phenomenon is different from that in an ordinary nozzle or diffuser, in which the heat release is considered to be nil, thus permitting the final values P, T, c to be in theoretical principle independent of the shape of the duct, provided the initial and final cross sections are given.

3. Special Case of Duct with Constant Cross Section

In this case $\psi = 1$; $\psi' = 0$, thus:

$$\tau = \mu_0 - (\mu_0 - 1)\sigma^2 + \varphi; \tag{12}$$

$$\tau = \pi\sigma; \tag{13}$$

$$d\pi + \kappa M_0^2 d\sigma = 0; \tag{14}$$

and after integration:

$$\pi + \kappa M_0^2\sigma = (\kappa M_0^2 + 1). \tag{15}$$

These equations, when solved, give, in accordance with the results already published by the author (10):

$$\pi = \frac{(\kappa M_0^2 + 1)}{(\kappa + 1)} + \frac{\kappa}{(\kappa + 1)}\sqrt{(1 - M_0^2)^2 - 2(\kappa + 1)M_0^2\varphi}\ ; \tag{16}$$

$$\sigma = \frac{(\kappa M_0^2 + 1)}{(\kappa + 1)M_0^2} - \frac{1}{(\kappa + 1)M_0^2}\sqrt{(1 - M_0^2)^2 - 2(\kappa + 1)M_0^2\varphi}\ ; \tag{17}$$

$$\tau = \pi\sigma = \frac{[4\kappa\mu_0^2 - (\kappa + 1)^2]}{(\kappa + 1)^2(\kappa - 1)M_0^2} + \frac{2\kappa}{(\kappa + 1)}\varphi + \frac{(\kappa - 1)(\kappa M_0^2 + 1)}{(\kappa + 1)^2 M_0^2}\sqrt{(1 - M_0^2)^2 - 2(\kappa + 1)M_0^2\varphi}. \tag{18}$$

Therefore:

$$\sigma = \frac{(\kappa M_0^2 + 1) - \pi}{\kappa M_0^2}\ ; \tag{19}$$

$$\tau = \frac{\pi}{\kappa M_0^2}[(\kappa M_0^2 + 1) - \pi] = \sigma[(\kappa M_0^2 + 1) - \kappa M_0^2\sigma]; \tag{20}$$

$$\pi + \kappa M_0^2\nu = (\kappa M_0^2 + 1), \tag{21}$$

where $\nu = \frac{v}{v_0}$ represents the specific volume; and

$$\varphi = \frac{1}{\kappa}\left[\frac{(\kappa - 1)}{2\kappa M_0^2} - 1\right] + \frac{1}{\kappa}\left(1 + \frac{1}{\kappa M_0^2}\right)\pi - \frac{(\kappa + 1)}{2\kappa^2 M_0^2}\pi^2$$

$$= (\kappa M_0^2 + 1)\sigma - \frac{(\kappa + 1)M_0^2}{2}\sigma^2 - \mu_0. \tag{22}$$

Discussion and graphical representation of these mathematical results have already been given in the author's publication cited above (10). The only detail that remains to be discussed, therefore, is the representation in the entropy diagram.

In order to define the entropy, express φ in function of temperature, eliminating σ from (20) and (22):

$$\varphi = \frac{(\kappa+1)}{2\kappa}\tau - \frac{[(\kappa-1)\kappa^2 M_0^4 + 2(\kappa+1)\kappa M_0^2 - (\kappa-1)]}{4\kappa^2 M_0^2} + \frac{(\kappa-1)}{2\kappa}(\kappa M_0^2+1)\sqrt{\frac{(\kappa M_0^2+1)^2}{4\kappa^2 M_0^4} - \frac{\tau}{\kappa M_0^2}}. \tag{23}$$

The entropy

$$d\Phi = \frac{dQ}{T},$$

is in dimensionless form expressed by

$$\frac{\Phi}{c_p} = \frac{(\kappa-1)J}{\kappa R}\Phi = \rho. \tag{24}$$

Thus

$$d\rho = \frac{d\varphi}{\tau} = \frac{(\kappa+1)}{2\kappa}\frac{d\tau}{\tau} - \frac{\frac{(\kappa-1)}{2\kappa}d\tau}{\tau\sqrt{1-\frac{4\kappa M_0^2}{(\kappa M_0^2+1)}\tau}}, \tag{25}$$

and after integration

$$(\rho-\rho_0) = \ln\tau - \frac{(\kappa-1)}{\kappa}\ln\left[\frac{(\kappa M_0^2+1)}{2} - \sqrt{\frac{(\kappa M_0^2+1)^2}{4} - \kappa M_0^2\tau}\right]. \tag{26}$$

The line representing this evolution in entropy diagram (τ, ρ) is limited both by a maximum of temperature

$$\tau_{max} = \frac{(\kappa M_0^2+1)^2}{4\kappa M_0^2}$$

for

$$(\rho-\rho_0)_e = \frac{(\kappa+1)}{\kappa}\ln\left(\frac{\kappa M_0^2+1}{2}\right) - \ln(\kappa M_0^2),$$

and by a maximum of entropy

$$(\rho-\rho_0)_{max} = \frac{(\kappa+1)}{\kappa}\ln\left(\frac{\kappa M_0^2+1}{\kappa+1}\right) - \ln(M_0^2)$$

for

$$\tau_e = \frac{(\kappa M_0^2+1)^2}{(\kappa+1)^2 M_0^2}.$$

In the latter case, according to (20), the velocity becomes:

$$\sigma_e = \frac{(\kappa M_0^2+1)}{(\kappa+1)M_0^2} = \frac{\sqrt{\tau_e}}{M_0},$$

wherefrom $c_e = \sqrt{g\kappa RT_e}$; this is, therefore, the velocity of sound.

The tangent to the line of evolution at the initial point $\tau = 1$ is

$$\left(\frac{d\rho}{d\tau}\right)_{\tau=1} = \frac{(1-M_0^2)}{(1-\kappa M_0^2)};$$

$$\left(\frac{d\tau}{d\rho}\right)_{\tau=1} = \frac{(1-\kappa M_0^2)}{(1-M_0^2)},$$

while for the classic isobar:

$$\rho - \rho_0 = \ln \tau;$$

$$\frac{d\tau}{d\rho} = \tau;$$

$$\left(\frac{d\tau}{d\rho}\right)_{\tau=1} = 1.$$

The evolutions which occur in a tube of constant cross section for different values of M_0 are shown in entropy diagram in Fig. 2.

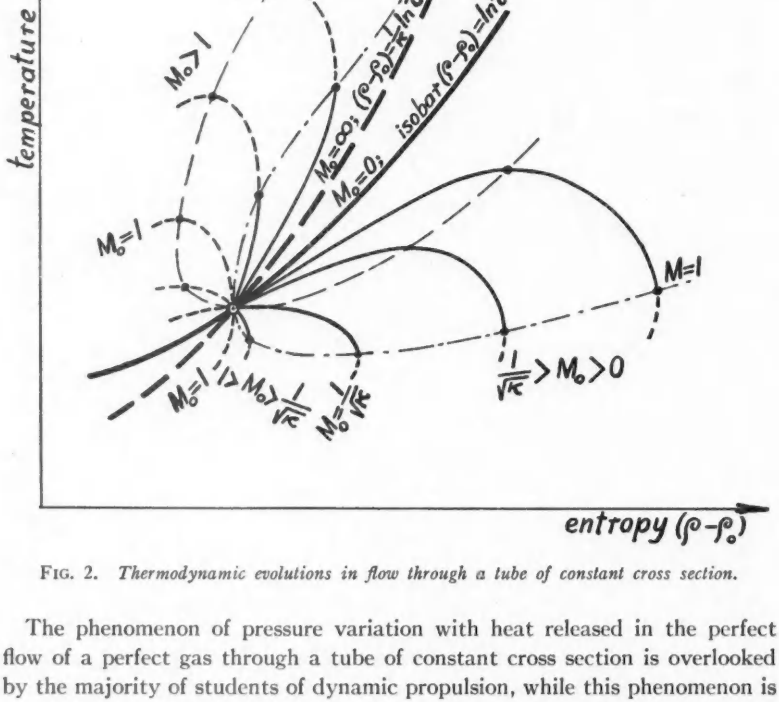

FIG. 2. *Thermodynamic evolutions in flow through a tube of constant cross section.*

The phenomenon of pressure variation with heat released in the perfect flow of a perfect gas through a tube of constant cross section is overlooked by the majority of students of dynamic propulsion, while this phenomenon is the more important the higher the velocity of flow in the combustion chamber. The results of computation given in this Section are, therefore, applied in the following Sections, instead of the generally admitted assumption P = Const. for perfect gas and flow in a combustion chamber.

4. The Problem of Ram-jet Propulsion as Interpreted in Entropy Diagram

The ram-jet propulsion system may be, in general, represented by a duct as given in Fig. 1. The air enters section 0 at a velocity c_0, numerically equal to flight speed, but of opposite direction. The heat is released by combustion along the length $x_1 = l$ or along a part of it. The burnt gases leave at section 1 at a velocity c_1 which, if a certain increase in mass output due to fuel introduction is disregarded, must be higher than c_0, in order to obtain an increase in momentum, thus giving the necessary thrust.

Another essential condition, from the viewpoint of the performance of the engine as considered alone, is

$$P_1 = P_0,$$

i.e., the initial and final static pressures are the same and are equal to the atmospheric pressure. If the pressure P_1 is different from P_0, this will cause an additional loss of energy, apart from the additional static portion of thrust.

The mathematical form of the laws governing the phenomenon studied, as given by Equations (5), (6), and (7), may be rewritten as follows, taking into account the dimensionless coefficients:

$$\frac{\sigma\pi}{\tau}\psi = 1; \tag{27}$$

$$\tau\frac{d\pi}{\pi} + \kappa M_0^2\sigma d\sigma = 0; \tag{10}$$

$$\varphi = \tau + \frac{(\kappa - 1)}{2} M_0^2\sigma^2 - \mu_0. \tag{28}$$

Supposing for the moment that the pressure remains constant during the process, this latter will be represented in entropy diagram by the path $0 - 1$ of the isobar $P = P_0$ (Fig. 3). But, according to (10), the velocity will also remain constant. Thus, the thrust becomes nil here, if the mass output increase by adding fuel is disregarded. Such being the case, and remembering that, in general, $P_1 = P_0$, this isobaric path may be considered as the main skeleton line, which will serve as a comparative basis, while Equation (28) will serve as the main basis for discussion of energy exchanges. This latter equation may be rewritten as follows:

$$\varphi_1 = (\tau_1 - 1) + \frac{(\kappa - 1)}{2} M_0^2(\sigma_1^2 - 1), \tag{29}$$

where τ_1, σ_1, and φ_1 are the final values. As is seen, for isobaric evolution the total amount of energy introduced in form of combustion heat φ_1 is spent in increasing the "total heat", which is proportional to the temperature ($Q_1 = c_pT_1 - c_pT_0$). In other words, the heat released served only to increase the internal energy of the gas, $c_v(T_1 - T_0)$, apart from a certain amount of external work done $(v_1 - v_0)P_0$ in "repulsing surroundings", due to the increase of specific volume $(v_1 - v_0)$.

The first term on the right side of Equation (29) thus represents the increase in "total heat", and the second the increase in kinetic energy, the only energy which is useful in our case.

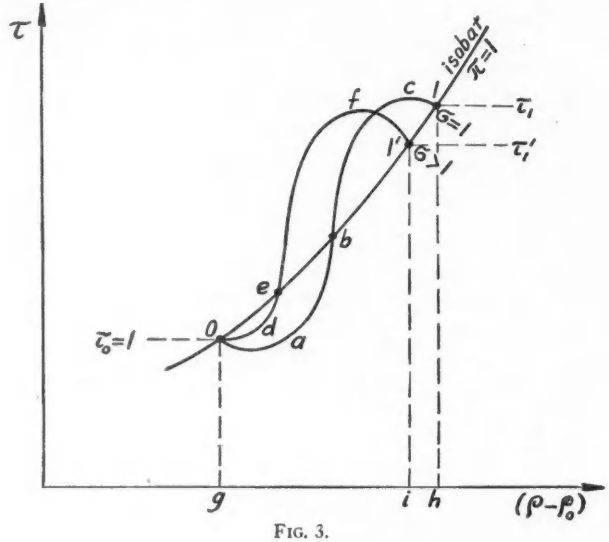

FIG. 3.

It is, of course, possible to apply any kind of evolution arbitrarily given, by forming appropriately the duct form, i.e., $\psi(x)$, provided the variation of the rate of heat release $\varphi(x)$ is given. Let, for instance, the evolution be arbitrarily given as $\pi = f_e(\tau)$. (Polytropic evolution, where $\pi = \tau^{\frac{m}{m-1}}$ with m = Const. might serve here as an example.) Thus, Equations (27), (28), and (10) will give:

$$\kappa M_0^2 (\sigma^2 - 1) + 2\int_1^\tau \frac{f_e'(\tau)}{f_e(\tau)}\,\tau d\tau = 0;$$

$$\sigma = \sqrt{1 - \frac{2}{\kappa M_0^2}\int_1^\tau \frac{f_e'(\tau)}{f_e(\tau)}\,\tau d\tau}\ ; \tag{30}$$

$$\tau - 1 - \frac{(\kappa - 1)}{\kappa}\int_1^\tau \frac{f_e'(\tau)}{f_e(\tau)}\,\tau d\tau = \varphi(x); \tag{31}$$

$$\psi(x) = \frac{\tau}{f_e(\tau)\sqrt{1 - \frac{2}{\kappa M_0^2}\int_1^\tau \frac{f_e'(\tau)}{f_e(\tau)}\,\tau d\tau}}\ . \tag{32}$$

Function $\varphi(x)$ being given, Equation (31) expresses τ in function of x; thus $\psi(x)$ will be found in function of x from (32).

Let the evolution be represented by the line $0abc1$. It is shaped arbitrarily, with the only condition that areas $0ab0$ and $11'bc1$ are equal. As the area comprised between the line of evolution, the two abscissae $0g$ and $1h$, and the path gh on abscissa axis, represents the total amount of heat φ_1 introduced, the evolution will really finish at point 1, the same as for an isobaric evolution.

If both the kind of fuel and the air excess coefficient are given, the total amount of heat released φ_1 remains the same for any evolution, and the same is true for the area below the line of evolution. On the other hand, in order to get positive thrust, the actual final point must be placed to the left of 1, say at 1′, as there $\tau_1' < \tau_1$, thus $\sigma_1' > \sigma_0 = 1$. This means that the actual evolution, say $0def1'$, must be such as to have area $ef1'be$ larger than $0de0$, the difference being equal to $1hi1'$.

One important conclusion may be immediately drawn here: *if the combustion chamber, i.e., the part of the duct in which combustion occurs, has to be shaped for practical reasons as a tube of a constant cross section, it is impossible, in subsonic flight, to obtain positive thrust without prior dynamic compression by a diffuser.* This is to say that the ram-jet engine for a subsonic flight, as shown in Fig. 4, is impossible.

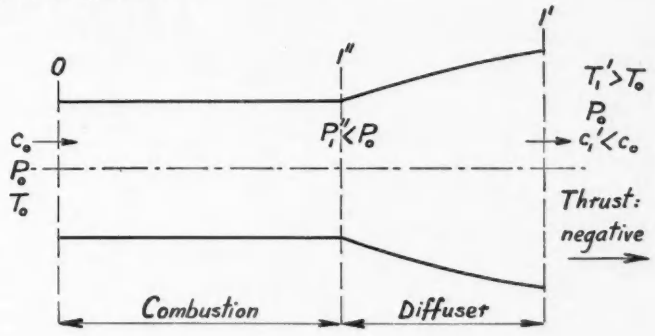

FIG. 4.

The corresponding graphical representation in entropy diagram is given in Fig. 5 for $M_0 < 1$ (subsonic region). Here the two shaded areas must be equal; thus, after isentropic compression $1'' - 1'$ of burnt gases, point 1′ will be placed to the right of 1; consequently $\sigma < 1$ and thrust becomes negative.

Applying as combustion chamber a cone (in general curvilinear) of sufficient divergency, a line of evolution passing above the isobar $0 - 1$ is obtainable, with the final point 1′ lying to the left of 1. Such a solution is, however, inefficient, as will be seen later.

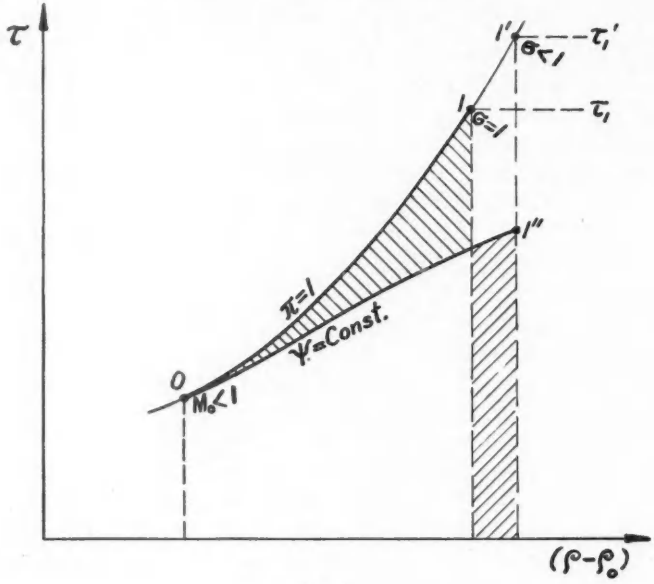

FIG. 5.

If the combustion chamber is to be of constant cross section type, prior dynamic compression by a diffuser is unavoidable (see Figs. 6 and 7).

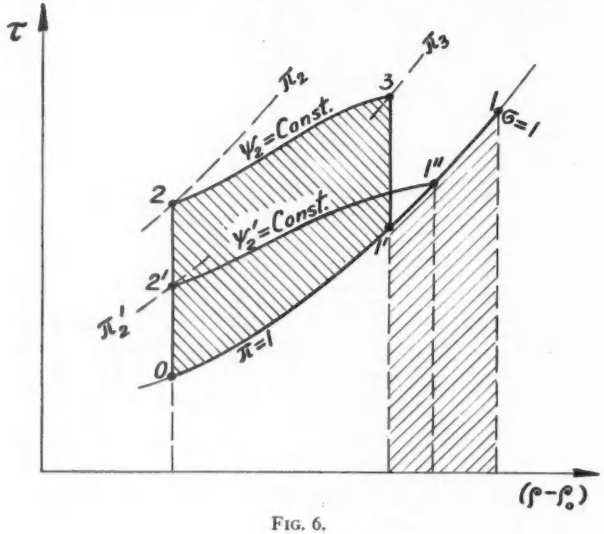

FIG. 6.

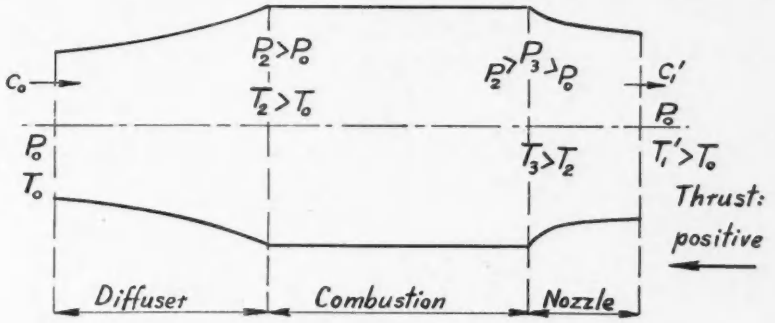

FIG. 7.

The prior compression ends here at a certain pressure $\pi_2 > 1$ at which the velocity σ_2 is still positive. The combustion being finished at 3, applying the nozzle to expand burnt gases from π_3 to $\pi_1' = 1$ is in general necessary. In a certain particular case when $\pi_2 = \pi_2'$ the nozzle is not necessary, the combustion being finished at 1'', on isobar $\pi = 1$. If the prior dynamic compression is extended only to the pressure $\pi_2 < \pi_2'$, obtaining final pressure $\pi_1' = 1$ is no longer possible.

In the supersonic region, a combustion chamber with constant cross section and without the initial diffuser may give a positive thrust (see Figs. 8 and 9).

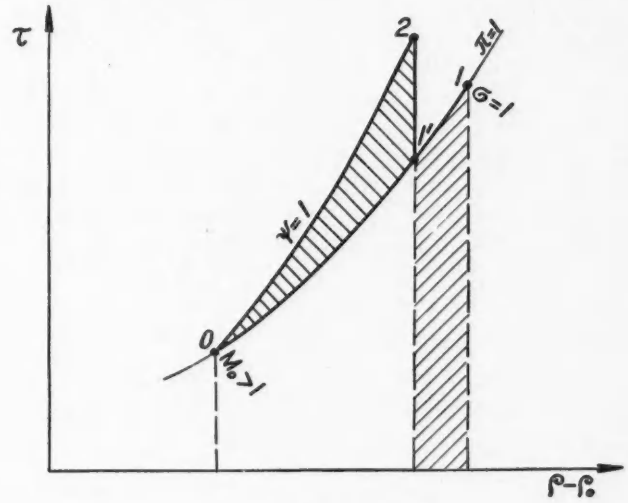

FIG. 8.

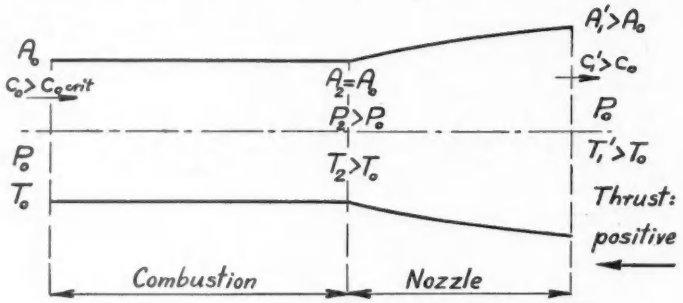

FIG. 9.

The nozzle to enable the expansion $2 - 1'$ is here divergent, as is needed in a supersonic region. Such a solution is, however, inefficient, as will be seen later.

In order to obtain the best working conditions of ram-jet engine, point $1'$ must be placed as far to the left of 1 as possible, according to (28). This will give both the maximum increase in velocity, i.e., maximum thrust and maximum efficiency, also minimum temperature, the total amount of heat φ_1 released by combustion remaining constant.

This is a geometrical problem, at least in part: to apply such a line of evolution which, together with the two abscissae and the path of abscissa axis, encloses a given area in such a manner as to have the difference $(\rho_1' - \rho_0)$ as small as possible, this being incidentally in accordance with the thermodynamic principle of minimum increase of entropy for maximum efficiency.

The first thing to be done is, therefore, an isentropic compression $0 - 2$ by a diffuser (Fig. 10), extended as far as possible. Of course, this is possible only up to $M_2 = 0$ and then the cross section becomes infinite. Although such a "perfect ram-jet engine" is not actually feasible, consider such an ideal case as the limit to which the actual solution has to approach as close as the actual conditions will permit. The corresponding form of the channel is symbolically represented in Fig. 11 for subsonic region and in Fig. 12 for supersonic.

In this case $M_2 = 0$ and, if on the line $2 - 3$ $\psi_2 = \text{Const.} = \infty$, also $\sigma = \dfrac{w}{w_0} = \text{Const.} = 0$, i.e., $\sigma_3 = \dfrac{w_3}{w_0} = 0$, and $\pi = \text{Const.} = \pi_2 = \pi_3$, according to (16) and (17) where $M_0 = 0$ is put (which corresponds to $\sigma_2 = 0$). At the same time, it is found from (18), as a limit:

$$\frac{\tau_3}{\tau_2} = \frac{(\kappa - 1)JQ_4}{\kappa RT_2} + 1 = \frac{\varphi_4}{\tau_2} + 1.$$

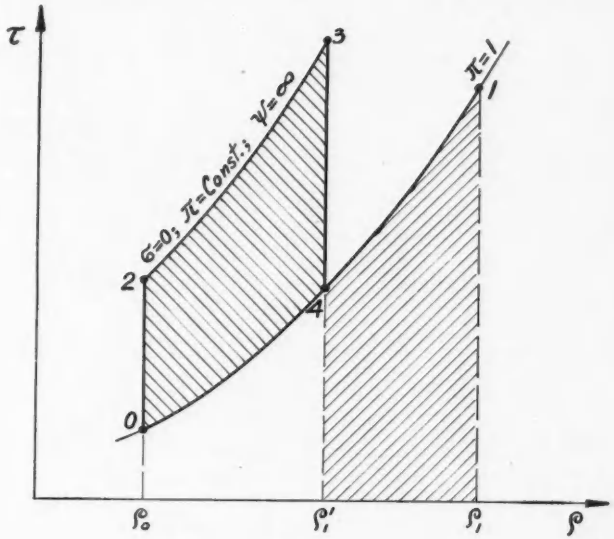

FIG. 10.

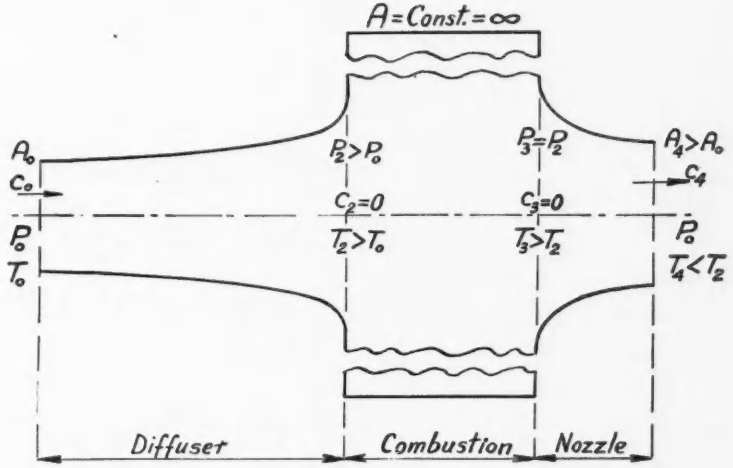

FIG. 11.

The evolution 0 − 2 being simply isentropic, Equation (28) gives:

$$\tau = \mu_0 - \frac{(\kappa - 1)}{2} M_0^2 \sigma^2 = 1 + \frac{(\kappa - 1)}{2} M_0^2 (1 - \sigma^2);$$

$$\tau_2 = \mu_0 = 1 + \frac{(\kappa - 1)}{2} M_0^2, \tag{33}$$

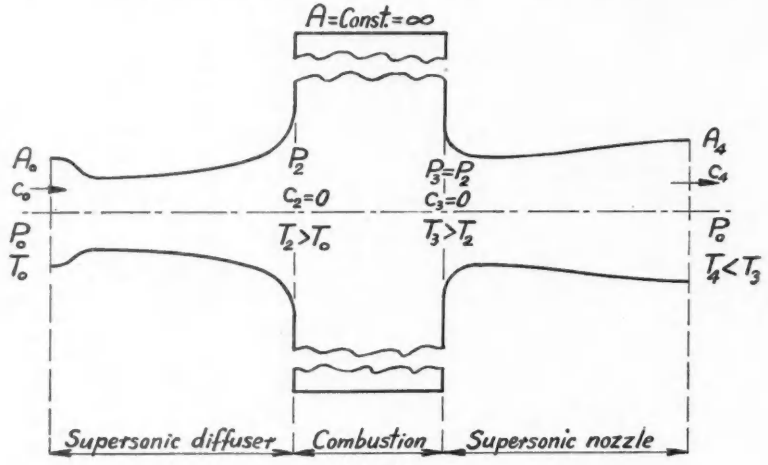

FIG. 12.

and Equation (10) gives:

$$\frac{d\pi}{\pi} + \frac{\kappa M_0^2 \sigma d\sigma}{\left[\mu_0 - \frac{(\kappa-1)}{2} M_0^2\sigma^2\right]} = 0 ;$$

$$\frac{\pi^{\frac{\kappa-1}{\kappa}}}{\left[\mu_0 - \frac{(\kappa-1)}{2} M_0^2\sigma^2\right]} = 1;$$

$$\sigma_2 = 0;$$

$$\pi_2 = \mu_0^{\frac{\kappa}{\kappa-1}} = \left[1 + \frac{(\kappa-1)}{2} M_0^2\right]^{\frac{\kappa}{\kappa-1}} = \pi_3 ; \qquad (34)$$

therefore

$$\tau_3 = \varphi_4 + \tau_2 = \left[1 + \frac{(\kappa-1)}{2} M_0^2 + \varphi_4\right]; \qquad (35)$$

$$\sigma_3 = 0.$$

Next comes the simple isentropic expansion 3 − 4, similar to evolution 0 − 2;

$$\frac{\tau_4}{\tau_3} = 1 + \frac{(\kappa-1)c_3^2}{2g\kappa RT_3}\left(1 - \frac{c_4^2}{c_3^2}\right)$$

$$= 1 - \frac{(\kappa-1)M_0^2\sigma_3^2}{2\tau_3}\left(\frac{\sigma_4^2}{\sigma_3^2} - 1\right);$$

$$\tau_4 = \tau_3 - \frac{(\kappa-1)}{2} M_0^2(\sigma_4^2 - \sigma_3^2)$$

$$= \tau_3 - \frac{(\kappa-1)}{2} M_0^2\sigma_4^2 = \tau_3 - (\mu_0 - 1)\sigma_4^2 ;$$

$$\pi_4 = 1;$$

$$\frac{\pi_4}{\pi_3} = \frac{1}{\pi_3} = \left(\frac{\tau_4}{\tau_3}\right)^{\frac{\kappa}{\kappa-1}} ;$$

therefore:

$$\tau_4 = \frac{\tau_3}{\pi_3^{\frac{\kappa-1}{\kappa}}} = 1 + \frac{\varphi_4}{1 + \frac{(\kappa - 1)}{2} M_0^2}; \tag{36}$$

$$\varphi_4 = \sqrt{\frac{\tau_3 - \tau_4}{\tau_2 - 1}} = \sqrt{\tau_4} = \sqrt{1 + \frac{\varphi_4}{\tau_2}} = \sqrt{1 + \frac{\varphi_4}{1 + \frac{(\kappa - 1)}{2} M_0^2}}. \tag{37}$$

The final cross section will be

$$\psi_4 = \frac{\tau_4}{\sigma_4 \pi_4} = \sqrt{\tau_4} = \sqrt{1 + \frac{\varphi_4}{1 + \frac{(\kappa - 1)}{2} M_0^2}}. \tag{38}$$

5. Thrust and Efficiencies of the "Perfect Ram-jet Engine"

The explanations of the thrust in a jet engine, as given in the technical literature, are sometimes misleading. In order to avoid misunderstandings, the theoretical interpretation of the thrust is given below.

According to the law of conservation of momentum the sum of impulse and quantity of movement remains constant. Consider a mass element dG of the thickness dx of the gas entering the duct at 0 (Fig. 1). The force acting on this element in the direction of channel axis is $P_0 A_0$ and its momentum is $\frac{dG}{g} c_0$. At the exit the corresponding values are $P_1 A_1$ and $\frac{dG}{g} c_1$. Thus:

$$f_w + P_0 A_0 + \frac{c_0}{g} \int dG = P_1 A_1 + \frac{c_1}{g} \int dG,$$

where f_w is the force imparted to the gas by the duct walls. The reaction of gas on the duct walls is, therefore, $(-f_w)$. This is the internal reaction. On the other hand, supposing the duct to be at rest in an atmosphere of P_0 pressure, the external force acting on the duct walls will be $(A_1 - A_0)P_0$. Thus, assuming $P_1 = P_0$, the net thrust becomes:

$$Th = f_w - (A_1 - A_0)P_0 = \frac{(c_1 - c_0)}{g} \int dG = \frac{G}{g} (c_1 - c_0),$$

i.e., only the increase in momentum gives the thrust, provided the pressure is the same on both sides.

Taking as an example the duct of constant cross section, the thrust becomes, according to (16) and (17):

$$\begin{aligned} Th &= (P_1 - P_0)A_0 + \frac{G}{g} (c_1 - c_0) - P_0(A_1 - A_0) \\ &= P_0 A_0(\pi_1 - 1) + \frac{G c_0}{g} (\sigma_1 - 1) = \frac{GRT_0}{c_0} (\pi_1 - 1) + \frac{G c_0}{g} (\sigma_1 - 1) \\ &= \frac{G c_0}{g} \left[\frac{1}{\kappa M_0^2} (\pi_1 - 1) + (\sigma_1 - 1) \right] = 0. \end{aligned}$$

Let all idealizing assumptions so far made be conserved for a moment, and let the increase of mass by addition of fuel be disregarded. Thus the thrust will be:

$$Th = \frac{G}{g}(c_4 - c_0) \text{ lb.},$$

and the "specific thrust" as calculated per 1 lb. of air output:

$$\zeta = \frac{Th}{G} = \frac{c_0}{g}(\sigma_4 - 1) = \frac{c_0}{g}\left[\sqrt{1 + \frac{\varphi_4}{1 + \frac{(\kappa - 1)}{2} M_0^2}} - 1\right]. \quad (39)$$

The external efficiency:

$$\eta_{ex} = \frac{c_0(Th)}{\frac{G}{2g}(c_4^2 - c_0^2)} = \frac{2(\sigma_4 - 1)}{(\sigma_4^2 - 1)}$$

$$= \frac{2}{(\sigma_4 + 1)} = \frac{2}{1 + \sqrt{1 + \frac{\varphi_4}{1 + \frac{(\kappa - 1)}{2} M_0^2}}}. \quad (40)$$

The thermal efficiency (the only useful energy being the increase in kinetic energy):

$$\eta_{th} = \frac{G/2g(c_4^2 - c_0^2)}{JGQ_4}$$

$$= \frac{(\kappa - 1)M_0^2(\sigma_4^2 - 1)}{2\varphi_4} = \frac{\frac{(\kappa - 1)}{2} M_0^2}{\left[1 + \frac{(\kappa - 1)}{2} M_0^2\right]}. \quad (41)$$

The over-all efficiency:

$$\eta_0 = \eta_{ex}\eta_{th} = \frac{(\kappa - 1)M_0^2}{1 + \sqrt{1 + \frac{\varphi_4}{1 + \frac{(\kappa - 1)}{2} M_0^2}}}. \quad (42)$$

Thus, the conclusions for a "perfect ram-jet engine" are as follows:

(1) The specific thrust decreases with increasing altitude, while it increases with the total rate of heat release per 1 lb. of air output (i.e., with the total specific rate of heat release); it attains maximum value at a certain flight speed, being nil for $c_0 = 0$ and for $c_0 = \infty$.

(2) The external efficiency decreases with the total specific rate of heat release, while it increases with Mach number, i.e., with both the speed of flight and the altitude.

(3) The thermal efficiency is independent of the total specific rate of heat release, while it increases with the square of the initial Mach number, i.e., the square of flight speed has the same influence as the linearly increasing altitude.

(4) The over-all efficiency decreases with total specific rate of heat release and increases with Mach number.

(5) The maximum values of external and total efficiencies are obta... ' when the total specific rate of heat release is negligible:

$$(\eta_{ex})_{max} = 1.0;$$

$$(\eta_0)_{max} = \frac{\frac{(\kappa - 1)}{2} M_0^2}{1 + \frac{(\kappa - 1)}{2} M_0^2} = \eta_{th}.$$

In order to obtain in this case positive thrust, the air output must be infinitely large.

Rewriting Equations (40) and (42) for a certain given constant thrust Th, the following is obtained:

$$\sqrt{\frac{\varphi_4}{\mu_0} + 1} = 1 + \frac{g(Th)}{c_0 G};$$

$$\eta_{ex} = \frac{1}{1 + \frac{g(Th)}{2c_0 G}}; \tag{40'}$$

$$\eta_0 = \frac{\frac{1}{2}(\kappa - 1) M_0^2}{1 + \frac{g(Th)}{2c_0 G}}, \tag{42'}$$

while Equation (41) remains the same. As is seen, an increase in either flight speed or air output, as calculated per unit of thrust, is useful to improve efficiency.

It should be remembered here that the above conclusions are rather abstract, as they are based on assumptions of ideal gas and ideal flow, and of perfectly reversible thermodynamic process, excluding any friction and throttling losses, and also inlet shock wave phenomenon, the importance of which is actually considerable.

6. Perfect Ram-jet Engine with Mass of Fuel Involved

The next step to be accomplished in approaching actual conditions is to take into account the mass of fuel, other idealizing assumptions remaining valid.

In order to define more precisely the total rate of heat release, take first the chemically correct air–fuel mixture. The heat H_{m_0} released by burning 1 lb. of such a mixture, if regarded as a lower heat value, is incidentally constant and equals about 1130 B.t.u. per lb. for usual fluid fuels. The total specific rate of heat release φ_4 will, therefore, depend on the air excess coefficient λ.

The weight of air theoretically necessary to burn completely 1 lb. of fuel being denoted by α (for instance $\alpha \backsim 15.1$ for gasoline), thus, per 1 lb. of burning mixture:

$$Q_4 = Q_{2,3} = \frac{(\alpha + 1)}{(\alpha\lambda + 1)} H_{m_0}, \quad \text{B.t.u. per lb.;}$$

$$\varphi_4 = \varphi_{2,3} = \frac{(\kappa - 1)J}{\kappa R T_0} Q_{2,3}$$

$$= \frac{(\kappa - 1)J(\alpha + 1)H_{m_0}}{\kappa R T_0(\alpha\lambda + 1)} = \frac{(\alpha + 1)\beta}{(\alpha\lambda + 1)}, \tag{43}$$

where

$$\beta = \frac{(\kappa - 1)JH_{m_0}}{\kappa R T_0}. \tag{44}$$

The weight output of the active medium being G in compression $1 - 2$, it will be in combustion $2 - 3$ and in expansion $3 - 4$:

$$G_{2,3,4} = \frac{(\alpha\lambda + 1)}{\alpha\lambda} G = \delta G. \tag{45}$$

Equations (33) to (37) might be directly applied here to find temperatures, pressures, and velocities. This would be, however, an approximation only, which may raise the asymptotic limit of the external efficiency beyond 100%. To have all formulae theoretically exact, two quantities of energy, no matter how small they may actually be, must be taken into account.

The first is due to the fact that the fuel is introduced at the temperature T_0; it must, therefore, be reheated from T_0 to T_2. From the theoretical standpoint the same specific heat as for air will be applied here; therefore the actual amount of heat serving to raise the temperature of 1 lb. of the fuel–air mixture from T_2 to T_3 will be not Q_4 but

$$Q_4' = Q_4 - \frac{\kappa R}{(\kappa - 1)J}(T_2 - T_0)\frac{G}{\alpha\lambda} \times \frac{\alpha\lambda}{(\alpha\lambda + 1)G}$$

$$= \frac{(\alpha + 1)H_{m_0}}{(\alpha\lambda + 1)} - \frac{\kappa R T_0}{(\kappa - 1)J} \times \frac{(\tau_2 - 1)}{(\alpha\lambda + 1)};$$

$$\varphi_4' = \varphi_4 - \frac{(\tau_2 - 1)}{(\alpha\lambda + 1)} = \frac{(\alpha + 1)\beta - (\tau_2 - 1)}{(\alpha\lambda + 1)}. \tag{46}$$

The second quantity of energy lost is due to the fact that the fuel has to be delivered at the pressure P_2. This prior compression from P_0 to P_2 may be ideologically identical with the increase of kinetic energy of fuel from 0 to $\frac{c_0^2}{2g}$, as this was the kinetic energy of air at the intake, while for the fuel it was nil. The only means of doing this work is to utilize a small part of the kinetic energy of the gases leaving the engine, as there is no other way to drive auxiliaries—if the theoretical viewpoint is to be maintained. Thus the actual thrust will be diminished. Instead of the net work done by the thrust per unit of time

$$W = c_0(Th) = \frac{Gc_0}{g}(\delta c_4 - c_0),$$

it will be

$$W' = \frac{Gc_0}{g}(\delta c_4 - c_0) - \frac{Gc_0^2}{2g\alpha\lambda} \tag{47}$$

if any loss of energy which might occur here is disregarded. The actual net thrust will, therefore, be:

$$(Th)' = \frac{W'}{c_0} = \frac{G}{g}(\delta c_4 - c_0) - \frac{Gc_0}{2g\alpha\lambda}\,. \tag{48}$$

Applying now Equation (37) and those following, formulae as given below are obtained:

$$\tau_2 = 1 + \frac{(\kappa - 1)}{2} M_0^2\,;$$

$$\pi_2 = \left[1 + \frac{(\kappa - 1)}{2} M_0^2\right]^{\frac{\kappa}{\kappa - 1}} = \pi_3\,;$$

$$\sigma_2 = \sigma_3 = 0;$$

$$\tau_3 = \tau_2 + \varphi_4' = \frac{(\alpha + 1)\beta + 1 + \alpha\lambda \frac{(\kappa - 1)}{2} M_0^2}{(\alpha\lambda + 1)}\,;$$

$$\tau_4 = \frac{\tau_3}{\tau_2} = \frac{\varphi_4'}{\tau_2} + 1$$

$$= \frac{\left[(\alpha + 1)\beta + 1 + \alpha\lambda + \alpha\lambda \frac{(\kappa - 1)}{2} M_0^2\right]}{(\alpha\lambda + 1)\left[1 + \frac{(\kappa - 1)}{2} M_0^2\right]}\,;$$

$$\pi_4 = 1;$$

$$\sigma_4 = \sqrt{\frac{\tau_3 - \tau_4}{\frac{(\kappa - 1)}{2} M_0^2}} = \sqrt{\frac{\tau_3}{\tau_2}} = \sqrt{\frac{\varphi_4'}{\tau_2} + 1}$$

$$= \sqrt{\tau_4} = \sqrt{\frac{(\alpha + 1)\beta + 1 + \alpha\lambda + \alpha\lambda \frac{(\kappa - 1)}{2} M_0^2}{(\alpha\lambda + 1)\left[1 + \frac{(\kappa - 1)}{2} M_0^2\right]}}\,.$$

Thus, the final cross section:

$$\psi_4 = \delta\sqrt{\frac{\varphi_4'}{\tau_2} + 1} = \frac{\sqrt{\alpha\lambda + 1}}{\alpha\lambda}\sqrt{\frac{(\alpha + 1)\beta + 1 + \alpha\lambda + \alpha\lambda \frac{(\kappa - 1)}{2} M_0^2}{1 + \frac{(\kappa - 1)}{2} M_0^2}}\,. \tag{49}$$

Furthermore:

$$\left.\begin{aligned}(Th)' &= \frac{Gc_0}{g}\times \\ &\frac{\left[\sqrt{\alpha\lambda+1}\sqrt{(\alpha+1)\beta+1+\alpha\lambda+\alpha\lambda\frac{(\kappa-1)}{2}M_0^2}-(\alpha\lambda+\frac{1}{2})\sqrt{1+\frac{(\kappa-1)}{2}M_0^2}\right]}{\alpha\lambda\sqrt{1+\frac{(\kappa-1)}{2}M_0^2}};\\ \zeta' &= \frac{(Th)'}{G}\\ &= \frac{c_0}{g\alpha\lambda}\left[\frac{\sqrt{\alpha\lambda+1}\sqrt{(\alpha+1)\beta+1+\alpha\lambda+\alpha\lambda\frac{(\kappa-1)}{2}M_0^2}}{\sqrt{1+\frac{(\kappa-1)}{2}M_0^2}}-(\alpha\lambda+\tfrac{1}{2})\right];\end{aligned}\right\}\quad(50)$$

$$W' = c_0(Th)';$$

$$\eta_{ex} = \frac{W'}{\frac{G}{2g}(\delta c_4^2 - c_0^2)}$$

$$=\frac{2\left[\sqrt{\alpha\lambda+1}\sqrt{(\alpha+1)\beta+1+\alpha\lambda+\alpha\lambda\frac{(\kappa-1)}{2}M_0^2}-(\alpha\lambda+\frac{1}{2})\sqrt{1+\frac{(\kappa-1)}{2}M_0^2}\right]\sqrt{1+\frac{(\kappa-1)}{2}M_0^2}}{[(\alpha\lambda+1)\beta+1]};\quad(51)$$

$$\eta_{th} = \frac{\frac{G}{2g}(\delta c_4^2 - c_0^2)}{JGQ_4\delta} = \frac{(\kappa-1)M_0^2[(\alpha+1)\beta+1]}{2(\alpha+1)\beta\left[1+\frac{(\kappa-1)}{2}M_0^2\right]};\quad(52)$$

$$\eta_0 = \frac{(\kappa-1)M_0^2}{(\alpha+1)\beta}\left[\frac{\sqrt{\alpha\lambda+1}\sqrt{(\alpha+1)\beta+1+\alpha\lambda+\alpha\lambda\frac{(\kappa-1)}{2}M_0^2}}{\sqrt{1+\frac{(\kappa-1)}{2}M_0^2}}-(\alpha\lambda+\tfrac{1}{2})\right].\quad(53)$$

The "unit thrust", as calculated by the unit of the cross section area, will be:

$$\epsilon_0 = \frac{(Th)'}{A_0} = \frac{c_0P_0}{GRT_0}(Th)'$$

$$= \frac{\kappa M_0^2P_0}{\alpha\lambda}\left[\frac{\sqrt{\alpha\lambda+1}\sqrt{(\alpha+1)\beta+1+\alpha\lambda+\alpha\lambda\frac{(\kappa-1)}{2}M_0^2}}{\sqrt{1+\frac{(\kappa-1)}{2}M_0^2}}-(\alpha\lambda+\tfrac{1}{2})\right].\quad(54)$$

$$\epsilon_4 = \frac{(Th)'}{A_4} = \frac{\epsilon_0}{\psi_4}$$

$$= \kappa M_0^2 P_0 \frac{\left[\sqrt{\alpha\lambda+1}\sqrt{(\alpha+1)\beta+1+\alpha\lambda+\alpha\lambda\frac{(\kappa-1)}{2}M_0^2}-(\alpha\lambda+\tfrac{1}{2})\sqrt{1+\frac{(\kappa-1)}{2}M_0^2}\right]}{\sqrt{\alpha\lambda+1}\sqrt{(\alpha+1)\beta+1+\alpha\lambda+\alpha\lambda\frac{(\kappa-1)}{2}M_0^2}}. \tag{55}$$

Mathematical analysis of Equation (51) shows that η_{ex} attains the maximum value of 100% for $\lambda = \infty$, and continuously increases with λ. At the same time the specific thrust ζ' continuously decreases with increasing λ and becomes nil for $\lambda = \infty$, provided that $\mu_0 \leqslant 4[(\alpha + 1)\beta + 1]$, i.e.,

$$M_0 \leqslant \sqrt{\frac{2}{(\kappa - 1)}\{4[(\alpha + 1)\beta + 1] - 1\}}.$$

Considering now the initial Mach number as an independent variable, the external efficiency η_{ex} first increases with increasing M_0, attaining maximum value of 100% for

$$(M_0)_{\epsilon_1} = \sqrt{\frac{2}{(\kappa - 1)}(\alpha + 1)\beta},$$

and then decreases, becoming nil for

$$(M_0)_{\epsilon_2} = \sqrt{\frac{2}{(\kappa - 1)}\{4[\alpha + 1)\beta + 1](\alpha\lambda + 1) - 1\}}.$$

Of course, η_{ex} cannot be negative; therefore, the limit for the velocity of flight, expressed by the initial Mach number, is

$$M_0 \leqslant \sqrt{\frac{2}{(\kappa - 1)}\{4[(\alpha + 1)\beta + 1](\alpha\lambda + 1) - 1\}}, \tag{56}$$

as far as the dynamical phenomenon is concerned, this value of M_0 corresponding to the conditions in which the loss in kinetic energy of gas mass leaving the engine becomes equal to the total increase in kinetic energy created by the engine. For $\lambda = \infty$, i.e., in a case in which the mass of fuel may be disregarded, the limit (56) gives, of course, $M_0 = \infty$, which means $c_0 = \infty$ if $T_0 > 0$.

Likewise, the specific thrust first increases with increasing M_0, attaining a certain maximum value which does not coincide with the maximum of η_{ex}, and then decreases, becoming nil together with η_{ex}, i.e., for the value of M_0 as defined by (56).

The maximum value of thermal efficiency, equalling 100%, is obtained for $(M_0)_{e_1} = \sqrt{\frac{2}{(\kappa - 1)}(\alpha + 1)\beta}$, according to (52), i.e., if thermodynamic means for creating energy are applied. In the limiting case φ_4' becomes nil, i.e., all the heat released by combustion is utilized only for the reheating of fuel from T_0 to the ram temperature T_2. It follows that $T_4 = T_0$ and $c_4 = c_0$, i.e., both exit heat loss and exit loss in kinetic energy are nonexistent, which is in accordance with 100% value of all efficiencies (η_{ex} ; η_{th} ; η_0). Of course, heat φ_4' cannot be negative; value $(M_0)_{e_1}$ is, therefore, a physical limit for the velocity of flight, as regarded from the theoretical viewpoint:

$$M_0 \leqslant \sqrt{\frac{2}{(\kappa - 1)}(\alpha + 1)\beta}\,. \tag{56'}$$

This limiting value is independent (at least apparently so) of the air excess coefficient, i.e., of the ratio G_f/G_a. It, therefore, seems to be valid in any general case, even for $G_a = \infty$, provided the thermodynamic means to create energy are applied. As the limit (56') is more restricted than (56), it must be considered as the actual one.

7. Semiperfect Ram-jet Engine with Finite Combustion Chamber Cross Section

In the actual jet engine the bulk diameter will, of course, be limited by practical conditions. In order to let the perfect ram-jet engine approach actual conditions, suppose that the maximum cross section, no matter where it may be placed in the engine, is given, all other idealizing conditions being maintained. The best results in such a semiperfect jet engine will, of course, be obtained when this maximum cross section occurs at point 2, i.e., just after dynamic compression, the combustion chamber cross section remaining constant, i.e., $A_3 = A_2$. The corresponding form of the engine working in subsonic region is represented in Fig. 13 and the graphical representation in entropy diagram in Fig. 14.

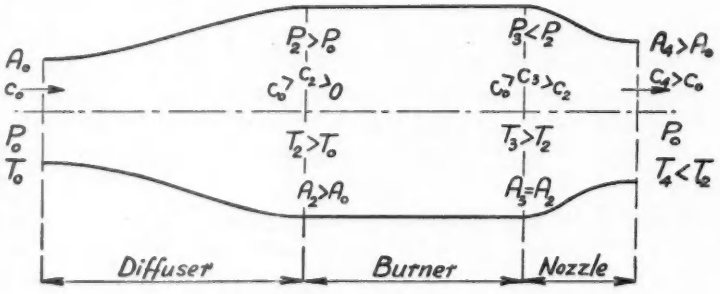

FIG. 13.

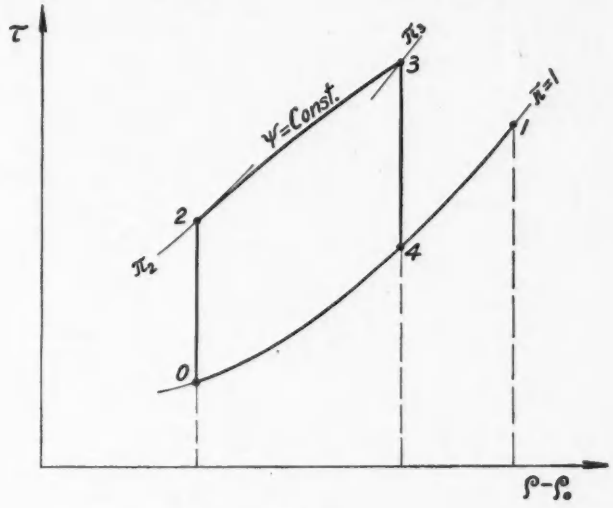

FIG. 14.

Another possible limitation is to consider the minimum admissible value for the velocity σ_2 after dynamic compression. Supposing that this value is given as $(\sigma_2)_{min}$, the following formulae are obtained:

$$\tau_2 = \left[1 + \frac{(\kappa - 1)}{2} M_0^2 (1 - \sigma_{2m}^2)\right]; \tag{57}$$

$$\pi_2 = \tau_2^{\frac{\kappa}{\kappa-1}} = \left[1 + \frac{(\kappa - 1)}{2} M_0^2 (1 - \sigma_{2m}^2)\right]^{\frac{\kappa}{\kappa-1}}; \tag{58}$$

$$\psi_2 = \frac{\tau_2}{\sigma_{2m}\pi_2} = \frac{1}{\sigma_{2m}\left[1 + \frac{(\kappa - 1)}{2} M_0^2 (1 - \sigma_{2m}^2)\right]^{\frac{1}{\kappa-1}}}; \tag{59}$$

$$\varphi_{2,3} = \frac{(\alpha + 1)\beta}{(\alpha\lambda + 1)}; \tag{60}$$

$$Q_{2,3} = \frac{\kappa R T_0}{(\kappa - 1) J} \varphi_{2,3};$$

$$\varphi'_{2,3} = \varphi_{2,3} - \frac{(\tau_2 - 1)}{(\alpha\lambda + 1)} = \frac{(\alpha + 1)\beta - \frac{(\kappa - 1)}{2} M_0^2 (1 - \sigma_{2m}^2)}{(\alpha\lambda + 1)}; \tag{61}$$

$$\pi_3 = \frac{\pi_2^{\frac{1}{\kappa-1}}}{(\kappa + 1)} \left[(\kappa M_0^2 \sigma_{2m}^2 + \tau_2) + \kappa \sqrt{(\tau_2 - M_0^2\sigma_{2m}^2)^2 - 2(\kappa+1) M_0^2 \sigma_{2m}^2 \varphi'_{2,3}}\right]; \tag{62}$$

$$\sigma_3 = \frac{1}{(\kappa+1)M_0^2\sigma_{2m}}\left[(\kappa M_0^2\sigma_{2m}^2+\tau_2) - \sqrt{(\tau_2+M_0^2\sigma_{2m}^2)^2-2(\kappa+1)M_0^2\sigma_{2m}^2\varphi'_{2,3}}\right]$$

$$= \frac{\sigma_{2m}[(\kappa-1)M_0^2\sigma_{2m}^2+2(\tau_2+\varphi'_{2,3})]}{(\kappa M_0^2\sigma_{2m}^2+\tau_2)+\sqrt{(\tau_2-M_0^2\sigma_{2m}^2)^2-2(\kappa+1)M_0^2\sigma_{2m}^2\varphi'_{2,3}}}\ ; \qquad (63)$$

$$\tau_3 = \tau_2\frac{\sigma_3}{\sigma_{2m}}\times\frac{\pi_3}{\pi_2} = \frac{\sigma_3\pi_3}{\sigma_{2m}\tau_2^{\frac{1}{\kappa-1}}}\ ; \qquad (64)$$

$$\tau_4 = \frac{\tau_3}{\pi_3^{\frac{\kappa-1}{\kappa}}}\ ; \qquad (65)$$

$$\sigma_4 = \sqrt{\frac{(\tau_3-\tau_4)}{\frac{(\kappa-1)}{2}M_0^2}+\sigma_3^2}\ ; \qquad (66)$$

$$\psi_4 = \frac{\delta\tau_4}{\pi_4\sigma_4} = \frac{\delta\tau_4}{\sigma_4}\ ; \qquad (67)$$

$$(Th)' = G\zeta' = \frac{Gc_0}{g}\left(\delta\sigma_4-1-\frac{1}{2\alpha\lambda}\right); \qquad (68)$$

$$\eta_{ex} = \frac{c_0(Th)'}{\frac{Gc_0^2}{2g}(\delta\sigma_4^2-1)} = \frac{2\left(\delta\sigma_4-1-\frac{1}{2\alpha\lambda}\right)}{(\delta\sigma_4^2-1)}\ ; \qquad (69)$$

$$\eta_{th} = \frac{Gc_0^2/2g\,(\delta\sigma_4^2-1)}{JGQ_{2,3}\delta} = \frac{(\kappa-1)M_0^2(\delta\sigma_4^2-1)}{2\delta\varphi_{2,3}}\ ; \qquad (70)$$

$$\eta_0 = \eta_{ex}\eta_{th}\ ; \qquad (71)$$

$$\epsilon_0 = \frac{(Th)'}{A_0} = \kappa M_0^2 P_0\left(\delta\sigma_4-1-\frac{1}{2\alpha\lambda}\right); \qquad (72)$$

$$\epsilon_2 = \frac{\epsilon_0}{\psi_2}\ ; \qquad (73)$$

$$\epsilon_4 = \frac{\epsilon_0}{\psi_4}\ . \qquad (74)$$

Suppose, as an example:

Velocity of flight c_0 = 600 m.p.h. = 880 ft. per sec.;

Sea level, standard atmosphere;

κ = 1.4; R = 53.3 ft. per °Rankine;

Fuel: gasoline, α = 15.0; H_{m_0} = 1130 B.t.u. per lb.;

Air excess coefficient: λ = 4.0;

Velocity at the combustion chamber inlet: c_2 = 100 ft. per sec.

This gives:

$M_0 = 0.789$; $M_0^2 = 0.6225$;
$\sigma_{2m} = 0.1137$; $\sigma_{2m}^2 = 0.01292$;
$\tau_2 = 1.1221$; $\pi_2 = 1.497$;
$\psi_2 = 6.595$; $\sqrt{\psi_2} = 2.568$;
$\beta = 9.09$; $\varphi_{2,3} = 2.384$; $\varphi'_{2,3} = 2.383$;
$\delta = 1.017$;
$\pi_3 = 1.463$; $\sigma_3 = 0.362$; $\tau_3 = 3.490$;
$\pi_4 = 1.000$; $\tau_4 = 3.130$; $\sigma_4 = 1.739$;
$\psi_4 = 1.830$; $\sqrt{\psi_4} = 1.354$;
$\zeta' = 20.80$ lb. per lb. per sec.;
$\eta_{ex} = 0.734 = 73.4\%$;
$\eta_{th} = 0.1064 = 10.64\%$;
$\eta_0 = 0.0781 = 7.81\%$;
$\epsilon_0 = 1415$ lb. per sq. ft. $= 9.67$ lb. per sq. in.;
$\epsilon_2 = 214.7$ lb. per sq. ft. $= 1.475$ lb. per sq. in.;
$\epsilon_4 = 774$ lb. per sq. ft. $= 5.330$ lb. per sq. in.

8. The Actual Ram-jet Engine

The aerothermodynamic process in an actual ram-jet engine will be as illustrated graphically in entropy diagram in Fig. 15.

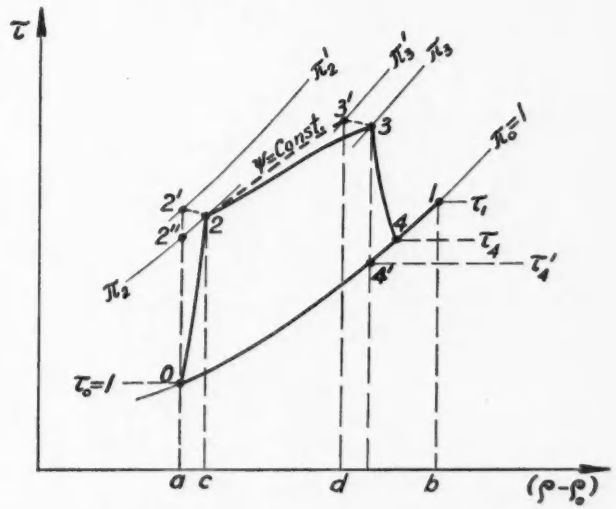

FIG. 15. *Entropy diagram of an actual ram-jet engine.*

Let the efficiency of the diffuser be η_d (probably of the order of 0.92); thus:

$$\frac{T_2'' - T_0}{T_2 - T_0} = \eta_d ;$$

$$\frac{P_2''}{P_0} = \frac{P_2}{P_0} = \pi_2 = \left(\frac{T_2}{T_0}\right)^{\frac{\kappa}{\kappa-1}} .$$

As equation of aerothermodynamics, in form (7) or (28), always holds true, even if throttling loss is involved, assuming that the process 0 − 2 is adiabatic in the general sense of the term (i.e., that no heat exchange is involved), this process may be considered as an isentropic compression 0 − 2′ accompanied by the throttling 2′ − 2. Thus

$$\tau_2 = \left[1 + \frac{(\kappa - 1)}{2} M_0^2(1 - \sigma_{2m}^2)\right], \tag{75}$$

where σ_{2m} is assumed to be given. Therefore:

$$T_2'' = T_0 + \eta_d(T_2 - T_0);$$

$$\pi_2 = [(1 - \eta_d) + \eta_d\tau_2]^{\frac{\kappa}{\kappa-1}}$$

$$= \left[1 + \eta_d \frac{(\kappa - 1)}{2} M_0^2(1 - \sigma_{2m}^2)\right]^{\frac{\kappa}{\kappa-1}} ; \tag{76}$$

$$\psi_2 = \frac{\tau_2}{\sigma_{2m}\pi_2} . \tag{77}$$

Pressure π_2' might be obtained if the evolution were isentropic, with no throttling loss involved and with the same cross section ψ_2.

The loss by incomplete combustion may be considered as nil, remembering the considerable air excess applied here, provided that the combustion chamber is properly designed. The loss of heat by conductivity is relatively small—of the order of 2%; this is due to the considerable magnitude of the heat release, as relating to the small surface corresponding to unit of flowing mass. Let the corresponding efficiency be η_h (probably about 0.98); thus:

$$\varphi_{2,3} = \eta_h \frac{(\alpha + 1)\beta}{(\alpha\lambda + 1)} ; \tag{78}$$

$$\varphi_{2,3}' = \varphi_{2,3} - \frac{(\tau_2 - 1)c_{p_f}}{(\alpha\lambda + 1)c_{p_a}} , \tag{79}$$

where c_{p_f}/c_{p_a} is the ratio of specific heats of fuel and air respectively; this ratio is so chosen as to take into account also the latent heat of vaporization of fuel. The actual value of this ratio is, therefore, about 10.

The gas constant and the isentropic exponent of the mixture during combustion are, of course, variable. The gas constant deviates only very slightly from that of air (this being due to a considerable air excess), and its mean

value may be evaluated as $R' = 53.0$. The mean value of the specific heat c_p' deviates much more from that of cold air, this being due mainly to the increase in temperature. It may be evaluated as $c_p' \backsim 0.28$ B.t.u. per lb., °F., in the case studied.

Therefore the isentropic exponent will be:

$$\kappa' = \frac{1}{1 - R'/c_p'J} = 1.322.$$

At the same time the formal value of Mach number M_0 will change to M_0':

$$M_0' = \sqrt{\frac{\kappa R}{\kappa' R'}}\, M_0 = 1.032\, M_0 .$$

In actual practice the loss by heat conductivity is often overestimated, values of η_h being estimated as low as 0.88 and even 0.85. This is due to the fact that, in applying computation based on the assumption of an ideal gas, values of R and κ are usually kept constant during the whole process. As is seen, the actual value κ' during combustion deviates considerably from κ for cold gas. Thus, remaining in the field of theoretical computation, final results are found to be less optimistic, the influence of the changing value of κ with temperature being much stronger than the heat loss by conductivity.

If, for the moment, the "hydraulic" loss in the combustion chamber of constant cross section is disregarded, the final state after combustion will be π_3', σ_3', τ_3':

$$\pi_3' = \frac{\pi_2}{(\kappa'+1)\tau_2}\left[(\kappa' M_0'^2\sigma_{2m}^2+\tau_2)+\kappa'\sqrt{(\tau_2-M_0'^2\sigma_{2m}^2)^2-2(\kappa'+1)M_0'^2\sigma_{2m}^2\varphi_{2,3}'}\right]; \tag{80}$$

$$\sigma_3' = \frac{1}{(\kappa'+1)M_0'^2\sigma_{2m}}\left[(\kappa' M_0'^2\sigma_{2m}^2+\tau_2)-\sqrt{(\tau_2-M_0'^2\sigma_{2m}^2)^2-2(\kappa'+1)M_0'^2\sigma_{2m}^2\varphi_{2,3}'}\right]$$

$$= \frac{\sigma_{2m}[(\kappa'-1)M_0'^2\sigma_{2m}^2+2(\varphi_{2,3}'+\tau_2)]}{[(\kappa' M_0'^2\sigma_{2m}^2+\tau_2)+\sqrt{(\tau_2-M_0'^2\sigma_{2m}^2)^2-2(\kappa'+1)M_0'^2\sigma_{2m}^2\varphi_{2,3}'}]}; \tag{81}$$

$$\tau_3' = \frac{\sigma_3'\pi_3'}{\sigma_{2m}\pi_2}\,\tau_2 . \tag{82}$$

The actual pressure π_3 will, of course, be less and it might be evaluated according to the well known routine method, involving Reynolds number and hydraulic radius. The loss $(\pi_3' - \pi_3)$ is, in the case studied, of the order of 2%. For the sake of simplicity it may be defined by the "pressure efficiency" η_p as follows:

$$\pi_3 = \eta_p \pi_3', \tag{83}$$

where η_p is of the order of 0.98. More precisely:

$$\eta_p = 1 - 2.5\, M_0^2\sigma_{2m}^2 ,$$

where the coefficient 2.5 was so chosen as to approach the actual conditions.

In actual practice the "hydraulic" loss of pressure during combustion is often overestimated, even if account is taken of the fact that some actual designs of burner are complicated and offer considerable resistance to flow through combustion chamber. This is due to the fact that the influence of heat exchange on pressure, as studied theoretically in Sections 3 and 4, is generally overlooked in actual computations, while this influence may be actually considerable, at least in case of high velocity.

As, in passing from 3′ to 3, both the equation of continuity and the equation of aerothermodynamics hold true, the throttling phenomenon being adiabatic in the general sense of the term; thus:

$$\frac{\sigma_3\pi_3}{\tau_3} = \frac{\sigma_3'\pi_3'}{\tau_3'};$$

$$\tau_3 = \tau_3' + \frac{(\kappa' - 1)}{2} M_0'^2(\sigma_3'^2 - \sigma_3^2),$$

wherefrom:

$$\sigma_3 = \frac{\sigma_3'}{\eta_p}\left[1 + \frac{(\kappa' - 1)M_0'^2}{2\tau_3'}(\sigma_3'^2 - \sigma_3^2)\right];$$

$$\sigma_3 = \frac{\sigma_3'[2\tau_3' + (\kappa' - 1)M_0'^2\sigma_3'^2]}{\sqrt{[(\kappa' - 1)M_0'^2\sigma_3'^2 + \tau_3']^2 - (1 - \eta_p^2)\tau_3'^2} + \eta_p\tau_3'}; \quad (84)$$

$$\tau_3 = \frac{\eta_p\tau_3'}{\sigma_3'}\sigma_3. \quad (85)$$

Now let the efficiency of the nozzle be η_n (probably of the order of 0.96); thus:

$$\frac{T_3 - T_4}{T_3 - T_4'} = \eta_n;$$

$$\pi_4 = 1;$$

$$\left(\frac{T_3}{T_4'}\right)^{\frac{\kappa'}{\kappa'-1}} = \pi_3;$$

$$\tau_4 = \tau_3\left[(1 - \eta_n) + \frac{\eta_n}{(\pi_3)^{\frac{\kappa'-1}{\kappa'}}}\right]; \quad (86)$$

$$\sigma_4 = \sqrt{\sigma_3^2 + \frac{2}{(\kappa' - 1)M_0'^2}(\tau_3 - \tau_4)}; \quad (87)$$

$$\psi_4 = \frac{\delta\tau_4}{\sigma_4}. \quad (88)$$

The efficiency of the pumping of fuel η_f is of the order of 0.10 only, as a part of final thrust is supposed to be utilized here; thus:

$$\zeta' = \frac{c_0}{g}\left(\delta\sigma_4 - 1 - \frac{1}{2\alpha\lambda\eta_f}\right); \quad (89)$$

$$\eta_{ex} = \frac{2\left(\delta\sigma_4 - 1 - \frac{1}{2\alpha\lambda\eta_f}\right)}{(\delta\sigma_4^2 - 1)}; \tag{90}$$

$$\eta_{th} = \frac{(\kappa - 1)M_0^2\eta_h(\delta\sigma_4^2 - 1)}{2\delta\varphi_{2,3}}; \tag{91}$$

$$\eta_0 = \eta_{ex}\eta_{th}; \tag{92}$$

$$\epsilon_0 = \kappa M_0^2 P_0\left(\delta\sigma_4 - 1 - \frac{1}{2\alpha\lambda\eta_f}\right); \tag{93}$$

$$\epsilon_2 = \frac{\epsilon_0}{\psi_2}; \tag{94}$$

$$\epsilon_4 = \frac{\epsilon_0}{\psi_4}. \tag{95}$$

Let, for example:

$c_0 = 880$ ft. per sec.; $c_2 = 100$ ft. per sec.;

sea level, standard atmosphere;

$\kappa = 1.40$; $R = 53.3$ ft. per °Rankine; $\lambda = 4.0$;

$\kappa' = 1.322$; $R' = 53.0$;

$\alpha = 15.0$; $H_{m_0} = 1130$ B.t.u. per lb. ($\beta = 9.09$; $\delta = 1.017$);

$\eta_d = 0.92$; $\eta_n = 0.96$;

$\eta_h = 0.98$; $\frac{c_{p_f}}{c_{p_a}} = 10.0$;

$\eta_p = 0.98$; $\eta_f = 0.10$.

This gives:

$M_0 = 0.789$; $M_0^2 = 0.6225$;

$\sigma_{2m} = 0.1137$; $\sigma_{2m}^2 = 0.01292$;

$M_0' = 0.8135$; $M_0'^2 = 0.6625$;

$\tau_2 = 1.1221$; $\pi_2 = 1.448$;

$\psi_2 = 6.820$; $\sqrt{\psi_2} = 2.614$;

$\varphi_{2,3} = 2.536$; $\varphi'_{2,3} = 2.316$;

$\pi_3' = 1.414$; $\sigma_3' = 0.355$; $\tau_3' = 3.422$;

$\pi_3 = 1.386$; $\sigma_3 = 0.3573$; $\tau_3 = 3.374$;

$\pi_4 = 1.000$; $\tau_4 = 3.122$; $\sigma_4 = 1.578$;

$\psi_4 = 2.014$; $\sqrt{\psi_4} = 1.420$;

$\zeta' = 14.22$ lb. per lb. per sec.;

$\eta_{ex} = 0.6800 = 68.00\%$;

$\eta_{th} = 0.0724 = 7.24\%$;

$\eta_0 = 0.0492 = 4.92\%$;

$\epsilon_0 = 960$ lb. per sq. ft. $= 6.670$ lb. per sq. in.;

$\epsilon_2 = 140.8$ lb. per sq. ft. $= 0.978$ lb. per sq. in.;

$\epsilon_4 = 477.0$ lb. per sq. ft. $= 3.312$ lb. per sq. in.

It should be pointed out here that the property of a semiperfect ram-jet engine to have the higher efficiency, the closer the velocity σ_{2m} of flow in the combustion chamber is to zero, no longer exists in the actual engine. Of course, all the heat released in an actual engine is represented by the area $c23'd$, according to Fig. 15, as the two throttling phenomena $2' - 2$ and $3' - 3$ are adiabatic, and the expansion $3 - 4$, bound with a certain throttling, is also adiabatic. The heat released is also represented by the area $a01b$, the two areas being equal. As, however, in an actual engine point 2 is shifted to the right of 0 and point 4 is shifted to the right of 3', therefore, the higher the pressure π_2 (i.e., the lower the velocity σ_{2m}), the closer the point 4 is shifted to 1. It is therefore possible that the total efficiency does not increase continuously with π_2 but it passes through a maximum for a certain value of $\sigma_{2m} > 0$, at least at very high supersonic velocities of flight.

9. Conclusions

The main emphasis in this paper is placed on the theoretical background of the problem of ram-jet propulsion, while numerical calculation in regard to an actual engine, as given in Section 8, is only approximate.

The conclusion showing the necessity of applying both the diffuser for dynamic compression and the combustion chamber of constant cross section, as well as the nozzle at the rear, is rather disappointing, as this will result in considerable length of the whole unit. Fortunately, some recent solutions permitting a considerable shortening of the combustion chamber are just making their appearance. The same holds true for a diffuser. These questions are, however, beyond the scope of this paper.

The method of discussion on the basis of entropy diagram, as applied in this paper, seems to be successful; therefore, it will perhaps be desirable to apply it also in the case of a conventional turbo-jet engine.

References

1. CHAMBRÉ, P. and LIN, C.-C. J. Aeronaut. Sci. 13 : 537. 1946.
2. EXERGIAN, R. J. Franklin Inst. 237 : 401. 1944.
3. KEIRN, D. J. and SHOULTS, D. R. J. Aeronaut. Sci. 13 : 411. 1946. (See also references in that paper.)
4. MALINA, F. J. J. Franklin Inst. 230 : 433. 1940.
5. MOSS, S. A. and FOOTE, W. R. J. Aeronaut. Sci. 13 : 111. 1946.
6. REISSNER, H. J. Aeronaut. Sci. 14 : 197. 1947.
7. SAMARAS, D. G. Can. J. Research, F, 24 : 272. 1946.
8. SAMARAS, D. G. Eng. J. 29 : 398. 1946.
9. SEIFERT, H. S., MILLS, M. M., and SUMMERFIELD, M. Am. J. Phys. 15 : 1. 1947.
10. SZCZENIOWSKI, B. Can. J. Research, A, 23 : 1. 1945.

REMARKS ON THE EXCITATION OF HYDROGEN AND HELIUM IN THE UPPER ATMOSPHERE[1]

By William Petrie

Abstract

A number of hydrogen and helium lines have been identified as features of the auroral spectrum. The relative intensities of these lines suggest that the excitation process is electron collision. Furthermore, the intensities of the helium lines indicate an "excitation temperature" of 4600°K., and the intensities of the hydrogen lines an "excitation temperature" of 7600°K.

Introduction

There is little doubt that on certain occasions hydrogen lines appear in the auroral spectrum. Vegard (15) has obtained spectra which show relatively strong lines at wave lengths coinciding with the first two members of the Balmer series. The rare appearance of these lines raises an interesting question regarding the source of the hydrogen and the excitation of the spectrum. It is not likely that hydrogen in the earth's atmosphere is the source of the observed Balmer spectrum, since we would then expect these lines to be a permanent feature of the auroral spectrum. This spectrum shows that excitation conditions in the upper atmosphere are sufficiently high to produce the Balmer lines, but little is known regarding the hydrogen content of the auroral region. The percentage by volume of hydrogen in dry tropospheric air is 5×10^{-5}. Owing to the differential densities of the various constituents of air, the percentage of hydrogen should increase with altitude. There is experimental evidence (11) to show that the percentage of helium is increasing at a height of 20 km.; and the same should be true to an even greater degree for hydrogen. On the other hand, the lighter gases are undoubtedly escaping from the upper atmosphere, which fact probably explains the usual absence of hydrogen lines from the auroral spectrum. Vegard (15) suggests that on occasions showers of hydrogen from the sun enter the earth's atmosphere; at such times the auroral spectrum shows the Balmer lines. This suggestion is very reasonable; it is known that solar "eruptive" prominences eject matter into space, and these prominences are largely hydrogen.

We will discuss the intensity distribution in the Balmer spectrum for different methods of excitation, and attempt to decide which method applies to the hydrogen lines in the auroral spectrum.

Excitation of the Balmer Spectrum

It might be thought that the hydrogen lines in the auroral spectrum are produced by the recombination of electrons and protons. Actually, we have no information on the proton content of the upper atmosphere, although

[1] *Manuscript received May 27, 1948.*
Contribution from the Department of Physics, University of Saskatchewan, Saskatoon, Sask.

cosmic ray studies indicate that protons are present in this region. If protons are supplied by the ionization of hydrogen or enter the atmosphere from an external source, we would expect the recombination process to operate continually and result in the hydrogen lines being a permanent feature of the auroral spectrum. Quite apart from these considerations we will explain that the recombination process produces a spectrum in which the intensities of the lines H_α, H_β, H_γ decrease relatively slowly unless the temperature of the free electrons is very high.

To compute the relative intensities of the Balmer lines in a pure capture spectrum, we need to know the fractions of electrons captured on the various levels of the atom. The number of captures per cubic centimeter per second per velocity range dv may be represented by the following expression,

$$N_v = N_i N_e v f(v) \sigma_n dv \tag{1}$$

N_i = the number of protons per cubic centimeter,

N_e = the number of electrons per cubic centimeter,

$f(v)$ = the fraction of the electrons which have velocities between v and $(v + dv)$,

σ_n = the target area for capture on level n.

Kramers (8) has derived an expression for σ_n from the correspondence principle, i.e. $\sigma_n = \frac{K}{v^2 n^3 \nu}$. The factor ν is obtained from the relation $h\nu = W_n + \frac{1}{2}mv^2$, W_n being the energy of level n measured from the ionization level. Then $\sigma_n = \frac{2\,h\,K}{v^2\,n^3\,(2\,W_n + m\,v^2)}$. If the velocity distribution of the free electrons is Maxwellian, then

$$f(v)dv = 4\pi \left(\frac{m}{2\pi k T_e}\right)^{\frac{3}{2}} v^2 e^{-\frac{1}{2}mv^2/kT_e} dv.$$

$$\text{Then } N_v = N_i N_e 4\pi \left(\frac{m}{2\pi k T_e}\right)^{\frac{3}{2}} v^3 e^{-\frac{1}{2}mv^2/kT_e} \frac{2hK}{v^2 n^3 (2W_n + mv^2)} dv.$$

The number of captures per cubic centimeter per second over all velocities

$$N = N_i N_e 4\pi \left(\frac{m}{2\pi k T_e}\right)^{\frac{3}{2}} \frac{2hK}{n^3} \int_0^\infty \frac{v e^{-\frac{1}{2}mv^2/kT_e}}{(2W_n + mv^2)} dv.$$

We may write

$$N = \frac{C_1}{T_e^{\frac{3}{2}} n^3 2W_n} \int_0^\infty \frac{v e^{-\frac{1}{2}mv^2/kT_e}}{(1 + C_2 v^2)} dv, \tag{2}$$

where

$$C_1 = N_i N_e 4\pi \left(\frac{m}{2\pi k}\right)^{\frac{3}{2}} 2hK \text{ and } C_2 = \frac{m}{2W_n}.$$

The integral is standard and results in a series the general term of which is

$$\frac{x!}{2\left(\frac{m}{2kT_e}\right)^{x+1}}, \qquad x = 1, 2, 3, \text{-------} \infty.$$

The intensities of the first three members of the Balmer series in a capture spectrum may be computed from the following expressions (14),

$$\begin{aligned} I(H_\alpha) &= A_{32} h\nu_{32} [N_3 + N_4 X_{43} + N_5 X_{53} + N_6 X_{63} + \text{-----}] \\ I(H_\beta) &= A_{42} h\nu_{42} [N_4 + N_5 X_{54} + N_6 X_{64} + N_7 X_{74} + \text{-----}] \\ I(H_\gamma) &= A_{52} h\nu_{52} [N_5 + N_6 X_{65} + N_7 X_{75} + N_8 X_{85} + \text{-----}], \end{aligned} \tag{3}$$

where A_{n3} is the Einstein transition coefficient from levels n to 2, N_n the number of captures per second on level n, and X_{ni} the fraction of atoms in level n which reach level i by spontaneous emission. The X_{ni} values may be obtained from the following equation,

$$X_{n3} = \frac{1}{\sum_{i=1}^{n-1} A_{ni}} [A_{n3} + A_{n4} X_{43} + A_{n5} X_{53} + \text{-----}]. \tag{4}$$

ΣA_{ni} is the total number of ways of leaving level n per second by spontaneous emission. We have used the A_{ni} and ΣA_{ni} values as computed by Menzel and Pekeris (10) to calculate X_{ni} values from (4). Substituting the X_{ni} and N values in Equations (3), we calculate the relative intensities of the first three members of the Balmer series. The results are approximately 3.5 : 1 : 0.3. This result is for an electron temperature of 5000°K. The relative intensities are not sensitive to the temperature of the free electrons; at very high temperatures the intensities still decrease slowly. More accurate expressions for σ_n have been derived by Gaunt (5) and Cillié (4). Menzel and Baker (9) have presented a more accurate method of calculating Balmer intensities, and have pointed out the inaccuracies of the above approach. They give for the relative intensities of the first three members of the Balmer series in a capture spectrum the values 2 : 1 : 0.6. Laboratory experiments on the recombination spectrum of hydrogen substantiate the theoretical result that the intensities decrease slowly. See for example the experiments of Herzberg (7). On the other hand, Vegard (15) gives the relative intensities of $H_\alpha : H_\beta$ in the auroral spectrum as 6 : 1. Hence we can say with some certainty that the hydrogen lines in the auroral spectrum are not the result of electron and proton recombination.

A second possible but unlikely excitation process is the absorption of ultraviolet radiation from the sun. It is readily understood that the atmosphere is not exposed to short wave length solar radiation during the night, hence any excitation from this source must come about by absorption of energy during the day and the subsequent release of this energy at night. For example, oxygen and perhaps other molecules may absorb ultraviolet radiation and dissociate into atoms. During the night, recombination will take place, and the energy released in this process may excite certain constituents of the

atmosphere. However, there is no apparent dissociation and recombination process which will supply the energy necessary to excite hydrogen atoms and produce the observed intensity distribution in the spectrum. Furthermore, the observed intensity changes in auroral structure are difficult to explain by a radiation excitation process.

Collisional excitation is a process which will certainly operate to a certain extent in the upper atmosphere. It is well known that colliding electrons are effective in producing the hydrogen spectrum, and the many experiments with hydrogen discharge tubes indicate that the intensities of the Balmer lines decrease rapidly towards higher members of the series. For example, Bongers (3) has measured the intensities of the Balmer lines in a long discharge tube, and gives the relative intensities of the first three members of the series as 79 : 10 : 2. Since hydrogen cross-sectional areas for electron collision are not known, we are unable to compute the numbers of atoms excited to the various energy levels, and hence determine the intensities of the Balmer lines. However, the experimental evidence indicates that when hydrogen atoms are excited by electron impact the relative intensities of the Balmer lines are comparable to the relative intensities observed in the auroral spectrum. In a recent paper, Bernard (1) has attributed some fifteen lines in the auroral spectrum to the neutral helium atom. He shows that the intensity distribution in these lines is comparable to the intensity distribution in the spectrum of the radiation from a helium discharge tube. This evidence suggests that electron collisions are the source of the excitation of hydrogen and helium in the upper atmosphere. However, if hydrogen and helium atoms from the sun are incident on the earth's upper atmosphere, collisions between these particles and atmospheric atoms and molecules may produce both the hydrogen and helium lines as well as other features of the auroral spectrum.

Excitation Temperatures in the Auroral Region

The emission per cubic centimeter per second in a spectral line is given by $E_{nn'} = N_n A_{nn'} h \nu_{nn'}$, N_n being the number of atoms in the upper level involved in the production of the line. For a condition of thermal equilibrium, N_n may be represented by the Boltzmann law,

$$N_n = N_0 \frac{\tilde{\omega}_n}{\tilde{\omega}_0} e^{-\chi_n/kT} .$$

N_0 is the number of atoms in the ground level, $\tilde{\omega}_n$ and $\tilde{\omega}_0$ the statistical weights of levels n and the ground level, and χ_n the excitation potential of level n. Hence,

$$E_{nn'} = N_0 \frac{\tilde{\omega}_n}{\tilde{\omega}_0} e^{-\chi_n/kT} A_{nn'} h\nu_{nn'} . \qquad (5)$$

It is very unlikely that the auroral region as a whole approximates thermal equilibrium. However, free electrons may experience elastic collisions with other electrons, ions, or neutral atoms and molecules, inelastic collisions which result in the excitation of ions, atoms, or molecules, collisions of the second kind with ions, atoms, or molecules in excited metastable levels, free-

free transitions in the neighborhood of nuclei with the resulting emission of radiation, or capture by an ion with the emission of radiation. Bohm and Aller (2) have considered the motions of the free electrons in the atmosphere of a planetary nebula, and conclude that the process of elastic scattering is by far the most probable. Their arguments are quite general and probably apply to conditions in the upper atmosphere, in which case the free electrons will reach a velocity distribution which is close to a Maxwellian distribution. If this is so, atoms excited by collisions with these electrons will be distributed among the various energy levels according to the Boltzmann law. It is worth while then to apply Equation (5) to the intensities of the hydrogen and helium lines in the auroral spectrum. The relative intensities of the first two members of the Balmer series will be given by,

$$\frac{H_\alpha}{H_\beta} = \frac{\tilde{\omega}_3}{\tilde{\omega}_4} \frac{e^{-\chi_3/kT}}{e^{-\chi_4/kT}} \frac{A_{32}}{A_{42}} \frac{\nu_{32}}{\nu_{42}} .$$

Putting the equation in logarithmic form and expressing the χ-values in volts,

$$\log \frac{H_\alpha}{H_\beta} = \log \frac{\tilde{\omega}_3}{\tilde{\omega}_4} + \log \frac{A_{32}}{A_{42}} + \log \frac{\nu_{32}}{\nu_{42}} + \frac{5040\ (\chi_4 - \chi_3)}{T} . \qquad (6)$$

For the hydrogen levels the $\tilde{\omega}$ values are $2n^2$. Hence $\tilde{\omega}_3 = 18$, $\tilde{\omega}_4 = 32$. Also $A_{32} = 4.39 \times 10^7$, $A_{42} = 8.37 \times 10^6$, $\nu_{32} = 4.57 \times 10^{14}$, $\nu_{42} = 6.17 \times 10^{14}$, and $(\chi_4 - \chi_3) = 0.66$ volts. Substituting these values in (6) we find T is approximately 7600° K. The above results do not indicate whether or not the hydrogen energy levels are populated according to the Boltzmann law. On the other hand, this problem may be investigated by considering the intensities of the helium lines in the auroral spectrum. Table I gives the intensities of these lines as determined by Bernard, and other relevant data.

TABLE I

λ	$E_{nn'}$	Transition	$A_{nn'}$	$\tilde{\omega}_n$	χ_n	log D
5876	6	$^3P - {}^3D$	64.7×10^6	15	23.0	23.70
4471	10	$^3P - {}^3D$	25.9×10^6	15	23.6	23.43
4026	4	$^3P - {}^3D$	12.8×10^6	15	23.9	23.16
5016	12	$^1S - {}^1P$	14.0×10^6	3	23.0	22.40
3965	6	$^1S - {}^1P$	8.13×10^6	3	23.6	22.27
4922	5	$^1P - {}^1D$	19.7×10^6	5	23.6	22.79
4388	4	$^1P - {}^1D$	8.67×10^6	5	23.9	22.49
4009	1	$^1P - {}^1D$	2.82×10^6	5	24.2	22.05

Writing Equation (5) in logarithmic form and letting $\frac{N_0}{\tilde{\omega}_0} h = C_1$, we have,

$$\log E_{nn'} = \log C_1 + \log \tilde{\omega}_n - \frac{5040\ \chi_n}{T} + \log A_{nn'} + \log \nu_{nn'}$$

Let $\tilde{\omega}_n A_{nn'} \nu_{nn'} = D$. Then,

$$\log \frac{E_{nn'}}{D} = \log C_1 - \frac{5040\ \chi_n}{T} . \qquad (7)$$

A plot of log $\frac{E_{nn'}}{D}$ against χ_n will produce a straight line if the energy levels are populated according to the Boltzmann law. Fig. 1 shows this plot for the

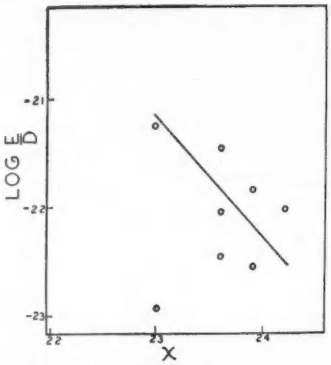

FIG. 1. *The distribution of helium atoms in a number of energy levels.*

HeI lines. It is apparent that deviations from the Boltzmann law are appreciable, and the slope of the line $\frac{5040}{T}$ simply gives an indication of the "excitation temperature" for the various energy levels. The temperature obtained from this slope is 4600° K. This method has been used by Goldberg (6) and Petrie (12) to compute the temperature of the solar chromosphere.

The results indicate that hydrogen and helium atoms are excited by particles which have velocities characteristic of a high temperature. Similar results have been obtained by Petrie (13) from a study of the intensities of a number of OII lines in the auroral spectrum. On the other hand, Vegard has found that the energy responsible for the excitation of nitrogen molecules is characteristic of a temperature of 300° K. These results show that the upper atmosphere deviates considerably from a condition of thermal equilibrium. This condition is not surprising, since it is likely that different excitation mechanisms are operating in the upper atmosphere. Certain features of the auroral spectrum are likely to result from collisions between atmospheric electrons and atoms or molecules. "Excitation temperatures" computed from the intensities of these spectral features give information on the velocities of the particles involved. On the other hand, if collisions between atmospheric particles and hydrogen or helium atoms from the sun are responsible for the appearance of hydrogen and helium lines in the auroral spectrum, then temperatures derived from these spectral features give information on the velocities of the incoming particles. Detailed studies of the intensities of all auroral spectral features are necessary, if we are to understand fully the problem of auroral excitation.

References

1. BERNARD, M. R. Compt. rend. 225 (7) : 352. 1947.
2. BOHM, D. and ALLER, L. H. Astrophys. J. 105 : 131. 1947.
3. BONGERS, I. A. Dissertation, Utrecht. 1927.
4. CILLIÉ, G. G. Monthly Notices Roy. Astron. Soc. 96 : 771. 1936.
5. GAUNT, J. A. Trans. Roy. Soc. London, A, 229 : 163. 1930.
6. GOLDBERG, L. Astrophys. J. 89 : 673. 1939.
7. HERZBERG, G. Ann. Physik, 84 : 553. 1927.
8. KRAMERS, H. A. Phil. Mag. 46 : 836. 1923.
9. MENZEL, D. H. and BAKER, J. G. Astrophys. J. 86 : 70. 1937.
10. MENZEL, D. H. and PEKERIS, C. L. Monthly Notices Roy. Astron. Soc. 96 : 77. 1935.
11. PANETH, F. A. Quart. J. Roy. Meteor. Soc. 63 : 433. 1937.
12. PETRIE, W. J. Roy. Astron. Soc. Can. 38 : 137. 1944.
13. PETRIE, W. Can. J. Research, A, 25 : 293. 1947.
14. PLASKETT, H. H. Pubs. Dominion Astrophys. Observ. Victoria, B.C. 4 : 187. 1928.
15. VEGARD, L. Geofys. Publikasjoner. Norske Videnskaps.-Akad. Oslo. 12 (14) : 1. 1940.

GAMMA RAYS FROM THE DISINTEGRATION OF BORON BY SLOW NEUTRONS[1]

By B. Rose[2]

Abstract

The slow neutron disintegration of B^{10} yields two groups of α-particles, corresponding to the production of Li^7 in either the ground state or an excited state. The γ-radiation accompanying the de-excitation of the excited nucleus was studied. Boron in the form of boron trifluoride in a proportional counter was irradiated with slow neutrons from a Ra–α–Be source. Coincidences were counted between α-particle pulses in the proportional counter and γ-ray pulses in an adjacent Geiger–Müller counter. The ratio of the α–γ coincidence rate to the α-rate gave the product of the efficiency of the Geiger-Müller counter and the number of quanta emitted per boron disintegration. The absorption coefficient of the γ-radiation in lead was measured, and, by comparison with the absorption coefficients for the γ-radiation from Cu^{64} and Au^{198}, the energy was found to be 0.48 ± 0.015 Mev. The quantum efficiency of the Geiger–Müller counter for radiation of this energy was determined by calibration with standard sources of Co^{60} and thorium active deposit. Hence the number of quanta per boron disintegration was found to be 0.90 ± 0.08, in satisfactory agreement with the value to be expected from the relative abundance of the α-particle groups from this reaction.

Introduction

The slow neutron disintegration of B^{10} yields two groups of α-particles corresponding to the formation of the product nucleus Li^7 either in the ground state, or in a state of about 0.45 Mev. excitation. Measurements by Wilson (23) in a proportional counter, by Bøggild (3) and by Gilbert (8) in a cloud chamber, show that only 7% of the disintegrations go directly to the ground state. There should therefore be a γ-ray of energy about 0.45 Mev. accompanying 93% of the disintegrations, corresponding to the de-excitation of the Li^{7*} nucleus. Soft γ-rays from this reaction have been observed by Kikuchi, Aoki and Husimi (13). Wilson (23) observed $\alpha-\gamma$ coincidences and estimated the γ-ray energy by a very rough absorption measurement to be in the neighborhood of 0.5 Mev.

The object of the present investigation was to test the simple disintegration scheme suggested by the above results, and shown in Fig. 1, by measurement of the intensity and energy of the γ-ray.

Outline of Method

Boron, in the form of gaseous boron trifluoride contained in a proportional counter, was irradiated with slow neutrons from a 1.2 gm. Ra–α–Be source. The γ-radiation accompanying the neutron-induced disintegration of the

[1] *Manuscript received in original form June 17, 1948, and, as revised, August 31, 1948. Contribution from the Nuclear Physics Branch, Chalk River Laboratory, Atomic Energy Research Division of the National Research Council of Canada. Issued as N.R.C. No. 1835.*

[2] *Member of United Kingdom Staff; now at the Atomic Energy Research Establishment, Harwell, England.*

boron was detected in an adjacent aluminum-walled Geiger–Müller counter, of which the net efficiency for the energy of the radiation in question was determined by subsidiary experiments.

Let N disintegrations per minute be produced in the proportional counter,

ϵ_α be the efficiency of the proportional counter,

ϵ_{Li} be the efficiency of the Geiger–Müller counter for the Li^{7*} γ-ray,

λ be the number of quanta produced per disintegration,

and

N_α and $N_{\alpha\gamma}$ be respectively the α- and genuine coincidence counting rates. Then $N_\alpha = N\epsilon_\alpha$; $N_{\alpha\gamma} = N\epsilon_\alpha\lambda\epsilon_{Li}$, so that $N_{\alpha\gamma}/N_\alpha = \lambda\epsilon_{Li}$.

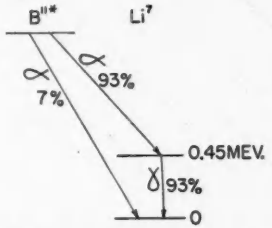

FIG. 1. *Disintegration scheme for the reaction* $B^{10}(n,\alpha)Li^7$.

The net efficiency of the Geiger–Müller counter was determined for the γ-radiation from Co^{60} by the use of a standard Co^{60} solution, and for the mixed γ-radiation from thorium active deposit by means of a source calibrated in terms of its α-particle activity.

The γ-ray energy was determined by measuring its absorption coefficient in lead, and comparing it with those of the γ-radiations from Cu^{64}, which is almost pure annihilation radiation (6), and from Au^{198}, which is predominantly of energy 0.408 Mev. (5, 16). Using the curves published by Bradt *et al.* (4), showing the variation of absolute efficiency of a Geiger–Müller counter with quantum energy, the net efficiency ϵ_{Li} may be determined for the energy of the γ-ray from the boron disintegration, and hence λ, the number of quanta per disintegration.

Measurement of $\lambda\epsilon_{Li}$

The proportional counter used was made of aluminum, of inside diameter ¾ in., active volume 2½ in. long, and of ⅛ in. wall thickness. It was filled with boron trifluoride to a pressure of 12 cm. of mercury. The Geiger–Müller counter was made of aluminum, with glass ends waxed in, the dimensions of the cathode being length 2 in., inside diameter 1 in. and wall thickness 0.9 mm. The arrangement of source and counters is shown in Fig. 2. The neutron source F was set in a bismuth block D, which was surrounded by eight inches of paraffin, E. The counters, A and B, were mounted in a light aluminum frame with their axes parallel and 36 mm. apart, and installed in a

bismuth block *C*, vertically above *F* and *D*. The function of the block *D* was to shield the Geiger–Müller counter *A* from the γ-radiation direct from the source *F*, and of the block *C* to shield it from γ-rays of neutron capture in the

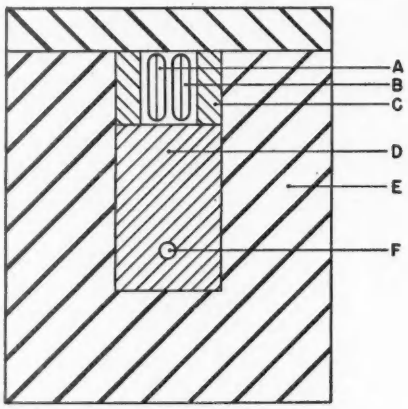

FIG. 2. *Experimental arrangement. A, B, counters; C, D, bismuth; E, paraffin; F, neutron source.*

paraffin. Bismuth was used in preference to lead as it is almost as efficient as lead for γ-ray shielding, and has a smaller slow neutron capture cross-section. The block *D* provided 11 in. of shielding, the block *C* 2.4 in. and together they reduced the γ-counting rate to approximately the same rate as that due to the activation of the aluminum cathode by the slow neutron flux (of the order of 1500 and 1000 counts per minute respectively). The latter rate was measured by removing the counter from the neutron flux and following the decay of the counting rate. The rate in the proportional counter was 2500 counts per minute.

The pulses from both counters, after amplification and discrimination, were fed into a Rossi coincidence circuit, and the ratio of the α-particle rate to the genuine coincidence rate was determined for coincidence resolving times of 0.25, 0.70 and 1.51 μsec. to ensure that no coincidences were lost. As the random coincidence rate at the longest resolving time was almost half the true coincidence rate, and the total coincidence rate was only about 0.7 count per minute, long counting periods were necessary. It was therefore decided to keep continuous check on the coincidence resolving time in order to be confident of the accuracy of the random coincidence rate. In alternate half hours, regularly spaced pulses from a pulse generator were fed into the Rossi circuit at 20,000 pulses per minute. The generator pulses and the coincidences between the generator pulses and those from the Geiger–Müller counter were counted, and from these figures and the measured γ-ray counting rate, the resolving time of the circuit was determined for each run. The ratio $N_{\alpha\gamma}/N_{\alpha}$

obtained was corrected for counting losses in the Geiger–Müller circuit, due to a 300 μsec. dead time in the discriminator. This long dead time was used throughout the experiment in order to minimize effects due to multiple pulsing in the Geiger–Müller counter. The dead time of the counter alone was 180 μsec. The circuit dead time was measured both by a counting loss determination and by direct measurement on an oscilloscope of known writing speed.

It should be pointed out that there could arise coincidences due to a γ-ray and a neutron, emitted simultaneously from the source, being registered by the two counters. However, the cross section for the B^{10} $(n,\alpha)Li^7$ disintegration is very small except for slow neutrons. The slowing down process takes several microseconds in the great majority of cases. Hence the number of coincidences from this effect is negligibly small, owing to the coincidence resolving times used.

The values obtained are shown in Table I, the errors shown, as elsewhere throughout this paper being the standard errors. There is no significant difference in the values of $N_{\alpha\gamma}/N_\alpha$ obtained for the three resolving times. Therefore the mean of those values in Column 3 was taken, giving $(1.43 \pm 0.04)10^{-4}$.

In order to use Bradt and collaborators' curves, as mentioned earlier, it was necessary to correct this quantity for

(*a*) Back scattering into the Geiger–Müller counter from the block,

(*b*) Absorption in the wall of the proportional counter,

and

(*c*) Absorption in the wall of the Geiger–Müller counter.

These corrections were determined from subsidiary experiments using annihilation radiation from Cu^{64}, which was shown later to have an energy very similar to that of the γ-ray from Li^{7*}.

TABLE I

$N_{\alpha\gamma}/N_\alpha$ AS A FUNCTION OF COINCIDENCE RESOLVING TIME

Resolving time, μsec.	$N_{\alpha\gamma}/N_\alpha$, × 10^4	Mean value
0.23 (± 5%)	1.42 ± 0.11	1.38 ± 0.07
0.27 (± 6%)	1.34 ± 0.10	
0.68	1.25 ± 0.12	
0.71 (± 3%)	1.53 ± 0.12	1.40 ± 0.07
0.71	1.43 ± 0.12	
1.54	1.64 ± 0.15	
1.52	1.36 ± 0.14	
1.46 (± 2½%)	1.65 ± 0.16	1.52 ± 0.07
1.50	1.50 ± 0.15	
1.54	1.44 ± 0.15	

The Cu^{64} was prepared by irradiating electrolytic copper in the pile. After irradiation it was dissolved in nitric acid, the excess acid being neutralized with ammonia, and allowed to stand for two hours before use to remove the five minute activity due to Cu^{66}. The solution was then diluted to a volume equal to that of the active volume of the proportional counter. A dummy counter, made from a piece of aluminum tube of the same dimensions as the proportional counter, and coated inside with glyptal, was then substituted for the proportional counter and filled with active copper solution. The γ-ray counting rate was measured with the counter and dummy in the block *C*, closely surrounded by bismuth as in the coincidence experiment, and also measured with the counter and dummy remote from scattering material. After correction for source decay and the different background rates inside and outside the block, the counting rate was found to have increased by $1\frac{1}{2}\%$, owing to back-scattering.

To determine the absorption in the wall of the proportional counter, a half-cylinder of aluminum $\frac{1}{8}$ in. thick and closely fitting the wall of the dummy, was interposed between the Geiger–Müller counter and the dummy containing active copper solution. The reduction in the counting rate observed, after correction for background and source decay, showed an absorption of 5.8% in the wall of the proportional counter.

The absorption in the wall of the Geiger–Müller counter, which in this energy range is due entirely to the Compton process, is small since the wall is thin. The Compton absorption process will result in electrons of maximum energy 0.33 Mev. from a quantum of energy 0.5 Mev. Therefore a recoil electron produced in the counter wall at a distance from the interior of the counter greater than 0.1 gm. per sq. cm., the range of a 0.33 Mev. electron in aluminum (18), cannot produce a discharge in the counter. The total absorption in the counter wall cannot then be less than that due to the Compton absorption cross section alone in the portion of the wall that is more than 0.1 gm. per sq. cm. distant from the interior of the counter. The absorption cross section per electron for a 0.5 Mev. γ-ray is 10^{-25} cm.^{2}, and the thickness of that portion of the wall concerned 0.14 gm. per sq. cm. From these figures, we see that the absorption in the counter wall must exceed $\frac{1}{2}\%$.

An upper limit for the absorption in the counter wall may be made by assuming that it occurs at the same rate as in the wall of the proportional counter. The absorption in the wall of the proportional counter is due to the degradation of the radiation and to the production of recoil electrons. Since we have conditions of 'bad geometry', scattering into and out of the counter may be expected to compensate each other, so that the production of degraded radiation should be at the same rate in the two walls. However, the production of recoil electrons will be less effective in the wall of the Geiger–Müller counter than in the wall of the proportional counter, as argued in the previous paragraph. In this way we obtain $1\frac{1}{2}\%$ as an upper limit for the absorption in the wall of the Geiger–Müller counter.

We shall therefore take 1%, the mean of these two limits, as the best estimate of the absorption in the wall of the Geiger–Müller counter.

Hence the total correction to be made to the value of $N_{\alpha\gamma}/N_\alpha$ is an increase of 5%, giving

$$\lambda\epsilon_{Li} = (1.50 \pm 0.05)10^{-4}.$$

Calibration of the Geiger-Müller Counter

The thickness of the wall of the Geiger–Müller counter was considerably less than the maximum range of the recoil electrons from Co^{60} γ-radiation (1.16 and 1.32 Mev. γ-rays in cascade (11)) and from the hard component (2.62 Mev.) of the thorium radiation. The wall thickness was therefore increased, by loading it with a close fitting split brass cylinder, to a mass 1.4 gm. per sq. cm., which is greater than the range of the recoil electron of maximum energy from the hardest component. The same loading was used for both calibration measurements.

The Co^{60} was obtained in the form of a solution of which the specific activity had been determined by β–γ coincidence methods by Dr. W. B. Mann in this laboratory, by the National Bureau of Standards in Washington, and by the Oak Ridge standardization laboratory, with concordant results. A known volume of this solution was diluted to a volume equal to that of the active volume of the proportional counter, introduced into the dummy counter, and the γ-ray counting rate determined. After correction for source decay, background, and counting losses, the counts per γ-ray emitted from the dummy counter was found to be $(6.16 \pm 0.12)10^{-4}$.

Subsidiary experiments showed that the γ-ray sensitivity was almost independent of the total volume over a 3 cc. range of solution introduced into the dummy counter (and hence of the precise assumptions about the active volume of the proportional counter). The sensitivity also varied very slowly with movements of the dummy counter along its axis, a movement of 1 cm. in this direction producing less than 1% difference in counting rate.

To determine the net efficiency of the counter for the γ-rays of Co^{60} and the geometry concerned, the counts per γ-ray must be corrected for self-absorption in the cobalt solution, absorption in the wall of the dummy counter, and absorption in the wall of the Geiger–Müller counter.

In order to measure the self-absorption, a linear source was prepared by filling a thin-walled glass tube of 2 mm. inside diameter with Co^{60} solution, the length of the source being equal to the length of the active volume of the counter. The counting rates were determined for a position of the linear source in the dummy counter, and then immediately redetermined with the dummy counter filled with water. In this way the change of counting rate due to the presence of the water was determined for each element of volume of the dummy counter. The total self-absorption due to the water, determined by numerical integration, was 3 ± 1%.

The absorption in the wall of the dummy counter was determined as before, giving 4.5 ± 1%.

The absorption in the wall of the Geiger–Müller counter was determined by inserting an additional half-cylinder of brass of mass 1.06 gm. per sq. cm. between the dummy and the Geiger–Müller counter, closely fitting the latter. This reduced the counting rate by $5.5 \pm 1\%$. We may therefore overestimate the absorption in the wall of the Geiger–Müller counter by assuming that it is the same per millimeter thickness as in the additional absorber, giving an absorption of 7%. We may underestimate it by assuming that it is due only to that thickness of the wall which exceeds the range of the fastest recoil electron. The latter would have an energy of 1.1 Mev. and therefore a range of 0.45 gm. per sq. cm. (18). The underestimate of the absorption is 5%. The mean of these two values was taken as the best value for the absorption in the counter wall, namely $6 \pm 1\%$.

The total value of the corrections to be applied is therefore about 14%. Hence the net efficiency of the Geiger–Müller counter for a γ-ray of energy 1.24 Mev. is $(7.02 \pm 0.21)10^{-4}$.

The difference between the efficiency of an aluminum and a brass counter was neglected here, since the brass loading increased the efficiency by a few per cent only in this case. It had to be considered, however, in the calibration with the thorium radiation, where a substantial portion of the efficiency was due to the brass.

In this method of determining the net efficiency of the Geiger–Müller counter for a volume source occupying the same position relative to it as did the proportional counter in the coincidence experiment, it has been assumed implicitly that the neutron-induced disintegration rate has its center of gravity at the geometric center of the proportional counter. This was investigated by measuring the counting rate in the proportional counter as a function of its position. The magnitude of the variation was such that the effective center of gravity of the disintegrations was displaced only a few millimeters from the geometric center. Displacements of the dummy counter by this amount were shown earlier to have a negligibly small effect on the counting rate in the Geiger–Müller counter, so that the assumption made is justified.

In order to calibrate the counter with a point source of thorium radiation, it was necessary to determine the effective center of gravity of the proportional counter relative to the Geiger–Müller counter. This was determined by the use of a point source of Co^{60} of which the strength relative to a standard Co^{60} solution was measured by γ-ray comparison. The counting rate was then measured as a function of the distance of the point source from the axis of the Geiger–Müller counter, and from the known strength of the source, that point on the equatorial plane determined at which the net efficiency of the Geiger–Müller counter was equal to that found by the calibration with the volume source. This was found to be at a distance of 37.8 ± 0.5 mm. from the axis of the Geiger–Müller counter, with the net efficiency changing by 6% per mm. at this point.

This location for the center of gravity was in reasonable agreement with a determination made from a point by point exploration of the counting rate as a function of the position of the point source for various distances from the Geiger–Müller counter.

The thorium source was deposited on a thin aluminum foil, and after being allowed to decay for two hours to establish transient equilibrium, the α-particle activity was measured by counting α-particles from both sides of the foil simultaneously. The foil was then stuck with Scotch tape to a small Lucite holder and mounted in the frame at a distance of 36.7 mm. from the axis of the Geiger–Müller counter. The γ-ray counting rate was measured, and corrected for background, counting losses, and source decay to determine the γ-ray counting rate per α-particle emitted. This measurement was repeated with another source, the mean of the two values being $(6.97 \pm 0.14)10^{-4}$. This figure was then corrected for the slight displacement of the thorium source from the experimentally determined center of gravity of the proportional counter. The displacement was 1.1 ± 0.5 mm., so that the corresponding correction was a reduction by $6.5 \pm 3\%$.

It was also necessary to correct for the absorption in the wall of the Geiger–Müller counter. The weighted mean energy per γ-ray from a thorium active deposit source is 1.03 Mev., computed from the results of Johansson (12) and Latyschev and Kulchitsky (14). It was therefore assumed that the absorption in the counter wall would be the same as for the 1.24 Mev. γ-rays from Co^{60}, namely $6 \pm 1\%$, since the Compton cross section does not differ by more than 10% for these two energies. The net correction to be made was then $-0.5 \pm 3\%$.

Hence the mean efficiency of the counter for the thorium radiation was $(6.93 \pm 0.35)10^{-4}$ per α-particle. The experimentally determined ratio of the efficiencies for thorium and Co radiations was therefore

$$\epsilon_{Th}/\epsilon_{Co} = \frac{6.93 \pm 0.35}{7.02 \pm 0.21} = 0.99 \pm 0.06.$$

The ratio of the efficiencies was also computed from Bradt's curves for the variation of counter efficiency with quantum energy. The efficiency per α-particle was calculated by weighting the intensities of the various components by their relative efficiencies, for the softer components taking the efficiency for an aluminum cathode, for the radiations at 1.60 Mev. and 1.80 Mev. taking the mean of the efficiencies for aluminum and brass, and for the 2.2 Mev. and 2.62 Mev. radiations, taking the efficiency for a brass cathode. The efficiency for Co^{60} radiation was determined similarly, using the curve for an aluminum cathode. This gave the ratio of efficiencies

$$\epsilon_{Th}/\epsilon_{Co} = 1.07 \pm 0.05 \text{ (computed)}.$$

This agrees with the experimental value within the combined errors.

Absorption Coefficient in Lead of the Li^{7*} γ-Radiation

The energy of the Li^{7*} γ-ray was determined by comparing its absorption coefficient with those of the 0.511 Mev. annihilation radiation and the 0.408 Mev. γ-radiation of gold. The absorption coefficient was determined by measuring the α–γ coincidence rate as a function of the thickness of lead between the counters. Another proportional counter was used with twice the active volume of the one previously in use and filled with 30 cm. of boron trifluoride and 1.5 cm. of argon. A larger Geiger–Müller counter was also used, with a lead cathode. The counting rates were then approximately 10,000 counts per minute in each counter. The counters were installed in a different mounting which increased their separation to permit the insertion between them of $1\frac{1}{2}$ cm. of lead, in the form of sheets of mean thickness 0.177 cm.

As the coincidence resolving time measured in the earlier part of the experiment had remained constant within statistical error, the continuous checking method was abandoned, but the resolving time, nominally $\frac{1}{4}$ μsec. was checked daily. Owing to the increased counting rates, it was possible to take several runs during a day with a small number of absorbers, the runs with a large number, when the genuine coincidence rate was equal to or less than the random rate, being carried out overnight. This had the advantage of avoiding any systematic drift of sensitivity of the counters producing a change in the measured absorption curve. The genuine coincidence rate varied from 4 to 0.25 counts per minute, and the counting periods from 40 min. to 16 hr. The rates obtained were corrected for counting losses in the Geiger–Müller circuit. The results obtained are shown in Table II. The errors shown are the standard errors of the number of counts. The average value of all determinations of the coincidence resolving time was used to determine the random coincidences.

TABLE II

$N_{\alpha\gamma}/N_\alpha$ AS A FUNCTION OF THICKNESS OF LEAD BETWEEN THE COUNTERS

Number of absorbers	Genuine coincidences	Random coincidences	$N_{\alpha\gamma}/N_\alpha$, $\times 10^4$	Number of runs
0	1843	332	4.12 ± 0.11	5
1	508	119	2.88 ± 0.15	3
2	1211	379	2.14 ± 0.08	4
3	530	266	1.31 ± 0.08	2
4	856	578	0.96 ± 0.05	1
5	666	601	0.71 ± 0.05	1
6	1039	1231	0.53 ± 0.04	2
8	241	644	0.23 ± 0.04	1

A least squares fit to an exponential curve gave the absorption coefficient 1.98 ± 0.11 cm.$^{-1}$, the error in this case being estimated by inspection.

Absorption Coefficient for 0.511 Mev. and 0.408 Mev. Radiation

Another dummy counter was substituted for the proportional counter and the pair of counters was installed in a lead block, so that the geometry was the same as in the absorption experiment. The dummy counter was then filled with a solution containing Cu^{64} prepared as before, and the absorption coefficient determined in the usual manner, using the same absorbers as in the coincidence absorption experiment, giving an absorption coefficient $\mu = 1.70$ cm.$^{-1}$

The absorption coefficient for the γ-radiation from Au^{198} was determined in the same way, giving $\mu = 2.55$ cm.$^{-1}$ Au^{198} was prepared by irradiating gold in the pile. The active gold was dissolved in aqua regia, the excess acid neutralized with ammonia, and the precipitated hydroxide redissolved in bromine water.

The γ-radiation from Cu^{64} consists of almost pure annihilation radiation, the admixture being a radiation of energy 1.35 Mev., with an intensity of one γ-ray per 40 ± 5 positrons (6). A computation based on the theoretical values of the good geometry absorption coefficients was made for this mixed radiation over the range of absorption used in these measurements, and showed that the mean absorption coefficient would be decreased by 0.03 cm.$^{-1}$ from the value for pure annihilation radiation. Since the measured absorption coefficients agreed closely with the theoretical values, this correction was applied directly, to give 1.73 cm.$^{-1}$ for the absorption coefficient for annihilation radiation.

The γ-radiation from Au^{198} consists principally of a line of energy 0.408 Mev. (5, 16), with possibly a weak admixture of softer components at 0.208 and 0.157 (16) of intensity less than 18% of that of the harder γ-ray. Computation based on the theoretical absorption coefficients showed that the effect of these components, even if present to the maximum intensity suggested, would be negligible after the first or second absorber, so that the measured absorption coefficient of 2.55 cm.$^{-1}$ needed no correction.

The absorption curves obtained are shown in Fig. 3. The statistical errors in the points on the Au^{198} and Cu^{64} curves are very small. The errors remaining, due to counter fluctuations, are difficult to estimate and are not shown. The curves for Au^{198} and Cu^{64} are each the mean of two separate determinations, which had no significant differences between them.

Energy of Li^{7*} γ-Ray

From the measured absorption coefficients, and the assumption of a linear variation of absorption coefficient with energy, the energy of the Li^{7*} γ-ray was found to be 0.48 ± 0.015 Mev.†

† *Since this paper was written DuMond, Lind, and Watson (Phys. Rev. 73, 1392 (1948)) have published the very precise value 0.4112 ± 0.0001 Mev. for the energy of the γ-ray from Au^{198}. Although this value supersedes 0.408 Mev. assumed in the present paper, the derived energy of the Li^{7*} γ-ray given to two significant figures needs no alteration.*

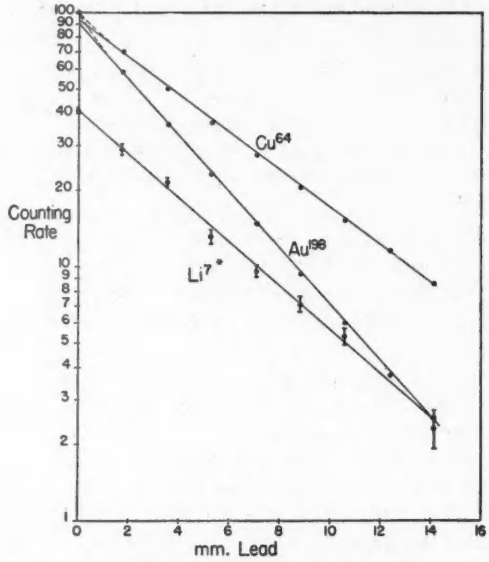

FIG. 3. *Absorption curves of radiations from Li^{7*}, Au^{198}, and Cu^{64} with the same geometry.*

Number of Quanta per Boron Disintegration

From the curves given by Bradt and collaborators (4), we obtain the following efficiency ratios, in the manner described earlier.

$$\epsilon_{Li}/\epsilon_{Co} = 0.243; \quad \epsilon_{Li}/\epsilon_{Th} = 0.226.$$

These ratios will be subject to a 5% standard error due to the 3% error in the γ-ray energy and an estimated 5% from the errors in Bradt's curves. We thus obtain for the efficiency of the counter for the γ-rays from Li^{7*} the values 1.71×10^{-4} and 1.57×10^{-4} as determined from the calibrations with Co^{60} and with thorium active deposit respectively. Weighting these results respectively by three and one, corresponding to the errors in the determination of ϵ_{Co} and ϵ_{Th}, we obtain for the weighted mean

$$\epsilon_{Li} = (1.67 \pm 0.13)10^{-4}.$$

From the previously determined value of $\lambda\epsilon_{Li}$ we obtain the value $\lambda = 0.90 \pm 0.08$.

Discussion

A summary of the work carried out before 1940 relating to the excited state of Li^7 is contained in Graves' paper (10), and a later summary of work up to 1947 is given by Siegbahn (20, 21). Later work is included in Table III. There remain two distinct groups of values, centered around 0.485 Mev. and 0.455 Mev. respectively. There is no clear evidence for two different energy

levels being concerned, for in each case when two different reactions have been studied in the same instrument, the determinations have been in satisfactory agreement with each other. Siegbahn (20, 21) obtained 0.453 Mev. and 0.462 Mev. by measurement in a β-spectrometer of the γ-rays from the decay of Be^7, and from the inelastic scattering of α-particles by lithium. Lauritsen and collaborators' results (15) are shown in Table III. The present work is in better agreement with the high than the low value.

The value of λ determined here is in satisfactory agreement with the value to be expected from the disintegration scheme shown in Fig. 1. The energy available to the α-particles in this reaction is greater than the barrier height for the lithium nucleus, and therefore more disintegrations would be expected to pass to the ground state than to the excited state of Li^7, as is in fact observed in another reaction involving the same intermediate nucleus and end products, namely $Be^9(d,\alpha)Li^7$ (10) and in the similar reaction $Li^6(d,p)Li^7$ which yields two proton groups (19).

TABLE III

Author	Reaction	Measurement	Method	Energy of Li^{7*}, Mev.
Wilson (23)	$B^{10}(n,\alpha)$	Total disintegration energy	Proportional counter	0.42 ± 0.05
Bøggild (3)	$B^{10}(n,\alpha)$	Total disintegration range	Cloud chamber	0.42
Lauritsen *et al.* (15)	$Li^7(p,p')Li^{7*}$	γ-Energy	β-Spectrometer	0.48 ± 0.010
Lauritsen *et al.* (15)	$Be^9(d,\alpha)Li^{7*}$	γ-Energy	β-Spectrometer	0.48 ± 0.010
Strait *et al.* (22)	$Be^9(d,\alpha)$	α-Groups	Annular magnet	0.481†
Elliott and Bell (7)	$B^{10}(n,\alpha)Li^{7*}$	γ-Energy	β-Spectrometer	0.479 ± 0.005††
Present work	$B^{10}(n,\alpha)Li^{7*}$	γ-Energy	Absorption coefficient	0.48 ± 0.015

† *The value given by Strait et al. in the reference was changed to the value quoted here in the presentation of the paper before the American Physical Society.*

†† *This measurement was made after the present work had been completed.*

It is normally assumed that both the ground and first excited state of Li^7 have odd parity, and angular momentum 3/2 and ½ respectively (9, 17). B^{10} has unit angular momentum (1) and is assumed to have even parity since it has an even number of particles (2). For this condition, the possible combinations of orbital angular momenta and spins are shown in the first part of Table IV. It will be clear that neither of these possible modes of disintegration can favor the production of the excited state of Li^7.

If, however, B^{10} has odd parity, the bias in favor of the excited state is readily explained. Remembering that the neutron and α-particle have even parity and that the reaction is produced by slow neutrons, it is necessary that the parity of the relative motion of the α-particle and of the residual nucleus be even. The possible combinations of angular momenta are given in the lower half of Table IV. It is clear that the only possible disintegration

that will favor the excited state is the last one, viz., that with zero relative angular momentum. The disintegration leading to the ground state will then have two units of orbital angular momentum, and in this case the penetrability is appreciably decreased.

TABLE IV

Parity of B^{10}	Angular momentum of B^{11*}	Relative angular momentum of α and Li	
		Ground state	Excited state
Even	3/2	1, 3	1
Even	½	1	1
Odd	3/2	0, 2	2
Odd	½	2	0

Acknowledgments

The author is indebted to Dr. B. B. Kinsey for suggesting the problem and for many helpful discussions, and to Mr. W. H. Walker for the construction of the proportional counters.

References

1. BETHE, H. A. Elementary nuclear theory. John Wiley & Sons, Inc., New York. 1947.
2. BETHE, H. A. Revs. Modern Phys. 9 : 69. 1937.
3. BØGGILD, T. K. Kgl. Danske Videnskab. Selskab., Math.-fys. Medd. 23, No. 4. 1945.
4. BRADT, H., GUGELOT, P. C., HUBER, O., MEDICUS, H., PREISWERK, P., and SCHERRER, P. Helv. Phys. Acta, 19 : 77. 1946.
5. CORK, J. M. Phys. Rev. 72 : 581. 1947.
6. DEUTSCH, M. Phys. Rev. 72 : 729. 1947.
7. ELLIOTT, L. G. and BELL, R. E. To be published.
8. GILBERT, C. W. See note at end of reference 23.
9. GOLDHABER, M. Proc. Cambridge Phil. Soc. 30 : 561. 1934.
10. GRAVES, E. R. Phys. Rev. 57 : 855. 1940.
11. JENSEN, E. N., LASLETT, L. J., and PRATT, W. W. Phys. Rev. 73 : 529. 1948.
12. JOHANSSON, A. Arkiv. Mat. Astron. Fysik, A, 34, No. 9. 1947.
13. KIKUCHI, S., AOKI, H., and HUSIMI, K. Nature, 137 : 745. 1936.
14. LATYSCHEV, G. D. and KULCHITSKY, L. A. J. Phys. U.S.S.R. 4 : 515. 1941.
15. LAURITSEN, T., FOWLER, W. A., LAURITSEN, C. C., and RASMUSSEN, V. K. Phys. Rev. 73 : 636. 1948.
16. LEVY, P. W. and GREULING, E. Phys. Rev. 73 : 83. 1948.
17. LIVINGSTON, M. S. and BETHE, H. A. Revs. Modern Phys. 9 : 245. 1937.
18. RASETTI, F. Elements of nuclear physics. Blackie & Son, Ltd., London & Glasgow. 1947.
19. RUMBAUGH, L. H., ROBERTS, R. B., and HAFSTAD, L. R. Phys. Rev. 54 : 657. 1938.
20. SIEGBAHN, K. Arkiv. Mat. Astron. Fysik, B, 34, No. 6. 1946.
21. SIEGBAHN, K. and SLÄTIS, H. Arkiv. Mat. Astron. Fysik, A, 34, No. 15. 1947.
22. STRAIT, E. N., STERGIOPOULOS, C. G., SPERDUTO, A., and BUECHNER, W. W. Bull. Am. Phys. Soc. 23, No. 3 : J6. 1948.
23. WILSON, R. S. Proc. Roy. Soc. London, A, 177 : 382. 1940-41.

SEARCH FOR A 3.20 MEV. γ-RAY IN THE DISINTEGRATION OF THORIUM C'' [1]

By R. E. Bell and L. G. Elliott

Abstract

In about 70% of the disintegrations, thorium C'' transforms to the ground state of thorium D by the emission of a β-ray and two successive γ-rays of energy 0.58 and 2.62 Mev. A search has been made for a γ-ray of energy 3.20 Mev. which would be emitted if a single radiative transition occurred. Using a source of radiothorium in equilibrium with its decay products, the secondary electrons ejected by the γ-rays from thin radiators of lead and uranium were analyzed in a magnetic lens spectrometer. No photoelectrons ejected by a 3.20 Mev. γ-ray were observed. If the γ-ray occurs its intensity is less than 0.2% of the intensity of the γ-ray at 2.62 Mev. This result is discussed in the light of the proposed disintegration schemes of thorium C''.

Introduction

Disintegration schemes have been proposed for the transition thorium C'' to thorium D by Ellis (8), Oppenheimer (13), and Arnoult (3). The last two of these are the most recent, and they agree well in their main features. The scheme suggested by Oppenheimer is shown in Fig. 1. According to this

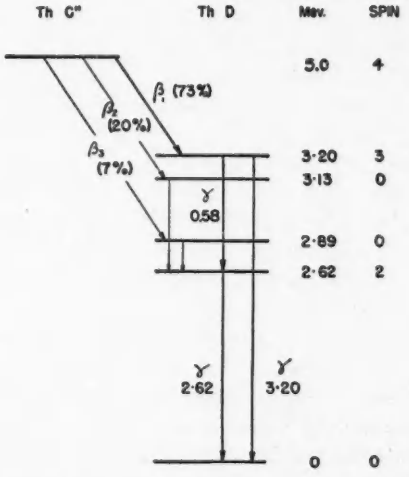

FIG. 1. *The disintegration scheme of thorium C'' according to Oppenheimer (13).*

scheme, 73% of the β-disintegrations of thorium C'' take place to an excited state of thorium D having an excitation energy of 3.20 Mev. De-excitation

[1] *Manuscript received June 3, 1948.*

Contribution from the Nuclear Physics Branch, Chalk River Laboratory, Division of Atomic Energy Research of the National Research Council of Canada. Issued as N.R.C. No. 1831. This paper was read on May 28, 1947 at the Quebec meeting of the Royal Society of Canada.

of this state is supposed to occur mainly by the emission of two successive γ-rays of energies 0.58 and 2.62 Mev. respectively. The direct 3.20 Mev. transition to the ground state occurs, according to this scheme, in some fraction of the cases. Ellis (9) has commented on the importance of knowing the intensity of the 3.20 Mev. γ-ray in assigning nuclear spins in this disintegration scheme. The present paper reports a search for a 3.20 Mev. γ-ray, and gives an upper limit for its intensity which is well below the values previously reported.

Previous Work

The first suggestion of the existence of a 3.20 Mev. γ-ray from thorium C″ was made by Chadwick, Blackett, and Occhialini (4), who studied the positron-electron pairs produced in lead in a cloud chamber. They noticed a few pairs whose total energy seemed too great to be accounted for by the 2.62 Mev. γ-ray. Alichanow, Alichanian, and Kosodaev (1) studied the secondary electron spectrum produced in lead in a 180°-focusing β-ray spectrometer, and found photoelectrons which they ascribed to a γ-ray of energy 3.20 Mev. The intensity is described only as "small". A method similar to that of Chadwick *et al.* has been used by Zuber (16) and Simons and Zuber (14), who estimate the intensity of the 3.20 Mev. γ-ray as $12 \pm 6\%$ of that of the 2.62 Mev. γ-ray. Ellis (9) and Stetter and Jentschke (15) have attempted to detect the 3.20 Mev. γ-ray by observing the photodisintegration of the deuteron with a pulse ionization chamber and linear amplifier. The intensities quoted are 2 to 3% and 0.8% respectively. In all the work mentioned here the statistical accuracy has been very low, with the result that the quoted intensities vary by a factor of 15.

A 3.20 Mev. transition taking place by internal pair production has been observed by Alichanow and Dzelepow (2), who studied the resulting positrons in a 180°-focusing β-ray spectrometer. This result, however, does not imply that 3.20 Mev. γ-ray quanta are being emitted, and in fact Latyschev and Kulchitsky (12) failed to detect Compton recoil electrons from any 3.20 Mev. γ-rays from a source of radiothorium in equilibrium with its products.

It is worth noting that the two quoted investigations which employed β-ray spectrometers (1, 12) did not verify the relatively large intensities found by the other methods. Neither investigation, however, was directly concerned with the question of the existence of the 3.20 Mev. γ-ray, and no quantitative estimate of intensity was given in either case.

Experimental Method

In the present study a search was made for γ-rays in the energy region of 3.20 Mev. from sources of radiothorium in equilibrium with its products. The secondary electrons ejected from thin radiators of lead and uranium were studied using a thin magnetic lens β-ray spectrometer (6). The radioactive source is placed at one end of an evacuated cylinder about one meter in length

(Fig. 2), and a thin-window Geiger counter at the other end records the β-particles which have passed through the baffle system under the action of the focusing coil. The geometry of the instrument is kept fixed and the coil

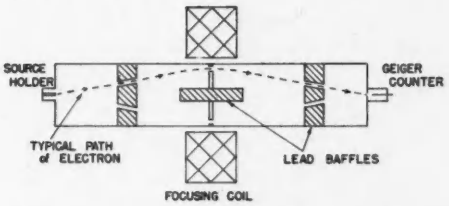

FIG. 2. *Schematic diagram of the magnetic lens β-ray spectrometer.*

current is varied to focus electrons of different momenta on the counter. Since no iron is used in the system, the current in the coil is exactly proportional to the momentum of the focused electrons.

The source, shown in Fig. 3, is covered with sufficient material of low atomic number (aluminum) to stop all the primary β-rays, and only the secondary electrons produced by γ-rays are observed. When no radiator of high atomic

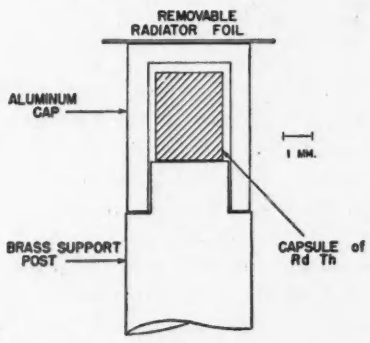

FIG. 3. *Diagram of the radiothorium source arrangement in the spectrometer.*

number is present on the source, the secondary electron spectrum consists almost entirely of Compton recoil electrons, for γ-ray energies of the order of magnitude considered here. When a thin radiator of high atomic number is placed over the source, there appears in addition to the Compton electron background a series of lines due to photoelectric conversion of the γ-rays. A typical pair of curves with and without the high atomic number radiator is shown in Fig. 4. Taking account of the fact that a particular γ-ray may be converted in the K, L, etc., shells of the atoms of the radiator, the difference

between the two curves is practically a line spectrum of the γ-rays from the source. It will be seen from Fig. 4 that this method is very sensitive to weak γ-rays of high energy because of the low counting background existing in that region.

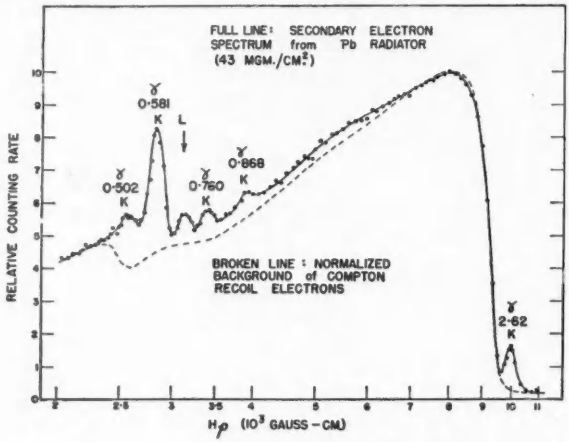
FULL LINE: SECONDARY ELECTRON SPECTRUM from Pb RADIATOR (43 MGM./CM.²)
γ 0·581 K L
γ 0·502 K
γ 0·760 K
γ 0·868 K
BROKEN LINE: NORMALIZED BACKGROUND of COMPTON RECOIL ELECTRONS
γ 2·62 K
RELATIVE COUNTING RATE
Hρ (10³ GAUSS – CM)

FIG. 4. *A typical pair of curves with and without the Pb radiator (43 mgm. per cm.²), showing the momentum distribution of the secondary electrons ejected by the γ-rays from the source of radiothorium in equilibrium with its decay products.*

In order to obtain the highest ratio of photoelectric line to Compton electron background, measurements were made on the 2.62 Mev. γ-ray using a series of radiators of different thicknesses. In the course of these measurements the first two runs were made with lead radiators ($Z = 82$) and the last two with uranium radiators ($Z = 92$). Since the photoelectric cross section varies approximately as the 4.5 power of Z (5), the change from lead to uranium gives roughly a 60% increase in the number of photoelectrons for a given radiator thickness. The results of these runs are shown in Fig. 5, the thickness of radiator being given above each curve. (The change from 43 mgm. per cm.² lead to 86 mgm. per cm.² lead was accompanied by improvements in the spectrometer alignment, accounting for the large improvement in line height in the case of the 86 mgm. per cm.² radiator.)

The uranium radiator of 82 mgm. per cm.² thickness was chosen as that giving the best visibility to the photoelectron line, having regard to the height of the line and its separation from the Compton background. The 150 mgm. per cm.² radiator gives a somewhat higher line, but the effect of electron scattering in the radiator prevents the line from reaching the height otherwise to be expected, and the scattered electrons, slightly degraded in energy, cause the line to be less well separated from the Compton background.

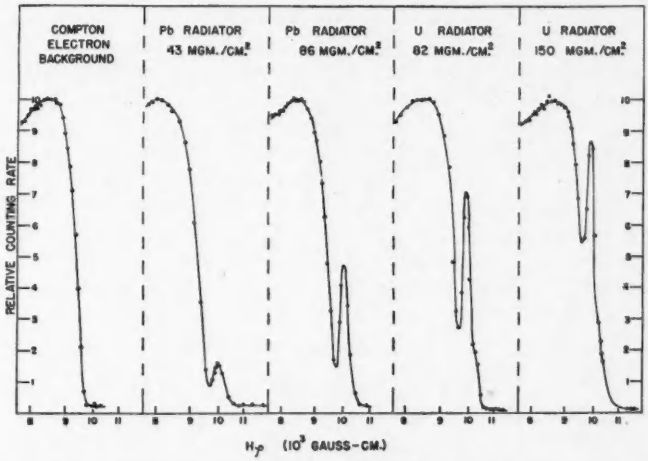

FIG. 5. *Curves showing the variation in the height of the photoelectron line ejected by the 2.62 Mev. γ-ray of thorium C'' from lead and uranium radiators of different thicknesses. The change from 43 mgm. per cm.² lead to 86 mgm. per cm.² lead was accompanied by improvements in the spectrometer alignment, accounting for the large improvement in line height in the case of the 86 mgm. per cm.² radiator.*

Experimental Results

The result of a typical run in search of γ-radiation in the region of 3.20 Mev. is shown in Fig. 6, using the 82 mgm. per cm.² uranium radiator. This curve

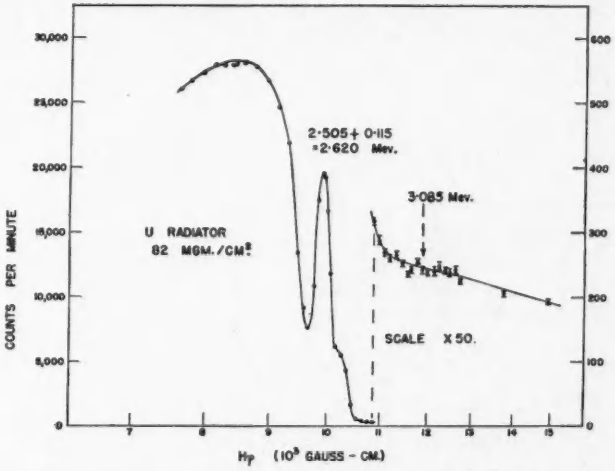

FIG. 6. *The result of a typical run in search of γ-radiation in the region of 3.20 Mev. A line at 3.20 Mev. having an intensity of 0.2% of that of the 2.62 Mev. line would give a peak of 32 counts per minute at the point marked 3.085 Mev.*

represents one of three runs of comparable accuracy over this energy region. The height of the 2.62 Mev. photoelectric conversion line, for reference, is 19,500 counts per minute. The ordinates of the curve in the high-energy region to the right of the 2.62 Mev. line have been expanded by a factor of 50. Taking account of the variation of the photoelectric cross section with energy, a 3.20 Mev. line having an intensity of 0.2% of that of the 2.62 Mev. line would give a peak of 32 counts per minute at the point marked 3.085 Mev. in Fig. 6. This line height corresponds to about three times the standard deviation of the points shown. No such line is detectable in any of the three runs taken, which demonstrates that the intensity of the 3.20 Mev. line must be less than 0.2% of that of the 2.62 Mev. line, and may be very much less than this amount or even zero.

Discussion of Results

The fact that a 3.20 Mev. excited state exists in thorium D is well attested by the results of Alichanow and Dzelepow (2), as well as by the fact that the 0.58 and 2.62 Mev. γ-rays have been shown to be emitted in cascade (7). The present study shows that direct γ-ray transitions from the 3.20 Mev. excited state to the ground state of thorium D are either very improbable or completely forbidden.

A theoretical estimate of the relative intensities of the γ-rays may be obtained from a formula quoted by Helmholtz (11), which gives the transition probabilities as follows: for electric 2^l-pole radiation of energy E, which occurs when the vector spin difference between the two states involved is l and the parity change is $(-1)^l$, the transition probability w is proportional to

$$\left(\frac{E}{23.7}\right)^{2l+1} \frac{1}{[1.3.5. \ldots (2l-1)]^2},$$

while for magnetic 2^l-pole radiation, which occurs when the vector spin difference is l and the parity change is $(-1)^{l+1}$, the transition probability w' is proportional to

$$\left(\frac{E}{23.7}\right)^{2l+3} \frac{1}{[1.3.5. \ldots (2l+1)]^2}.$$

Since both the 0.58 Mev. and 2.62 Mev. γ-rays are believed to be electric quadrupole radiations (10, 13), the three states involved have the same parity. Hence, according to Oppenheimer's disintegration scheme the 3.20 Mev. γ-ray is magnetic 2^3-pole radiation competing with the 0.58 Mev. electric 2^2-pole radiation. On this basis

$$\frac{w'_{3.20}}{w_{0.58}} = 0.0014.$$

On the data available the spin of the 3.20 Mev. level could be 4 instead of 3, in which case the 3.20 Mev. γ-ray is electric 2^4-pole radiation giving the same ratio $w_{3.20}/w_{0.58}$ as above. Taking into account the known intensity of the 0.58 Mev. γ-ray relative to the 2.62 Mev. γ-ray, the theoretical intensity ratio of the 3.20 Mev. γ-ray to the 2.62 Mev. γ-ray is 0.001.

From the present experimental results, the ratio of the intensity of the 3.20 Mev. γ-ray to that of the 2.62 Mev. γ-ray is known to be less than 0.002. This value is consistent with the theoretical estimate, but in view of the uncertainty in formulas of this type, the above agreement cannot be taken as a very positive support of the Oppenheimer disintegration scheme.

Acknowledgments

We are indebted to Dr. K. C. Mann and Mr. D. V. Booker for assistance in preliminary work on the experiment.

References

1. ALICHANOW, A. I., ALICHANIAN, A. I., and KOSODAEV, M. S. J. phys. radium, 7 : 163. 1936.
2. ALICHANOW, A. I. and DZELEPOW, B. Compt. rend. acad. sci. U.R.S.S. 20 : 113. 1938.
3. ARNOULT, R. Ann. phys. [11] 12 : 241. 1939.
4. CHADWICK, J., BLACKETT, P. M. S., and OCCHIALINI, G. Proc. Roy. Soc. London, A, 144 : 235. 1934.
5. DAVIDSON, Z. S. and LATYSCHEV, G. D. J. Phys. U.S.S.R. 6 : 15. 1942.
6. DEUTSCH, M., ELLIOTT, L. G., and EVANS, R. D. Rev. Sci. Instruments, 15 : 178. 1944.
7. DUNWORTH, J. V. Rev. Sci. Instruments, 11 : 167. 1940.
8. ELLIS, C. D. Report of the International Conference on Physics, London. 1934.
9. ELLIS, C. D. Proc. Phys. Soc. London, 50 : 213. 1938.
10. FLAMMERSFELD, A. Z. Physik, 114 : 227. 1939.
11. HELMHOLTZ, A. C. Phys. Rev. 60 : 415. 1941.
12. LATYSCHEV, G. D. and KULCHITSKY, L. A. J. Phys. U.S.S.R. 4 : 515. 1941.
13. OPPENHEIMER, F. Proc. Cambridge Phil. Soc. 32 : 328. 1936.
14. SIMONS, L. and ZUBER, K. Proc. Roy. Soc. London, A, 159 : 383. 1937.
15. STETTER, G. and JENTSCHKE, W. Physik. Z. 40 : 104. 1939.
16. ZUBER, K. Helv. Phys. Acta, 11–3 : 207. 1938.

ATTEMPT TO DETECT AN $(n,2n)$ REACTION IN DEUTERIUM[1]

BY L. G. ELLIOTT[2], E. P. HINCKS[2], AND A. N. MAY[3]

Abstract

A detailed account is given of experiments carried out to detect an $(n,2n)$ reaction in deuterium. A Po-α-Be neutron source was surrounded by a hollow aluminum sphere 30 cm. in diameter, which could be filled with heavy water. The sphere was surrounded by an effectively infinite medium of paraffin oil. The neutron density distribution outside the sphere was measured with a small boron trifluoride chamber (6 mm. diameter $\times$ 20 mm. long). The total integrated densities of neutrons were determined both with the sphere empty and filled with heavy water. After correcting for absorption of thermal neutrons by the heavy water, the aluminum sphere, and the source, and of fast neutrons by the oxygen of the heavy water, it is shown that the fraction of neutrons giving an $(n,2n)$ effect is $0.1 \pm 2.7\%$. This indicates that the effect is less than both that predicted by Höcker's theory ($\sim$10%) and that reported from an earlier experiment by Halban and coworkers (18%). However it is in good agreement with measurements made by Fenning and Knowles ($1.4 \pm 5\%$).

Introduction

In 1941 Halban, Kowarski, Fenning, and Freundlich (10) at Cambridge University found an increase of $18 \pm 5\%$ in the number of neutrons from a Ra-α-Be source when it was surrounded by heavy water, after allowing for the photoneutrons produced by γ-rays from the source. This was interpreted as an $(n,2n)$ process on deuterium caused by fast neutrons. Subsequently, it was frequently stated that this effect made an important contribution to the multiplication factor of chain-reacting piles using heavy water as the moderator. Critical analysis of the Cambridge experiment (9) has revealed that sources of error in the method, which were not fully taken into account, might give rise to the large positive result that was obtained.

Fenning and Knowles (8) repeated the Cambridge experiment in 1943 at the Montreal Laboratory. They also used a Ra-α-Be source, but avoided some of the sources of error in the earlier work. Their result $0 \pm 3\%$ for the neutron production by an $(n,2n)$ reaction on deuterium, becomes $1.4 \pm 5\%$ when a correction is added for the fast neutron reaction on oxygen as described below.

In view of the uncertainty in the magnitude of the effect, it was decided to carry out a new determination with as great an accuracy as possible, and with thorough attention to all possible sources of error. This experiment was performed by the authors between November 1943 and August 1944 in the Montreal Laboratory of the National Research Council. The method used was similar in principle to that of Halban and coworkers, and of Fenning and Knowles, although differing in details.

[1] *Manuscript received June 3, 1948.*

Contribution from the Physics Branch, Montreal Laboratory, Division of Atomic Energy of the National Research Council of Canada. Issued as N.R.C. No. 1836.

This work was carried out between November 1943 and August 1944, and is described in Report MP-198 of the Montreal Laboratory, National Research Council of Canada.

[2] *Now at the Chalk River Laboratory, Chalk River, Ontario.*

[3] *Formerly member of United Kingdom Staff, Montreal Laboratory.*

The general method will be described briefly. A source of fast neutrons is placed at the center of a sphere, which may be alternately empty or filled with heavy water. Outside the sphere is an effectively infinite uniform medium in which all emergent neutrons are slowed down to thermal velocities, and subsequently captured. If Q is the total number of neutrons emerging in all directions from the sphere per unit time,

$$Q = \frac{1}{\tau}\int_V \rho(x,y,z)dV,$$

where τ is the mean life of thermal neutrons in the external medium, $\rho(x,y,z)$ is the thermal neutron density at a point (x, y, z) in the medium, and the integral is taken over all space outside the sphere. If the neutron distribution is spherically symmetrical throughout the whole system, we can write $4\pi\rho(r)\,r^2\,dr$ for $\rho(x,y,z)\,dV$, where r is the distance from the center of the sphere. Moreover, if we use a neutron detector whose output I is accurately proportional to ρ everywhere, we can replace $\rho\,(r)$ by $aI(r)$, where a is a constant representing the efficiency of the detector. We may then write

$$Q = \frac{4\pi a}{\tau}\int_{r_1}^{\infty} I(r)r^2dr,$$

where r_1 is the radius of the sphere, and $4\,\pi a/\tau$ is constant for a given experiment. The detector output I is therefore measured at various distances from the source, from the surface of the sphere outwards. When these values are multiplied by the corresponding values of r^2, and the product plotted as a function of the distance r, the area under the resulting curve may be used as a measure of the total number of neutrons emerging from the sphere in unit time. When the sphere is empty, this number is just the number of neutrons emitted by the source per unit time. Any $(n,2n)$ effect should appear as an increase in the total number of neutrons when the sphere is filled with heavy water. Corrections must be made for absorption of thermal neutrons by the heavy water when the sphere is full, absorption by the material of the sphere, and absorption by the source itself; these will be discussed in detail below.

The principal differences between this and the earlier measurements are the following:

(1) The use of a smaller sphere (30 cm. diameter instead of 60 cm.). This decreases the fraction of thermal neutrons captured by the heavy water and so makes the result less dependent on the measurement of the absorption cross section of the water. It also requires a smaller volume of heavy water. On the other hand the $(n,2n)$ effect will be almost as large in a 30 cm. as in a 60 cm. sphere, since the neutrons are ineffective after their energy has fallen below the 3.3 Mev. threshold for the reaction.

(2) The use of a Po-α-Be source instead of Ra-α-Be. This eliminates the production of neutrons in the heavy water by the $D^2(\gamma,n)H^1$ reaction, which complicated the previous measurements. Moreover, the proportion of high energy neutrons may be greater owing to the absence of the "Auger group" (2).

(3) The use of small boron trifluoride chambers for neutron density measurements. These have great reproducibility and low backgrounds when compared with "induced activity" detectors. Since the boron cross section is inversely proportional to the neutron velocity (13), the number of B^{10} disintegrations is accurately proportional to the mean thermal neutron density in the chamber. The degree to which the neutron absorption and finite size of the chambers might affect their representation of the true (undisturbed) neutron density in the medium was investigated by comparing them with thin dysprosium detectors.

Description of Apparatus

(1) *Tank*

The measurements were carried out in a rectangular iron tank, 90 cm. long, 60 cm. wide, and 60 cm. high. This was filled with paraffin oil (Imperial "Marcolix" medicinal paraffin: density 0.840 gm. per $cm.^3$ at 22° C., and hydrogen content, 14.1% by weight.) The tank stood on a 30 cm.-thick layer of paraffin wax and was surrounded on the sides (but not on top) by 50 cm. of paraffin wax in the form of plates.

Fig. 1 is a vertical section of the tank showing the sphere and boron chamber mounted in position. These were supported from a steel frame that normally rested on the top edge of the tank, but which could be lifted out bodily and put on a separate stand for adjustments and measurements of distances.

(2) *Sphere*

The sphere was made of 0.5 mm. thick aluminum spun in two hemispheres and welded together. The outside diameter was 30.3 cm. A neck, 15 cm. long and 8.5 cm. in diameter, on the top of the sphere held a tight-fitting hollow aluminum plug, which was filled with paraffin oil during the measurements. Attached to the plug was a dural rod, which supported the source at the center of the sphere, and through the plug passed tubes by means of which the sphere could be filled with heavy water from a reservoir, or emptied, without disturbing the source. Clamping rings held the plug in the neck, and a neoprene gasket made a water-tight seal. Measurements with a cathetometer showed that the sphere was spherical to within 1 mm. in diameter, and that the source was central to within 1 mm.

The sphere was carried by a collar on the neck, and the collar in turn was clamped to two rods which were carried on the main frame. When the sphere was emptied, lead weights were placed on the collar to compensate for its buoyancy in oil, thus preventing distortion of the frame by a change in weight.

(3) *Chamber*

The chambers were 6 mm. in diameter, about 2 cm. long, filled with 1.5 atm. of boron trifluoride, and were a standard single-ended type made by N. Veall (16) in the Montreal Laboratory. Two chambers were used alternately for the experiment, and the sensitivity of each remained constant throughout.

The chamber was supported by a thin metal tube as shown in detail in Fig. 1. This, together with the preamplifier, was mounted on a carriage which slid on two rods of the main frame, so that the chamber could be moved longitudinally in the tank along a line normal to the surface of the sphere.

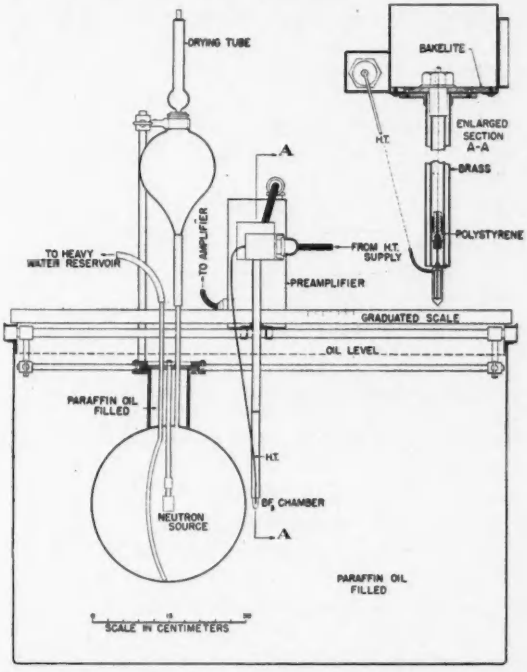

FIG. 1. *Vertical section of apparatus showing sphere and boron trifluoride chamber mounted in oil-filled tank.*

The use of an insulating medium such as paraffin oil in the tank had the advantage that the H.T. and collector leads could be brought out of the chamber without insulation, thus reducing the disturbance of the neutron distribution in the oil.

(4) *Counting Apparatus*

The electronic equipment used to count the pulses from the chamber comprised standard instruments used for similar work in the Montreal

Laboratory. A linear amplifier, with a gain of about 10^5, was followed by a discriminator with variable bias, and a scale-of-128. An oscilloscope was used for visual monitoring.

Considerable care was taken to reduce the background of spurious counts due to electrical pick-up in the laboratory. Double screening of the lead from the chamber to the preamplifier input was used, and the earthing-connections in the preamplifier and first stages of the main amplifier were chosen to secure minimum sensitivity to pick-up.

The counting rate did not change appreciably with normal drifts in the characteristics of the electronic circuits. The bias curves (counting rate vs. discriminator threshold) for the two chambers used are shown in Fig. 2. The

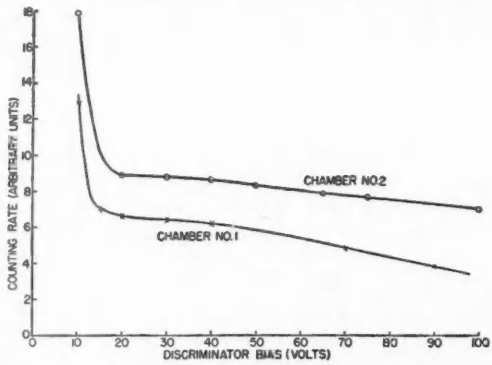

FIG. 2. *The bias curves for the two boron trifluoride chambers.*

operating points were chosen on the sections of minimum slope, where it may be seen that a 1% change in amplifier gain would cause less than 0.1% change in counting rate. The counting rate was also insensitive to small changes in H.T. voltage. The H.T. supply was stabilized, and all the equipment was operated from a constant-voltage transformer.

(5) *Measurement of Distances*

It was important to measure the distance r from the center of the sphere accurately since a change of 1 mm. in r led in some cases to a 2% change in the intensity. In some early runs the distances were measured by a scale placed along the top of the frame. The scale was calibrated frequently by measurements with a cathetometer when the frame was outside the tank. In view of the possibility of small relative displacements of sphere and chamber when moving the frame, in later runs direct cathetometer observations were made through the surface of the oil. The accuracy of this method was checked by measurements of a standard scale immersed in the oil.

(6) *Dysprosium Detectors*

Thin thermal neutron detectors were made by depositing dysprosium oxide (Dy_2O_3) on a 5 cm.^{2} area of aluminum foil. Two thicknesses of oxide were used, 1 mgm. per cm.^{2} and 2 mgm. per cm.^{2} The foils were supported in thin aluminum holders on thin brass rods. Distances between detectors and the sphere were determined by means of brass spacers. The detector activities were measured with standard cylindrical aluminum-wall counters (17) and scales-of-32.

(7) *Source*

The source consisted of 5 gm. of beryllium powder mixed with 0.5 curie of polonium and sealed in a brass holder. By comparison with a standard source it was found to be equivalent in neutron production to 0.07 curie of radon mixed with beryllium. Measurements made by H. Seligman at the Montreal Laboratory showed that the source did not decay appreciably during the whole period of measurement, so we can assume that the polonium is in equilibrium with radium D.

Experimental Results

Following the method outlined above, the neutron efflux from the sphere was derived by measuring the variation of neutron density with distance from the sphere. Each run therefore consisted of a sequence of counting rate determinations made at many points lying along a line normal to the sphere at various distances from it. About 10,000 counts were obtained at each point. Runs were taken with the sphere alternately empty and full of heavy water, and several complete sets of runs—each set comprising several emptyings and fillings—were made at intervals throughout the experiment. In comparable runs, the counting rates observed at a given distance repeated within the limits of statistical error (about 1%).

For analysis, the sets of runs were divided into two groups: those taken with one boron trifluoride chamber (No. 1) and those taken with the other chamber (No. 2). The results of these two groups were worked out separately in order to indicate the reproducibility that may be obtained by this method. Since the total number of measurements obtained in either group was large, measurements referring to approximately the same distance from the sphere have been lumped together in the following manner. Although the experimental procedure was to position the chamber at points which were an integral number of centimeters from the center of the sphere, as indicated by a meter scale attached to the frame, in general the accurate cathetometer reading showed a deviation from the integral position. The counting rate was corrected for this deviation by using the mean slope of the density curve at the point in question. All measurements thus corrected refer to integral distances, and measurements referring to the same distance were averaged. The final mean values of counting rates (I) at different distances from the center of the sphere for the two groups of runs are shown in Table I.

TABLE I

MEASURED INTENSITIES (COUNTS PER MINUTE) FOR EMPTY AND FULL SPHERES

Distance from center of sphere, r, cm.	Chamber No. 1		Chamber No. 2	
	Intensity, sphere empty, c.p.m.	Intensity, sphere full, c.p.m.	Intensity, sphere empty, c.p.m.	Intensity, sphere full, c.p.m.
15.2	660	2170	712	2260
16	655	1821	704	1930
17	640	1453	680	1545
18	604	1142	644	1215
19	560	877	596	926
20	510	665	544	705
21	460	500	490	527
22	410	373	436	395
23	—	—	385	297
24	314	218	337	226
25	—	—	293	174
26	233	126.5	252	135
27	—	—	216	106
28	172	78.8	184	84.5
29	—	—	156	68.2
30	127	51.9	132.5	55.3
31	—	—	112.5	45.0
32	92	34.9	95.8	36.7
34	67.2	24.1	69.8	25.2
36	48.5	17.2	50.7	17.8
38	35.0	12.5	37.0	12.7
40	25.3	9.0	27.0	9.05
42	18.3	6.4	19.75	6.52
44	13.2	4.6	14.3	4.70
46	9.70	3.3	10.5	3.39
48	7.10	2.4	7.62	2.45
50	5.23	1.7	5.61	1.78
52	3.85	—	4.16	1.32
54	—	—	3.08	—
56	—	—	2.29	0.7

The background count, taken with no source, was 0.03 counts per min. for both chambers. The constancy of this value, which was measured a number of times throughout the experiment, showed that spurious counts due to electrical pick-up, etc., were extremely unlikely. The contribution of the background is seen to be significant only for the points farthest from the sphere, and its effect on the area under the Ir^2 curve is negligible.

Some additional measurements were made with the sphere rotated about 180° through a vertical axis. In both the "full" and "empty" cases these agreed with the main results within 1%, showing that the source was well centered. Tests were also made with dysprosium detectors placed against the surface of the sphere at various latitudes, but again variation in intensity was found to be less than 1%.

The intensities given in Columns 2 and 3 (chamber No. 1) of Table I are plotted on a logarithmic scale against the distance r in Fig. 3. In the "empty" case the intensity is nearly constant near the sphere, corresponding to the

boundary condition $\partial\rho/\partial r = 0$ at the surface, and showing that there is little or no net generation or loss of thermal neutrons inside the sphere. At larger distances from the source ($r > 25$ cm.) the slope of the curve becomes

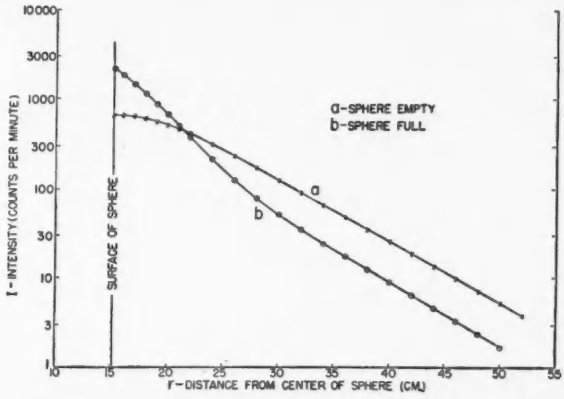

FIG. 3. *Logarithmic plot of the neutron intensity in the paraffin oil versus distance from center of the sphere: (a) sphere empty; (b) sphere filled with heavy water. (Chamber No. 1).*

nearly constant. This corresponds to an exponential decrease in density with a relaxation length of about 6.1 cm., which is characteristic of the energy of the fast neutrons from the source. The slope, however, decreases slightly with increasing distance, indicating a slight "hardening" of the neutrons.

The curve obtained with the full sphere shows quite different features. The slope near the sphere surface is large corresponding to a large outward flux of thermal neutrons generated in the sphere. For the same reason the intensity at the surface is larger than in the "empty" case. At $r = 21.4$ cm. the two curves cross. The "full" curve then straightens out at $r \sim 32$ cm. to become nearly parallel to the "empty" curve, but with about one-third the intensity. (The slope of the "full" curve actually appears to be slightly greater, the relaxation length for the exponential portion being 5.9 cm.) The comparison between the two curves in this region may be interpreted as showing that about one-third of the fast neutrons responsible for the exponential tail pass through the heavy water without much energy loss.*

The values of Ir^2 were calculated from the values in Table I, and plotted as a function of r. These curves for empty and full sphere in the case of chamber No. 1 are shown in Fig. 4. The area ($\int Ir^2 dr$) under the "empty" curve between the surface of the sphere (r_1) and the outermost point measured (r_2) gives the total number of neutrons emitted by the source and absorbed by the paraffin oil inside a spherical volume of radius r_2. A correction for those

* *This agrees quantitatively with results obtained in preliminary experiments with a 20 cm. diameter sphere. In this case the same behavior was observed but the intensity of the "full" curve was one-half that of the "empty" one in the exponential region.*

neutrons captured outside this volume was made by assuming the exponential tail on each curve to continue to infinity. The corrected area for empty sphere may then be compared with that for the full sphere, which will be greater or less depending on whether there is a net generation or absorption of neutrons in the heavy water.

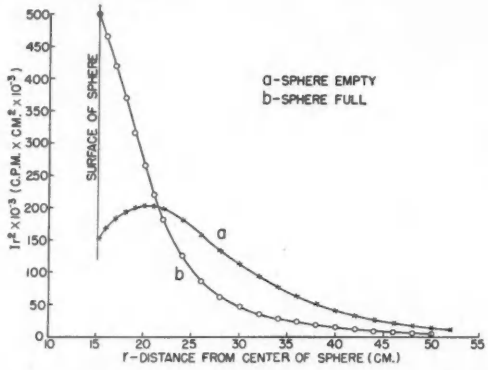

FIG. 4. *Plot of Ir^2 versus distance from center of the sphere: (a) sphere empty; (b) sphere filled with heavy water. (Chamber No. 1).*

Table II gives the results for the "empty" and "full" cases for each of chambers Nos. 1 and 2. Column 3 gives the value of r_2 at the outer limit of measurement; Column 4, the area measured between $r_1 = 15.15$ cm. and r_2;

TABLE II

AREAS UNDER Ir^2 CURVES FOR EMPTY AND FULL SPHERE

Chamber	Sphere	Outer limit of measurement r_2(cm.) ($r_1 = 15.15$cm.)	Measured area r_1 to r_2 $\times 10^{-3}$	Estimated area r_2 to ∞ $\times 10^{-3}$	Total area r_1 to ∞ $\times 10^{-3}$	Difference between "full" and "empty" areas $\times 10^{-3}$	Difference as percentage of "empty" area
1	Empty	52	3509	91	3600	−185	−5.1
	Full	50	3380	35	3415		
2	Empty	56	3750	64	3814	−198	−5.2
	Full	56	3597	19	3616		

Column 5, the correction for $r > r_2$, or the estimated area under the curve from r_2 to infinity; Column 6, the total (corrected) area; Column 7, the difference—"full" area minus "empty" area—for each chamber; and Column 8, the same difference as a percentage of the total "empty" area.

The results for both chambers indicate that about 5% less neutrons are "observed" when the sphere is full than when it is empty. This immediately precludes the presence of a large positive $(n,2n)$ effect such as found by Halban *et al.* (10)*. However the absence of an $(n,2n)$ effect cannot be presumed until allowance has been made for all other effects that may alter the neutron balance when the sphere is filled with heavy water. These effects are individually small, and will be considered in later sections as corrections to the differences of Table II.

Errors

The sources of error in the measurements of neutron density distribution may be divided into four groups:

(1) Counting errors—

(*a*) Statistical fluctuations,

(*b*) Non-linearity of counting circuit,

(*c*) Variations in sensitivity of boron trifluoride chamber and counting circuit.

(2) Failure of the boron trifluoride chamber to respond proportionally to the neutron density at all points of measurement.

(3) Imperfect extrapolation of the neutron distribution necessitated by the finite size of the paraffin oil medium.

(4) Errors in distance measurements.

The steps taken to minimize and estimate these errors will be discussed in turn.

(1) *Counting Errors.*—(*a*) Each point in each series of runs was obtained by observing more than 10,000 counts. Measurements were made at 1 cm. intervals over the greater part of the neutron distribution in the paraffin oil. Hence errors introduced in the area by statistical counting fluctuations are very small ($\ll 1\%$). (*b*) The counting circuit was tested at the highest counting rates used and found not to deviate from linearity by as much as 0.5%. (*c*) The constancy of the sensitivity of the chamber and counting circuit was frequently verified by observing the counting rate at a standard point close to the sphere.

(2) *Non-linearity of the Boron Trifluoride Chamber.*—To test whether the chamber was responding proportionally to the neutron density at all points in the paraffin oil, measurements were made with thin dysprosium detectors (described above) placed close to the sphere in both the "empty" and "full" cases. A further experiment was made with a stronger neutron source (600

* *The preliminary experiments with the 20 cm. diameter sphere similarly indicated the absence of any large effect.*

mc. Ra-α-Be), and the curves obtained with the chamber and thin dysprosium detectors at large distances from the sphere were compared. The shape of the neutron distribution obtained with 1 mgm. per cm.^{2} detectors was the same as that obtained with 2 mgm. per cm.^{2} detectors; this fact indicates that these detectors were sufficiently thin so as not to disturb appreciably the neutron distribution. The probable error in the detector measurements was 2%, and in all comparisons the agreement with the boron trifluoride chamber measurements was within this limit.

(3) *Extrapolation of the Neutron Distribution.*—There was no observable difference, even at the most distant point, between measurements taken with the oil tank alone and those taken with the tank surrounded on all sides by a 50 cm. thickness of paraffin wax. The residual area, obtained by extrapolating the measured curves to an infinite distance from the source, is the same to the required accuracy whether we assume either I or Ir^2 to decrease exponentially as r increases to infinity. It is seen in Table II, where the estimated residual area is given in Column 5, that it is less than 3% of the total area for each curve, so that any error introduced in the total area must be very small.

(4) *Distance Measurements.*—The distance measurements as described in the section on apparatus were reproducible to about 0.02 cm. The maximum error introduced by this uncertainty is 0.5% of the total neutrons in the differences between the full and empty sphere cases.

Corrections for Absorption of Thermal Neutrons

(1) *Absorption in the Heavy Water*

The fraction of neutrons absorbed by the heavy water depends upon the neutron density inside the sphere and the neutron lifetime in the water.

The distribution of neutron density within the sphere could be estimated with sufficient accuracy for this purpose from the density and the density gradient in the paraffin oil near the surface of the sphere. As a check one point was measured inside the sphere by fixing a thin dysprosium detector to the source rod. The estimated curve, together with the experimental point which lies on it, are shown in Fig. 5.

The neutron lifetime in the water is estimated in terms of that in the oil from the thermal neutron capture cross sections of the various nuclei involved, together with their relative abundances. In particular, we require a knowledge of the amount of hydrogen (H^1) contamination in the heavy water, since this is the nucleus chiefly responsible for the capture of thermal neutrons. It will be convenient and legitimate in the calculation of this correction to assume that the heavy water consists only of the molecules H_2O and D_2O, although in reality the hydrogen is found in the molecule HDO when in very small concentrations. P. Demers found both by freezing point and density

measurements that our heavy water contained 2.4% more ordinary water than did the main laboratory stock. Since the latter was known to have 0.6% ordinary water content, the actual contamination in our heavy water

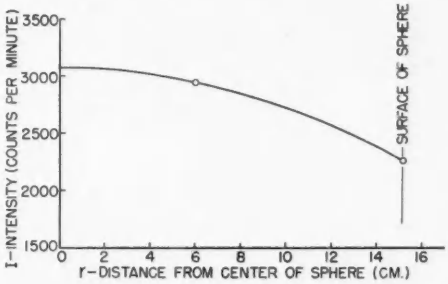

FIG. 5. *Neutron intensity inside the sphere when filled with heavy water. The solid line is estimated from the measurements outside the sphere; the circles are experimental points taken with dysprosium detectors. Both are normalized to the boron trifluoride chamber (No. 1) measurements at the surface of the sphere.*

was 3.0%. The ratio of the mean life for thermal neutrons in our heavy water (τ_s) to that in the paraffin oil (τ_{oil}) may be written

$$\frac{\tau_s}{\tau_{oil}} = \frac{d_{oil}}{d_s}\left(\frac{f_H\sigma_H + f_C\sigma_C/12}{f_{H_2O}\sigma_H/9 + f_{D_2O}\sigma_{D_2O}/20}\right)$$

where the symbols have the following meanings:

d_{oil} = Density of the oil (0.840 gm. per cm.^{3});

d_s = Density of the heavy water (1.10 gm. per cm.^{3});

f_H = Fraction by weight of hydrogen in the oil (0.141);

f_C = Fraction by weight of carbon in the oil (0.86);

f_{H_2O} = Fraction by weight of H_2O in our heavy water (0.030);

f_{D_2O} = Fraction by weight of D_2O in our heavy water (0.97);

σ_H = Cross section for thermal neutron absorption per H atom;

σ_C = Cross section for thermal neutron absorption per C atom;

σ_{D_2O} = Cross section for thermal neutron absorption per D_2O molecule.

We take the values $\sigma_H = 0.30 \times 10^{-24}$ cm.^{2}; $\sigma_C = 0.0045 \times 10^{-24}$ cm.^{2}*. Sargent *et al.* (15) have measured the diffusion length for thermal neutrons in heavy water and give a value $(0.92 \pm 0.22) \times 10^{-27}$ cm.^{2} for σ_{D_2O}. Substituting the above values we find for our heavy water

$$\frac{\tau_s}{\tau_{oil}} = 31.$$

* *See for example, nuclear chart compiled by E. H. Segrè. Revised Sept. 1946. Addison-Wesley Press Inc., Cambridge, Mass.*

To find the fraction f of neutrons absorbed by the heavy water we determine the ratio of the area A_z under the Ir^2 curve inside the full sphere (derived from the intensity curve of Fig. 5) to the total area A_{oil} under the corresponding curve outside (see Table II). Thus:

$$\frac{A_z}{A_{oil}} = \frac{\int_0^{r_1} Ir^2 dr}{\int_{r_1}^{\infty} Ir^2 dr}$$

$$= \frac{2690}{3415}$$

$$= 0.788.$$

Now

$$f = \left(\frac{A_z}{A_{oil}}\right)\left(\frac{\tau_{oil}}{\tau_z}\right)$$

$$= 0.788/31$$

$$= 0.025.$$

Thus the number of neutrons absorbed in the heavy water is 2.5% of the number absorbed outside the sphere. The probable error is estimated to be about 0.3%.

(2) *Absorption in the Aluminum Sphere*

The absorption in the aluminum can be estimated in a manner similar to that in the heavy water, where the net contribution is due to the differences in intensities at the sphere surface in the "empty" and "full" cases. The lifetime in pure aluminum can be derived from the absorption cross section for aluminum, but it is possible that the metal and the weld might contain impurities which would decrease the lifetime considerably. Analysis of samples of aluminum and welding rod showed traces of copper and silicon. The welding flux used contained lithium and boron, but tests of sample welds showed that simple washing removed all the flux.

To take into account the possibility of a large neutron absorption by impurities a test was made of the aluminum by a measurement with the 30 cm. sphere filled with pieces of aluminum sheet (totalling about 2.5 times the sphere weight) of the same kind as that used for the sphere. The area under the Ir^2 curve (Fig. 6, Curve *a*) was $0.6 \pm 1.0\%$ less than that in the case with the empty sphere, the shapes of the two curves being similar. Moreover, the thermal neutron density in the aluminum during this measurement was equal to the density in the empty sphere, which was 1/2.3 times the difference between the densities at the sphere surface in the "full" (of heavy water) and "empty" cases. Hence, this indicates a correction for absorption in the

aluminum sphere of $(0.6 \pm 1.0) \times 2.3/2.5 = 0.55 \pm 0.9\%$ of total neutrons. The value of the correction calculated from the lifetime, assuming pure aluminum, is 0.54%.

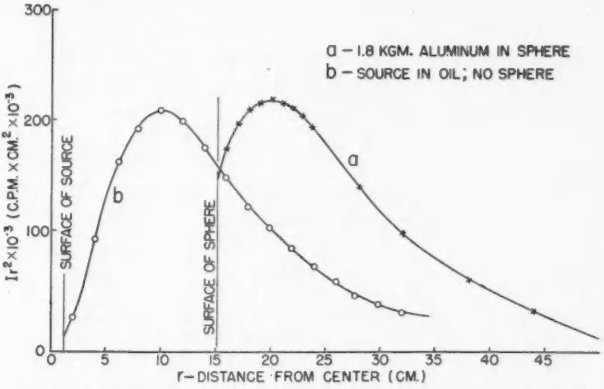

FIG. 6. *Plots of Ir^2 versus r: (a) source in sphere filled with pieces of aluminum sheet; (b) source placed directly in the paraffin oil.*

(3) *Absorption in the Source*

A test was made for the absorption of thermal neutrons in the source itself by placing the latter directly in the paraffin oil and integrating the density distribution. The Ir^2 curve under which the area is measured is shown in Fig. 6, Curve *b*. The increase in thermal neutron intensity at the source in this case over that with the empty 30 cm. sphere is about four times the difference in intensities between full and empty sphere. The difference in areas between the two cases is less than 1%. The correction for thermal neutron absorption in the source when comparing full and empty spheres is therefore less than 0.25% of total neutrons. The value calculated by assuming that all absorption is due to the brass container which holds the source is 0.11%.

(4) *Absorption in Air*

The absorption by the nitrogen of the air present when the sphere is emptied of heavy water is calculated to be 0.08% of total neutrons.

Correction for Absorption of Fast Neutrons

The absence of an increase in the number of neutrons on surrounding the source with heavy water may be interpreted to mean either that the effect of the $(n,2n)$ reaction with Po-α-Be neutrons is too small to be observed, or that it is masked by an equally large absorption of fast neutrons. For example, the following reactions between fast neutrons and O^{16} are known to occur:

$$O^{16} + n \longrightarrow C^{13} + He^4 - 2.3 \text{ Mev.} \quad (12, 7)$$

$$O^{16} + n \longrightarrow N^{16} + H^1 - \sim 5 \text{ Mev.} \quad (5)$$

Pulses due to these reactions may be observed when chambers filled with oxygen are used with fast neutrons, and are a source of error if they are interpreted as recoils. If the cross section for these reactions is of the order of 10^{-25} cm^2 per atom, it would lead to an absorption in the heavy water of a few per cent of the fast neutrons from the source.

The following experiment was performed to determine whether the effect from any O^{16} reaction is appreciable. The neutron distribution outside a 15 cm. diameter sphere immersed first (*a*) in ordinary water, and then (*b*) in paraffin oil, was measured using (1) a Ra-γ-Be neutron source, and (2) a Po-α-Be source, at the center of the empty sphere. The Ir^2 curves for the four cases, (*a*1), (*a*2), (*b*1) and (*b*2) are shown in Fig. 7. The results from integration under these curves are given in Table III.

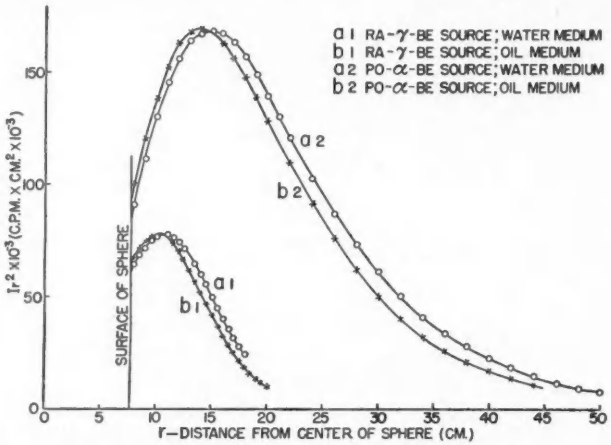

FIG. 7. *Plots of Ir^2 versus distance from center of sphere for a water medium (a) and an oil medium (b). Curves (a1) and (b1) are taken with a Ra-γ-Be source, while curves (a2) and (b2) are for a Po-α-Be source.*

TABLE III

COMPARISON OF AREAS UNDER Ir^2 CURVES TO DETERMINE THE EFFECT OF FAST NEUTRON REACTIONS ON OXYGEN

Source	$\int Ir^2 dr$ Water (*a*)	$\int Ir^2 dr$ Oil (*b*)	Difference in areas (water − oil)	Difference expressed as percentage of area for oil
Ra-γ-Be (1)	709	645	64	9.9 ± 1.5%
Po-α-Be (2)	3386	3180	206	6.5 ± 1.5%
Difference (1)–(2)				3.4 ± 2.1%

These results are interpreted in the following manner. The ratio of the area under the Ir^2 curve of case (*a*1) to that of case (*b*1) gives the ratio of the lifetimes for slow neutrons in ordinary water and paraffin oil. The difference

in areas expressed as a percentage of the area in case (*b*1) (Column (5)) is the fractional increase in lifetime of the Ra-γ-Be neutrons when the oil is replaced by water. We see that this increase is smaller for the Po-α-Be neutrons by an amount equal to 3.4% of the total neutrons. This effect, if real, can only be due to a greater absorption of the fast Po-α-Be neutrons by ordinary water than by paraffin oil. Our conclusion is consistent with the fact that the neutrons from the Ra-γ-Be source have energies below the threshold for the $O^{16}(n,\alpha)C^{13}$ reaction, while the Po-α-Be neutrons have energies above this threshold. In our heavy water experiment two-thirds of the fast neutrons were slowed down in the heavy water and one-third were slowed down in the paraffin oil which contains no oxygen. We estimate therefore that $2.2 \pm 1.6\%$ of the fast neutrons were lost by (n, α) or (n,p) reactions with the oxygen in the heavy water.

Conclusion and Discussion

The results of the measurements, together with the corrections, are summarized in Table IV. The decrease of 5.2% in the number of neutrons when the source is surrounded by heavy water is reduced to 2.1% when corrections

TABLE IV

SUMMARY OF RESULTS

Neutron absorption components	Difference as per cent of total neutrons: "full" case minus "empty" case	Estimated error, per cent of total neutrons
Neutrons absorbed in "infinite" paraffin medium	−5.2	±2.0
Neutrons absorbed in heavy water	+2.5	±0.3
Neutrons absorbed in aluminum sphere	+0.5	±0.9
Neutrons absorbed in source	+0.2	±0.1
Neutrons absorbed in air	−0.1	±0.0
Neutrons absorbed in entire system	−2.1	±2.2
Estimated fast neutrons absorbed in oxygen of heavy water	+2.2	±1.6
Net effect attributable to $(n,2n)$ reaction with deuterium	+0.1	±2.7

are made for absorption in heavy water, aluminum sphere, and source. Finally, when allowance is made for the fast neutron reaction with oxygen, we obtain an increase of $0.1 \pm 2.7\%$ which can be attributed to the $D^2(n,2n)H^1$ reaction.

Fenning and Knowles (8) in a repetition of the Cambridge experiment with a 60 cm. sphere and a Ra-α-Be source, found an effect due to the introduction of the heavy water equal to $-1.4 \pm 3\%$. However, this result does not take into account the absorption of fast neutrons by oxygen, and we have

estimated that when this correction is made the Fenning–Knowles experiment gives a value $+1.4 \pm 5\%$ for the $(n,2n)$ effect. Since both their experiment and the present one are consistent with the conclusion that the $(n,2n)$ effect is less than 3%, it seems that the value 18% found by Halban and coworkers must be due to experimental errors.

Höcker (11) has considered theoretically the $(n,2n)$ reaction with deuterium. He predicts a cross section that increases with the square of the excess neutron energy over the threshold, reaching a value 2×10^{-24} cm.^{2} at 10 Mev. We may combine this with the present information about the energy spectrum of Po-α-Be neutrons to calculate the effect to be expected on the basis of this theory. Thus the results of Richards, Speck, and Perlman (14)* and of Demers (6) give 10% and 30% respectively for the fraction of the neutrons from the source that would produce an $(n,2n)$ reaction in their first collision with deuterium. (Subsequent collisions are relatively unimportant because of the lower energy of the neutrons.) Since the present experiment shows that the effect with a Po-α-Be source is less than 3%, Höcker's values appear too large by a factor of at least three.

There is independent evidence that Höcker's cross sections are too large. Ageno *et al.* (1) found no appreciable difference between the total neutron cross section of deuterium as measured by beam experiments and the scattering cross section from the knocked-on deuterium nuclei at 13.5 Mev. At this energy Höcker's figures would lead to nearly every collision resulting in an $(n, 2n)$ reaction.

On the other hand, Bagge (3), in a cloud chamber investigation of recoil tracks in deuterium gas produced by fast neutrons from a Ra-α-Be source, found a group of tracks of about 10 cm. range in air which he ascribed to the protons from the $(n,2n)$ reaction. He estimated a mean cross section of 3×10^{-25} cm.^{2} per atom for neutrons of energy over 3.3 Mev. However, his interpretation of this group of tracks is doubtful, and even if it is correct the quantitative analysis of the results is complicated by the geometric conditions in the chamber—a point which is not adequately discussed in his paper.

The very similar reaction with fast protons, $D^2(p,n)2H^1$, has been studied by Barkas and White (4), who give a cross section that is much smaller than that to be expected from Höcker's theory.

Acknowledgments

We wish to express our gratitude to Mr. N. Veall who supplied the small boron trifluoride chambers, to Mr. H. F. Freundlich who supplied the electronic counting apparatus, to Mr. N. Q. Lawrence for his assistance in designing and supplying the mechanical components from the workshop, to Mr. P. Demers for his measurements on a sample of our heavy water, and to Dr. H. Seligman who checked the strength of our Po-α-Be source.

* *We are indebted to Dr. Richards for communicating his results to us.*

We are indebted to Dr. B. W. Sargent for his valuable criticism of the manuscript of this paper.

References

1. AGENO, M., AMALDI, E., BOCCIARELLI, D., and TRABACCHI, G. C. Naturwissenschaften, 31 : 231. 1943.
2. AUGER, P. Compt. rend. 195 : 234. 1932.
3. BAGGE, E. Physik. Z. 43 : 226. 1942.
4. BARKAS, W. H. and WHITE, M. G. Phys. Rev. 56 : 288. 1939.
5. CHANG, W. Y., GOLDHABER, M., and SAGANE, R. Nature, 139 : 962. 1937.
6. DEMERS, P. Unpublished report, MP-74. Photographic emulsion study of Po-Be neutrons. National Research Council of Canada. 1945.
7. FEATHER, N. Nature, 130 : 237. 1932.
8. FENNING, F. W. and KNOWLES, J. W. Unpublished report, MP-41. Capture cross-section of heavy water for thermal neutrons; *n*-2*n* effect in deuterium. National Research Council of Canada. 1944.
9. FENNING, F. W. and KOWARSKI, L. Private communication.
10. HALBAN, H., KOWARSKI, L., FENNING, F. W., and FREUNDLICH, H. F. Unpublished report, Br-3. Evidence for the disintegration of deuterium by fast neutrons. British Atomic Energy Project. 1941.
11. HÖCKER, K. H. Physik. Z. 43 : 236. 1942.
12. MEITNER, L. and PHILIPP, K. Naturwissenschaften, 20 : 929. 1932.
13. RAINWATER, J. and HAVENS, W. W., JR. Phys. Rev. 70 : 136. 1946.
14. RICHARDS, H. T., SPECK, L., and PERLMAN, I. H. Phys. Rev. 70 : 118. 1946.
15. SARGENT, B. W., BOOKER, D. V., CAVANAGH, P. E., HEREWARD, H. G., and NIEMI, N. J. Can. J. Research, A, 25 : 134. 1947.
16. VEALL, N. J. Sci. Instruments, 24 : 331. 1947.
17. VEALL, N. and WILSON, M. Unpublished report, MP-60. Geiger-Müller counters used in Montreal laboratory. National Research Council of Canada. 1944.

THE EMISSION OF L RADIATION FOLLOWING INTERNAL CONVERSION OF γ-RADIATION IN HEAVY ELEMENTS[1]

By B. B. Kinsey[2]

Abstract

The fluorescence yields of the L levels have been computed separately on the basis of radiation widths obtained from the work of Massey and Burhop, the widths of Auger transitions of the Coster–Kronig type measured by Cooper, and existing information on the widths of the L levels. In the case of fluorescence excitation, the total fluorescence yield calculated in this way is in general agreement with measurements of Lay. In the case of excitation by internal conversion of γ-radiation in the L levels, it is shown that the total fluorescence yield for elements in the vicinity of tantalum is appreciably less than the yield measured by Lay for fluorescence excitation, but that for the heavier elements near uranium, the yields should be comparable.

Introduction

The object of the present paper was to determine the fluorescence yield resulting from the internal conversion of γ-radiation in the L levels of the heavy elements and to determine the distribution of the energy in the spectrum. The L radiations emitted in the disintegration of RaD have been the subject of a careful study by Stahel (37). This author concluded that his results were consistent with the assumption that the γ-radiations produced by RaD are converted with nearly 100% efficiency; he based his results on the measurements of Lay (25) on the fluorescence yields obtained in fluorescence excitation. It is not clear that the use of Lay's results are relevant in this case because the relative excitations of the three levels by the fluorescence method are very different from that obtained with internal conversion. While the fluorescence excitations of the L_1, L_2, and L_3 levels are very roughly in the ratios of 1 : 2 : 3, the process of internal conversion in the L levels produces excitations in the ratios of 100 : 10 : 1. More recently, Frilley and Tsien (17) have examined the spectrum of the L radiation of RaD and have concluded that anomalies exist in the distribution of the energy among the various lines of the spectrum; in a later paper, Frilley *et al.* (16) point out that the distribution might be explained by the existence of Auger transitions of the type which have been discussed by Coster and Kronig (12).

This paper will show that there is no reason to suppose that an anomaly exists in the intensity distribution of the radiation emitted in the disintegration of RaD, although the quantitative information now available on the relative probabilities of the various Auger transitions which can occur does not make it possible to calculate the intensity distribution with any accuracy. In the following paper the author has described a measurement of the quantity of

[1] *Manuscript received June 17, 1948.*

Contribution from the Chalk River Laboratory, Division of Atomic Energy, National Research Council. Issued as N.R.C. No. 1841.

[2] *Member of the United Kingdom Staff.*

L radiation emitted by ThC and RaD and has shown that the radiations emitted by the latter element are less than predicted by the assumption of 100% conversion of the γ-radiation.

The Relative Intensities in the L Spectrum

The emission lines of the L series cover a considerable range of energy, but the most intense lines, which comprise the α and β groups, are concentrated into two relatively narrow bands. The γ group of lines are of weaker intensity and of higher energy. The transitions to which the more important lines correspond are shown in diagrammatic form in Fig. 1.

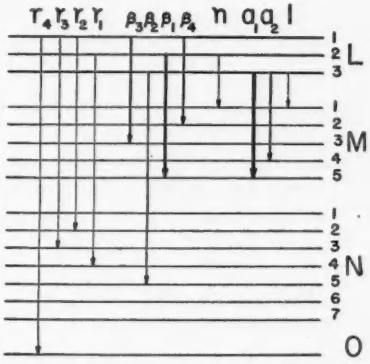

FIG. 1. *Energy level diagram for lines of the L spectrum.*

In general, the relative intensities of the various lines of the L spectrum depend on three factors: the relative excitation of the three L levels, the fluorescence yield of each level (which is itself a measure of the proportions of radiative and nonradiative transitions), and the probability of Auger transitions shifting the vacancy produced in one level to another L level. A numerical evaluation of each of these three effects will determine the relative intensities of the radiations associated with the three levels as initial states. A determination of the relative intensities of all the lines in the spectrum would require further information on the relative probabilities of the radiations associated with one level.

In principle, then, the basis of the calculations for the radiations emitted following internal conversion could be checked by using the formulae for the relative intensities of the L radiations emitted in cathode-ray or fluorescence excitation and comparing the results with those of experiment. However, the relative intensities of the L radiations due to fluorescence radiations do not seem to have been measured, and the intensities observed in cathode ray excitation do not admit of easy interpretation owing to the existence of secondary effects.

Formulation of the Problem

A formula will now be obtained for the radiation probabilities of the three L levels, the three effects discussed in a previous paragraph being taken into account.

In the absence of nonradiative transitions in which the vacancy in one L level can be shifted to another L level, the intensities of the lines characteristic of one L level as an initial state depend only on the extent of the primary excitation. Let u_1, u_2, and u_3 be the probabilities that the levels L_1, L_2, and L_3 are ionized, such that $\Sigma u = 1$; and let f_1, f_2, and f_3 be the fluorescence yields. The total probability of emission of a quantum characteristic of the level L_s is then proportional to $u_s f_s$. If Γ_s is the total width of the level, the total radiation width is $\Gamma_s f_s$, and if x is the fractional probability of emission of radiation of a particular line from that level, its contribution to the radiation width will be $\Gamma_s f_s x$. The difference $\Gamma_s(1 - f_s)$ measures the probability of occurrence of nonradiating transitions from the level L_s. If, however, Auger processes are possible which shift the vacancy from one L level to another and produce a doubly ionized atom by ejection of an electron from a level of lower energy, the probability of excitation of a level L_s may depend on the primary excitation of the L level of higher energy. Let A_{rs} be the probability that a vacancy produced in the level L_r is transferred to the level L_s by a nonradiative transition, the other vacancy in the doubly ionized atom being in an M level or one of lower energy. The number of quanta radiated by the three L levels will then be given by the quantities q_1, q_2, and q_3, where:

$$\begin{aligned} q_1 &= u_1 f_1 \\ q_2 &= f_2(u_2 + A_{12}u_1) \\ q_3 &= f_3(u_3 + A_{23}(u_2 + A_{12}u_1) + A_{13}u_1). \end{aligned} \tag{1}$$

In deducing these equations it has been assumed that the fluorescence yield of the state L_s, produced by a transition from the state L_r, is the same as in the case when the level L_s is excited by the primary process. The justification for this assumption is as follows. The probability per unit time of decay of the doubly ionized state is, to a first approximation, $\Gamma_s + \Gamma_p$, where Γ_s is the width of the L_s state and Γ_p is the width of the low energy state produced by the Auger transition. Let f_s be the fluorescence yield of the L_s level, and let f_s' be the effective fluorescence yield of this level in the doubly ionized state. When the L_s vacancy is filled first, the yield of radiation by transitions from L_s is $f_s'\Gamma_s/(\Gamma_s + \Gamma_p)$. When the low energy vacancy is filled first, the yield will be very nearly $f_s\Gamma_p/(\Gamma_s + \Gamma_p)$ since the new vacancy produced by this process will be of lower energy still and will have little effect on transitions from L_s. The total yield by transitions from L_s is therefore

$$(f_s\Gamma_p + f_s'\Gamma_s)/(\Gamma_s + \Gamma_p).$$

It will be shown that the most frequent double ionizations are vacancies in L_3 and either M_4 or M_5 (created by Auger transitions from L_1). The total width of the L_3 level is approximately equal to the total width of M_4 or M_5 in the case of heavy elements; hence approximately $\Gamma_s = \Gamma_p$. Moreover, f_s' must nearly equal f_s because the difference can result only from the vacancy in the M levels. The above expression, the total radiation yield by transitions from L_s, reduces to approximately f_s, as assumed in deriving Equations (1).

The Coster–Kronig Transitions

Transitions of the type which have just been described contribute to the coefficient A_{13}; it will now be shown that the greater part of that coefficient is derived from these transitions only, and that, to a first approximation, the other coefficients may be neglected.

The existence of an Auger transition, in which a vacancy in the L_1 level is filled to produce a vacancy in the L_3 level and another in the M levels, was invoked by Druyvesteyn (14) and others to explain the presence of the satellites of the line $L\alpha_1$ ($L_3 \rightarrow M_5$). These satellites, as is well known, are observed with appreciable intensity only for atoms with atomic numbers less than 50 and greater than 73. The explanation of this phenomenon was given by Coster and Kronig (12); they showed that the difference in the energies of the levels L_1 and L_3 should exceed that of the level M_5 corresponding to the element next above it in the periodic table. That the excitation of the satellites of the $L\alpha_1$ depends on the energy of the cathode rays exceeding the excitation potential of L_1 was demonstrated by Coster, Kuipers, and Huizinga (13) for Nb ($Z = 41$).

The probability of Auger transitions of this type, when permitted by the Coster–Kronig rule, depends, among other things, on the extent to which the wave function of the ejected electron overlaps the wave functions of the states of the atom involved in the transition. Only those electrons are ejected to an appreciable extent which can carry off an appreciable angular momentum. Further, those transitions will be most probable for which the energy of the ejected electron is least. For this reason transitions of the Coster–Kronig type are more probable than any others when they are permitted energetically. The increase in the probability of these transitions when the energy of the ejected electron is decreased has been demonstrated in experiments which have been made to determine the variation of intensity of the satellite line relative to the parent line as a function of atomic number (Z); as Z is increased, the satellite intensity increases to a maximum, followed by an abrupt decrease for atomic numbers within one or two units less than the maximum permissible by the energy condition of Coster and Kronig. This variation of the intensity of the $L\alpha$ satellites has been observed by Hirsh and Richtmeyer (21), and by Randall and Parratt (32); a similar intensity variation occurs in the satellites of $L\beta_2$ ($L_3 \rightarrow N_5$) which have been studied by Miss Pearsall (27). In the region of high atomic numbers, the intensities of the satellites of $L\alpha_1$ increase

abruptly at $Z = 74$, as shown in unpublished data of Shrader, quoted by Cooper (9). The onset of the transitions of the type $L_1 \rightarrow L_3M_{4,5}$ must be accompanied by an increase in the width of the L_1 state and a decrease in its fluorescence yield. Consequently, at this point the intensities of the radiations with L_1 as the initial state must decrease relatively to those characteristic of L_2 and L_3. This phenomenon has been studied by Cooper in elements of highest atomic numbers and by Coster and de Langen (11) in elements in the region of silver.

Coster and Kronig (12) have also showed that an Auger transition is possible from the L_1 level to the L_2 level with the ejection of an electron from the M_4 or M_5 level for atomic numbers less than that of Nb ($Z = 41$). This has been demonstrated in experiments on the intensity of the satellites of the line $L\beta_1$, characteristic of the L_2 level. Hirsh (20) has shown that an intensity anomaly exists in the vicinity of atomic number 40, and his observations have been confirmed by de Langen (24), by measurements of the intensities of the satellites of $L\beta_1$ for Zr($Z = 40$), Nb(41), and Mo(42). De Langen (24) has also shown that the relative intensities of the L_1 lines, $L\beta_3$ and $L\beta_4$, increase relatively to that of $L\beta_1$, from Zr to Mo, owing to the decreasing probability of this Auger transition. For atomic numbers in the region of 70 and above, transitions of this type are not possible.

Transitions in which the vacancy is shifted from the L_2 to the L_3 level are possible, energetically, with ejection of an M electron for atomic numbers above 90, and with ejection of electrons lying in states of lower energy, over the whole range of atomic number of interest in this paper. Generally, however, the ejection of an N electron in such a process is very much less probable than that of an M electron, when the energy conditions permit the latter.

When transitions of the Coster–Kronig type are permitted, they will have a predominating influence on the distribution of energy in the L spectrum; the radiation width of the L_1 level will be low compared with the total width of that level, and the excitation of the L_3 level will be increased. The coefficient, A_{13}, therefore, will be large and will be computed. Even when these transitions are energetically impossible, this coefficient, A_{13}, may not vanish, however, because transitions of the type $L_1 \rightarrow L_3N$ can still occur. Even if the probability of such a process is only 10% of that of the Coster–Kronig transition when fully developed, the value of A_{13} could be about 0.2, since the total width of the L_1 level is about 3 v. at tantalum, and 10% of the maximum width of the Coster–Kronig transitions is about 0.6 v. Transitions of this kind should produce satellites of $L\alpha$ and $L\beta_2$ which do not show the 'intensity anomaly'. Such satellites have been studied by Pincherle (30), but their origin is not entirely clear and the quantitative information is not sufficient for an estimate of the width of the L_1 level due to this cause.

Transitions of the type $L_2 \rightarrow L_3N$ must contribute to the width of the L_2 level. These transitions must also be associated with the production of satellites of $L\beta_2$ which do not show an 'intensity anomaly'; here again there is

no evidence to permit a computation of the width due to this process. However, the extremely low intensities of the satellites of $L\beta_2$ for the atomic numbers below 68 (cf. Richtmeyer and Kaufman (35)) indicate that the probabilities of the processes $L_1 \rightarrow L_3N$ and $L_2 \rightarrow L_3N$ are negligible in comparison with those of the other Auger processes which can occur.

Transitions of the type $L_1 \rightarrow L_2N$ are energetically possible for most of the N levels in the heavy elements. They should produce Auger electrons with less energy than those produced by either of the processes just considered and should be, therefore, more probable. These transitions contribute to the excitation of the L_2 level, but the magnitude of the coefficient A_{12} must be small except possibly at tantalum, because the probability of the process is certainly very much smaller than that of the Coster–Kronig transitions.

In the absence of quantitative information the coefficients A_{12} and A_{23} will be assumed to be zero and dropped from Equation (1). This assumption may be questioned on the grounds that the transition leading to doubly ionized M levels, or double ionization in the M and the N levels, might be less likely to occur because the energies of the Auger electrons are greater. The justification for the assumption can rest only on the results of experiment. Setting A_{12} and A_{23} equal to zero, Equation (1) reduces to:

$$q_1 = u_1 f_1 ; \qquad q_2 = u_2 f_2 ; \qquad q_3 = f_3(u_3 + A_{13}u_1). \tag{2}$$

A_{13} will be computed on the assumption that the Coster–Kronig process is the only one which contributes to it, as explained above.

Experimental Fluorescence Yields

Reliable experimental results are available only for the fluorescence yield of the L_3 levels. Measurements have been made by Küstner and Arends (23) for elements between tantalum and bismuth, and by Stephenson (38) for lead, thorium, and uranium. These authors used essentially the same method: a determination of the amount of the secondary radiation emitted from a target irradiated with X-rays with a wave length lying between the absorption limits of the L_2 and L_3 levels. Their results are given in the first and second rows of Table I, and are plotted in Fig. 2; the agreement between their results is satisfactory.

Küstner and Arends (23) have also attempted to measure the fluorescence yields of the L_2 and L_1 levels by decreasing the wave length of a monochromatic radiation until it lay between the absorption limits of the L_1 and L_2 levels and just shorter than the latter. The increase in yield of the secondary radiation was interpreted as being due to the characteristic radiation of the level for which the wave length of the absorption limit is just above that of the primary radiation. But above tantalum this interpretation of the results should not apply to the L_1 level owing to the secondary excitation of the L_3 level. Their figures for the fluorescence yield of the L_2 level are not subject to this objection, if the coefficient A_{12} is assumed to be zero; but the results show a decrease with

increasing atomic number which is very difficult to understand since the radiation width must increase rapidly with atomic number and the total width of the L_2 level changes very little.

TABLE I

EXPERIMENTAL VALUES FOR THE FLUORESCENCE YIELD OF THE L_3 LEVEL

Z	Ta(73)	W(74)	Ir(77)	Pt(78)	Au (79)	Pb(82)	Bi(83)	Th(90)	U(92)
Küstner & Arends (23)	0.191	0.207	0.244	0.262	0.276	0.337	0.367	—	—
Stephenson (38)	—	—	—	—	—	0.32	—	0.42	0.44

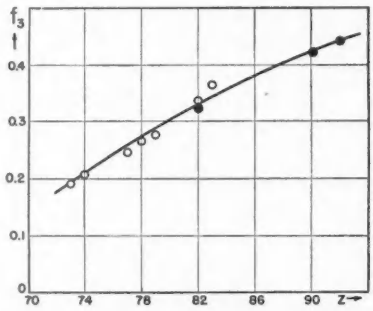

FIG. 2. *The fluorescence yield of the L_3 level as a function of the atomic number. Open circles: according to Küstner and Arends (23); full circles: according to Stephenson (38).*

Radiation Widths and Total Widths

Owing to the absence of experimental data on the fluorescence yields of the L_1 and L_2 levels, these quantities will be deduced by dividing theoretical radiation widths by the experimental values of the total widths. To check the validity of this method of calculation, the calculated values of the fluorescence yield of the L_3 level will be compared with the experimental values. The coefficient A_{13} is given by the ratio of the partial width of the L_1 level due to the Coster–Kronig transitions to the total width of that level. The partial width, in this case, can be deduced from measurements of the line widths. The total widths can be measured directly by studying the shapes of the absorption edges of the three levels. The differences in the widths, however, can be obtained much more accurately by measurement of the widths of the spectrum lines; since the width of a line is equal to the sum of the widths of the initial and final state, the difference in the widths of two lines with the same final state is equal to the difference in the widths of the initial states. When the average of this result is taken for several lines, an accurate value is obtained.

For gold ($Z = 79$), the widths of the three L levels have been measured by Richtmeyer, Barnes, and Ramberg (34) by fitting the constants of a theoretical formula to suit the experimental curve for the shape of the absorption edges. They showed that if the absorption in the edge is due to the ejection of the electron into a region of unoccupied levels in which the distribution in energy is uniform and continuous, the shape of the absorption edge should be given by the formula:

$$\mu(\nu) = c\left[\frac{1}{2} - \frac{1}{\pi}\tan^{-1}\left(\frac{\nu_{E_0} - \nu}{\Gamma/2}\right)\right],$$

where ν_{E_0} is the frequency of ionization of the level of the free atom, ν the frequency considered, c a constant, and Γ is the total width of the level for half-absorption. On the low frequency side the shape of the edge should correspond to that given by this formula; but on the high frequency side, the shape is distorted by the uneven distribution in energy of the states of the free electron in the solid material of the target. This phenomenon is particularly evident in the absorption edge of the L_1 level. Richtmeyer, Barnes and Ramberg considered the measurement of the width of the L_3 level to be the most accurate (4.4 v.). The widths of the remaining levels are calculated from this by using the differences in the widths of the levels obtained from their measurements of the line widths. They found that the width of the L_2 level is less than that of L_3 by 0.7 v. (a result which is confirmed by the measurements of Richtmeyer and Barnes (33) on the widths of the $K\alpha_1$ and $K\alpha_2$ lines of tungsten), and that the width of the L_1 level is greater by 4.3 v. Their final values are, therefore: L_1:8.7 v.; L_2:3.7 v.; and L_3:4.4 v.

The level widths for tungsten and platinum have been measured by Bearden and Snyder (4) and those of tungsten, more recently, by Coster and de Lang (10) by fitting the theoretical curve at the low frequency end to the observed shapes of the absorption edges. The results are summarized in Table II.

TABLE II

TOTAL WIDTHS OF L LEVELS IN VOLTS

C-L: Coster and de Lang, ref. (10); B-S: Bearden and Snyder, ref. (4); R-B-R: Richtmeyer, Barnes, and Ramberg ref. (34)

	Tungsten		Platinum	Gold
	C-L	B-S	B-S	R-B-R
L_1	9.5	4.9 ± 1.0	8.0 ± 1.0	8.7
L_2	—	3.0 ± 0.5	3.5 ± 0.5	3.7
L_3	3.1	3.4 ± 0.5	3.6 ± 0.5	4.4

Coster and de Lang's value for the width of the L_1 level is very discordant; this discrepancy illustrates the difficulty of these measurements, especially those relating to the L_1 level, which, for tungsten, is distorted by the presence of the 'white line' at the higher frequency end of the absorption edge.

The constancy of the widths of the L_2 and L_3 levels between tantalum and bismuth might seem surprising in view of the fact that the radiation widths are increasing rapidly with atomic number. This is explained by the fact that the radiation widths are small in comparison with the total widths, and probably change over this range by only about 0.5 v., which is of the order of the error in the measurements in the total width. The constancy of the total widths of these levels is demonstrated in the measurements of Williams (42) and of Cooper (9).

By plotting the results of Table II for the width of the L_3 levels against the atomic number, a mean value is obtained. For $Z = 76$, the width is 3.6 v.; this value will be used as the basis of further calculations.

Using a nonrelativistic theory, Ramberg and Richtmeyer (31) have calculated the Auger widths and the radiation widths of the levels for gold. For the radiation widths they give the following figures:

$$L_1 = 1.8 \text{ v.}; \qquad L_2 = 2.9 \text{ v.}; \qquad L_3 = 1.8 \text{ v.}$$

If the total width is taken to be 4.0 v. for the L_3 level in gold, the fluorescence yield is about 0.4 for this level, which is too high in comparison with the experimental value—about 0.27. Pincherle (28) has also calculated the radiation and Auger widths on a nonrelativistic basis, and finds 1.6 v. for the width of the L_3 level in gold. However, the nonrelativistic calculations are unsatisfactory. They do not give the correct ratio for the intensities of the $L\beta_3$ and $L\beta_4$ doublet, and in the case of Ramberg and Richtmeyer's work, they predict total widths which are too large (these authors find that the total width of the L_3 level in gold is in excess of 13.7 v.). The width of the K level is also too large; they find 66 v. for the width of this level and point out that the actual width is about 54 v., a value which is obtained by an extrapolation from the experimental width for tungsten by the fourth power of the atomic numbers of these elements (cf. Richtmeyer and Barnes (33)).

The relativistic calculations of Massey and Burhop (26) lead to a lower value for the width of the K level in gold (about 47 v.) nearer the correct figure and also give the correct ratio for the intensities of the $L\beta_3$ and $L\beta_4$ lines.* Their estimates are used for the basis of the calculations of the fluorescence yields in this paper. Since these authors did not calculate the radiation widths of some of the weaker lines, estimated values of the latter are included here in the total radiation width. In Table III, the contribution of the more important lines to the total width is given in terms of percentages, the calculations being made (for L_2 and L_3) on the basis of Jönnson's (22) measurements for tungsten, with the assumption that the relative intensities of the lines originating in one level remain approximately constant over the range of atomic numbers between tantalum and bismuth. For the L_1 radiations, the calculations are based on the measurements of Bötzkes (6).

* *Their predictions for the relative intensities of the Auger electrons ejected in the processes which produce a double ionization in the L levels do not seem to be in agreement with experiment (cf. Ellis (15)).*

Using the values given in Table III, the radiation widths obtained by Massey and Burhop, for gold, are equivalent to:*

L_1 : 0.70 v.; L_2 : 1.18 v.; L_3 : 0.92 v.

To obtain the radiation widths for neighboring elements, these figures may be multiplied by the ratio of the fifth power of the atomic numbers, which is approximately the variation with atomic number shown by Massey and Burhop's values for antimony, gold, and uranium. For $Z = 76$, the total width will be 3.6 v. (as discussed above) and the radiation width of the L_3 level will be 0.77 v. The Auger width is equal to the difference—2.8 v. If this width is assumed to be constant, the best value for the total width in gold is 3.7 v., giving a rather low value—0.25—for the fluorescence yield of the L_3 level, but possibly not outside the experimental error of the measurements of Küstner and Arends. The radiation width of this level in uranium is 2.16 v. if calculated from Massey and Burhop's figures and from Allison's (1) value of the intensity of the line $L\beta_2$ relative to that of $L\alpha_1$. Assuming that the Auger width is constant throughout this range of atomic number, at 2.8 v., the fluorescence yield of uranium in the L_3 level is found to be 0.43, which is in agreement with the results of Stephenson (see Fig. 2).

TABLE III

RELATIVE CONTRIBUTIONS TO THE RADIATION WIDTHS IN PERCENTAGES

L_1		L_2		L_3	
β_3	44	β_1	85	α_1	75
β_4	32	η	2	α_2	9
γ_2	8	γ_1	13	β_6	1
γ_3	13	γ_5	1	β_2	13
γ_4	3			1	3

The width of the lines characteristic of the L_1 level as an initial state have been studied in detail by Cooper (9). He measured the widths of the lines $L\beta_4(L_1 \rightarrow M_2)$, $L\beta_3(L_1 \rightarrow M_3)$, $L\gamma_2(L_1 \rightarrow N_2)$ and $L\gamma_3(L_1 \rightarrow N_3)$ and showed that they increased continuously from tungsten to thallium, and by the same amount. The variation of these widths with atomic numbers is illustrated in Fig. 3, which is taken from Cooper's results. In this figure, the mean difference of the width of a line for atomic number Z from that of the same line for tantalum is plotted against Z, the ordinate in each case being an average of the differences corresponding to the four lines referred to above. The accuracy of each point is about 0.2 v. The increase in widths at tantalum illustrates the appearance of the Coster–Kronig transitions above this element; at thallium, the probability of the two processes $L_1 \rightarrow L_3M_{4,5}$ was found to

* *The transition probabilities given by Massey and Burhop are measured in transitions per unit atomic time; it has been assumed in making these calculations that a probability of one in these units is equivalent to a width of 27.4 ev.*

be a maximum (not shown in the figure) by Shrader, according to some unpublished results quoted by Cooper. Shrader found that the intensity of the $L\alpha_1$ satellite relative to the parent line rising with increasing atomic number

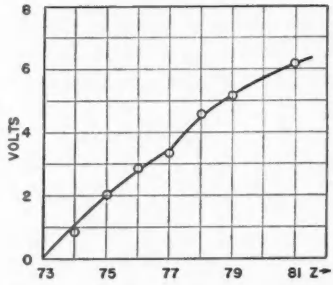

FIG. 3. *The difference between the width of the L_1 level in an element of atomic number Z and the width of the L_1 level in tantalum ($Z = 73$), after Cooper (9). The difference between the width of a line of the L spectrum for atomic number Z and that of the same line for tantalum is averaged over the lines $L\beta_3$, $L\beta_4$, $L\gamma_2$, and $L\gamma_3$, and is plotted, in volts, against the atomic number.*

from zero at tantalum on account of the $L_1 \rightarrow L_3M_5$ process has a discontinuity at platinum ($Z = 78$) owing to the onset of the $L_1 \rightarrow L_3M_4$ process, increases to a peak in the region of thallium, and then falls slowly to thorium. The reduction in the intensity of the satellites above the thallium–bismuth region is doubtless due, in part, to the rising radiation width and also to the increasing energy of the Auger electron.

Now the ordinates of Fig. 3 are equal to the partial widths of the L_1 levels due to the Coster–Kronig transitions. Since the experimental results for the total widths of the L_1 levels are unreliable, these widths must be obtained from the constituent parts: the radiation width, the Coster–Kronig width, and a constant width representing the remainder of the nonradiating transitions. The radiation width is obtained from the results of Massey and Burhop for gold with a suitable adjustment for the variation with atomic number; the constant width is obtained from the gold results. It has been shown that the best value for the width of the L_1 level in gold is 8.0 v.; the Coster–Kronig width is 5.1 v., and radiation width is 0.7 v.; the constant width is therefore 2.2 v. The total widths of the L_1 level are listed in the first row of Table IV: the fluorescence yield, f_1, in the second row. It will be seen that the yields are low and roughly constant over a wide range. The low value of this fluorescence yield is consistent, in general, with the low values deduced by Pincherle (29) which are necessary to account qualitatively for the very low intensities of the L_1 radiation which are observed in cathode ray excitation. The values obtained here are lower than that obtained by Küstner and Arends for tantalum ($f_1 = 0.28$), where their method might be expected to give accurate results.

TABLE IV

FLUORESCENCE YIELDS AND COEFFICIENTS CALCULATED FROM THE THEORETICAL RADIATION WIDTHS OF MASSEY AND BURHOP AND LEVEL WIDTHS OBTAINED FROM TABLE II

The values in brackets are obtained by interpolation or extrapolation of these figures

Z	73	75	77	79	81	83	90	92
Γ_1, v.	2.8	4.8	6.1	8.0	9.0	(9.2)	(9)	(9)
f_1, %	17	11.0	10.0	9.0	9.0	(10.0)	(15)	(16)
A_{13}, %	0	42	54	65	67	(70)	(60)	(60)
f_2, %	31	33	37	39	43	46	56	59
f_3, %	18	20	23	25	27	30	39	41

The values of the coefficient A_{13} are listed in the third row of the table. The numerical values for f_2 and f_3 are given in the fourth and fifth rows of the table. These quantities are equal to the ratios of the radiation widths (calculated from Massey and Burhops figures) to the total widths obtained by adding the sum of these radiation widths to a constant quantity representing the nonradiating transitions. The value for this constant quantity is taken from the figures for gold. The value of f_2 for tantalum is close to that obtained by Küstner and Arends for this element. It has already been pointed out that the theoretical figures of Massey and Burhop lead to a value for the fluorescence yield in gold which is about 10% lower than the experimental value. It is possible that all these yields are too low by a similar amount, but rather than make an arbitrary adjustment of the figures in this ratio in order to bring the fluorescence yield of L_3 into agreement with the experimental value for gold, the theoretical values for the fluorescence yields given in Table IV will be used in subsequent calculations as they stand.

X-Ray Intensities in Cathode Ray Excitation

A comparison of the intensities of the spectrum lines in cathode ray excitation might be expected to give a check on the ratios of the fluorescence yields which have been listed in Table IV. However, such a comparison is difficult to make because the relative excitation of the levels is not known with certainty. It appears that the greater part of the X-ray emission from thick targets arises from indirect or fluorescence excitation. The relative excitation of L radiation by fluorescence and cathode rays in targets of heavy elements does not seem to have received attention; but the work of Hansen and Stoddard (18), and of Stoddard (39, 40) on the excitation of the K radiations in copper, palladium, and in gold, shows that the indirect excitation greatly predominates in the heavy elements. If, as would appear very likely, this is also the case for the production of the L radiations, it is difficult to know what values to assign to the quantities u_1, u_2, and u_3. Further, the experimental results which are available have been corrected for equal probability of ionization for each electron in the levels on the assumption that cathode ray excitation only

is effective; even if these corrections are justified they are very dubious, because there in a lack of agreement between the variation in energy of the ionization function, as determined for the K level by Webster, Hansen, and Duveneck (41), and by Clark (7), and the theoretical curves of Rosseland(36), Bethe (5), and others, and because the relative values of the peaks of the ionization functions must be deduced from these theoretical formulae. Finally, the corrections do not allow for the secondary excitation of the L_3 level by the Coster–Kronig process.

A comparison of the intensities of the lines characteristic of the L_1 and L_2 levels might be expected to show the least discordance with experiment because the ionization energies of these levels are the closest together. If u_1 is equated to u_2, the value for the ratio of the intensities of the lines $L\beta_3$ and $L\beta_1$ will be obtained from the formula:

$$I\beta_3/I\beta_1 = \frac{f_1}{f_2} \cdot \frac{\lambda\beta_1}{\lambda\beta_3} \cdot \frac{C\beta_3}{C\beta_1},$$

where the λ's are the wave lengths of the lines and $C\beta_3$ and $C\beta_1$ are the fractional radiation probabilities given in Table III. If the excitation of these levels is indirect, in the main, the intensities would be expected to be less than those given by this equation. The wave length of these lines is very nearly equal in the range of atomic number of interest here. Hence,

$$I\beta_3/I\beta_1 = 0.52\, f_1/f_2. \qquad (3)$$

The ratios of the intensities of $L\beta_3$ to $L\beta_1$ have been measured in some instances by Hicks (19), Jönnson (22), and by Bötzkes (6). Cooper (9) has shown that the intensities of the L_1 lines fall relatively to that of $L\beta_1$ for increasing atomic numbers above tantalum, and has given uncorrected figures for the percentage intensities of $L\beta_3$, $L\beta_4$, $L\gamma_3$, and $L\gamma_2$ with respect to $L\beta_1$. The ratios of the observed intensities of $L\beta_3$ to $L\beta_1$, and $L\gamma_2$ to $L\gamma_1$ are collected in Table V.

TABLE V

EXPERIMENTAL VALUES FOR THE RATIOS OF THE INTENSITIES OF THE LINES $L\beta_3$ TO $L\beta_1$, AND $L\gamma_2$ TO $L\gamma_1$, IN PERCENTAGES

Z	Ta 73	W 74	Re 75	Os 76	Ir 77	Pt 78	Au 79	Tl 81
$L\beta_3$ to $L\beta_1$								
Hicks (19)	13	—	—	—	—	—	—	—
Jönnson (22)	—	16	—	—	—	—	—	—
Bötzkes (6)	12	—	—	—	—	—	—	—
Cooper (9)	18.5	16.2	15.2	13.9	14.2	14.1	13.0	9.4
$L\gamma_2$ to $L\gamma_1$								
Jönnson (22)	—	17	—	—	—	16	—	—
Bötzkes (6)	17	—	—	—	—	—	—	—
Cooper (9)	17.3	14.1	13.3	11.5	12.4	—	10.5	11.0

Substitution of the values for f_1 and f_2 from Table IV into Equation (3) gives ratios for the intensities of the lines $L\beta_3$ to $L\beta_1$ which are in general agreement with those of Table V, except at tantalum where the result is too high. At tantalum the ratio should be 28%, the observed value is about 17%; at Re ($Z = 75$), Equation (3) gives 17% in agreement with Table V; in Au (79), 12%; in Tl (81), 11%, also in general agreement. For the ratios of the γ lines, the ratio of $C\gamma_2$ to $C\gamma_1$ is 0.6, which gives figures about 10% higher than those for the ratios of $L\beta_3$ to $L\beta_1$. A large error at tantalum (73) is to be expected because it is in this element that the calculation of the total width of the L_1 level is the least accurate.

A comparison of the intensities of the lines $L\beta_1$ and $L\alpha_1$ may be made in a similar manner. For cathode ray excitation, the 'corrected' experimental results should be comparable with the values obtained from a formula with u_1 and u_2 proportional to unity, and u_3 proportional to 2. Thus:

$$I\beta_1/I\alpha_1 = \frac{u_2}{u_3 + A_{13}u_1} \cdot f_2/f_3 \cdot \left(\frac{\lambda\alpha_1}{\lambda\beta_1}\right) \cdot C\beta_1/C\alpha_1$$

$$= \frac{1}{2 + A_{13}} \cdot f_2/f_3 \left(\frac{\lambda\alpha_1}{\lambda\beta_1}\right) \cdot C\beta_1/C\alpha_1 \qquad (4)$$

Again, if fluorescence is the predominating mode of excitation, the calculated intensities should be appreciably less than those obtained from this equation, because the fluorescence processes, generally, favor the excitation of the L_3 level relative to that obtained with cathode ray bombardment. Equation (4) does not lead to satisfactory agreement with the experimental determinations. Some experimental values are listed in Table VI.

TABLE VI

EXPERIMENTAL VALUES FOR THE RATIOS OF THE INTENSITIES OF THE LINES $L\beta_1$ AND $L\alpha_1$ CORRECTED ACCORDING TO THE ROSSELAND FUNCTION

Ta			W	Pt
Hicks (19)	Andrew (2)	Bötzkes (6)	Jönnson (22)	Jönnson (22)
0.57	0.72	0.60	0.52	0.52

In the region of atomic number of interest here, the ratio $C\beta_1/C\alpha_1$ is 1.13 and $\lambda\alpha_1/\lambda\beta_1$ is about 1.15. For tantalum, the intensity ratio is found to be 1.1. The most accurate value of the intensity ratio is probably that of Andrew (2), who used an ionization chamber for detection of the radiation. His experimental result, corrected with the Rosseland function, is 0.72, and, corrected with the empirical Webster formula, it is 0.58. The disagreement, in this element, is not due to a lack of consideration of the Coster–Kronig processes: it is probably due to the indirect excitations, which, as pointed out above, favor the excitation of the L_3 level. That the ratios of the fluorescence

yields, f_2 and f_3, are approximately correct, at least for bismuth, is shown in the measurements of the L radiations emitted following the internal conversions produced in the disintegration of ThB, which are described in the following paper.

The Total Fluorescence Yields

(1) *Fluorescence Excitation*

The total fluorescence yield may be defined as the total number of quanta emitted per ionization of the L levels. Remembering that $\Sigma u = 1$, this quantity is given by adding the terms of Equation (2):

$$f_0 = f_1u_1 + f_2u_2 + f_3(u_3 + A_{13}u_1). \tag{5}$$

Experimental values for the total fluorescence yield have been given by Lay (25) using fluorescence excitation by the K radiation of molybdenum. In this case the relative excitations of the three L levels may be computed from the magnitudes of the absorption jumps given by Compton and Allison (8). From tungsten to uranium, the appropriate value of u_1 differs little from 0.18, u_2 varies between 0.29 to 0.35, and u_3 between 0.53 to 0.46. The results of the evaluation of Equation (5) are given in Table VII together with

TABLE VII

TOTAL FLUORESCENCE YIELDS WITH FLUORESCENCE EXCITATION (WITH MOLYBDENUM K RADIATION)

Z	W 74	Os 76	Pt 78	Au 79	Pb 82	Bi 83	U 92
Calculated from Eq. (5) and Table IV	0.23	0.26	0.29	0.29	0.33	0.36	0.47
Lay's results (25)	0.30	0.35	0.35	0.36	0.40	0.40	0.45

the results of Lay. It will be seen that the calculated figures are somewhat lower than the empirical results; since the excitation of the L_3 level is the most important, this lack of agreement is probably due to the low figures for the fluorescence yields, f_3, which have been used (Table IV).

(2) *Internal Conversion in L Levels*

The total fluorescence yields to be expected from conversion in the L levels are given in Table VIII. These have been calculated for $u_1 = 0.90$, $u_2 = 0.09$, and $u_3 = 0.01$, which are approximately in the ratios of the excitations observed by Arnoult (3) for the internal conversion of the 40 kev. transition of ThC–C″. The results are very similar to the figures calculated for fluorescence excitation although the relative excitations are very different.

In the following paper, the results of Table VIII have been compared with the experimental results for the fluorescence yield for L conversions in the disintegration of ThC (for which the product nucleus is thallium) and for

TABLE VIII

TOTAL FLUORESCENCE YIELDS FOR L CONVERSION

	q_1	q_2	q_3	f_0
Ta 73	0.15	0.02	0	0.18
Re 75	0.10	0.03	0.08	0.21
Ir 77	0.095	0.033	0.112	0.24
Au 79	0.081	0.035	0.150	0.27
Tl 81	0.081	0.039	0.165	0.29
Bi 83	0.090	0.041	0.192	0.32
Th 90	0.135	0.050	0.215	0.40
U 92	0.144	0.053	0.225	0.42

RaD (bismuth). The ratio of f_2 to f_3 is estimated from selective absorption measurements on the L radiations emitted following internal conversion in the K levels in bismuth; it is shown that the values used for these quantities are about 10% too low, in general agreement with a remark in a previous paragraph in this paper. This leads to the conclusion that the figures of Table VIII are also too low by about the same amount and for the same reason. Further, the results for RaD indicate that the yield of radiation from the L_2 level given in Table VIII is too low; this would seem to show that the neglect of the coefficient A_{12} is not justified in the case of internal conversion in the L levels where the excitation of the L_1 level greatly exceeds the excitation of the other levels. Taking this into account, the figures for f_0 in the table should be increased by some 25%.

References

1. ALLISON, S. K. Phys. Rev. 32 : 1. 1928.
2. ANDREW, V. J. Phys. Rev. 42 : 591. 1932.
3. ARNOULT, R. Ann. phys. 12 : 240. 1939.
4. BEARDEN, J. A. and SNYDER, T. M. Phys. Rev. 59 : 162. 1941.
5. BETHE, H. A. Ann. Physik, 5 : 325. 1930.
6. BÖTZKES, M. Z. Physik, 89 : 667. 1934.
7. CLARK, J. C. Phys. Rev. 48 : 30. 1935.
8. COMPTON, A. H. and ALLISON, S. K. X-rays in theory and experiment. 2nd ed. D. Van Nostrand Company, Inc., New York. 1935.
9. COOPER, J. M. Phys. Rev. 61 : 234. 1942.
10. COSTER, D. and DE LANG, H. Physica, 13 : 385. 1947.
11. COSTER, D. and LANGEN, K. W. DE. Physica, 3 : 282. 1936.
12. COSTER, D. and KRONIG, R. DE L. Physica, 2 : 13. 1935.
13. COSTER, D., KUIPERS, H. H., and HUIZINGA, W. J. Physica, 2 : 870. 1935.
14. DRUYVESTEYN, M. J. Dissertation, Groningen. 1928.
15. ELLIS, C. D. Proc. Roy. Soc. London, A, 139 : 336. 1933.
16. FRILLEY, M., SURUGUE, J., and TSIEN, S-T. J. phys. radium, 7 : 350. 1946.
17. FRILLEY, M. and TSIEN, S-T. Compt. rend. 220 : 144. 1945.
18. HANSEN, W. W. and STODDARD, K. B. Phys. Rev. 43 : 701. 1933.
19. HICKS, V. Phys. Rev. 36 : 1273. 1930.
20. HIRSH, F. R. Phys. Rev. 50 : 191. 1936.
21. HIRSH, F. R. and RICHTMEYER, F. K. Phys Rev. 44 : 955. 1933.
22. JÖNNSON, A. Z. Physik, 36 : 426. 1926.

23. KÜSTNER, H. and ARENDS, E. Ann. Physik, 22 : 443. 1935.
24. LANGEN, K. W. DE. Physica, 6 : 27. 1939.
25. LAY, H. Z. Physik, 91 : 533. 1934.
26. MASSEY, H. W. S. and BURHOP, E. H. S. Proc. Cambridge Phil. Soc. 32 : 451. 1936.
27. PEARSALL, A. Phys. Rev. 46 : 694. 1934.
28. PINCHERLE, L. Nuovo cimento, 12 : 81. 1935.
29. PINCHERLE, L. Nuovo cimento, 12 : 162. 1935.
30. PINCHERLE, L. Phys. Rev. 61 : 225. 1942.
31. RAMBERG, E. G. and RICHTMEYER, F. K. Phys. Rev. 51 : 913. 1937.
32. RANDALL, C. A. and PARRATT, C. G. Phys. Rev. 57 : 786. 1940.
33. RICHTMEYER, F. K. and BARNES, S. W. Phys. Rev. 46 : 352. 1934.
34. RICHTMEYER, F. K., BARNES, S. W., and RAMBERG, E. G. Phys. Rev. 46 : 843. 1934.
35. RICHTMEYER, F. K. and KAUFMAN, S. Phys. Rev. 44 : 605. 1933.
36. ROSSELAND, S. Phil. Mag. 45 : 65. 1923.
37. STAHEL, E. Helv. Phys. Acta, 8 : 651. 1935.
38. STEPHENSON, R. J. Phys. Rev. 51 : 637. 1937.
39. STODDARD, K. B. Phys. Rev. 46 : 837. 1934.
40. STODDARD, K. B. Phys. Rev. 48 : 43. 1935.
41. WEBSTER, D. J., HANSEN, W. W., and DUVENECK, F. B. Phys. Rev. 43 : 839. 1933.
42. WILLIAMS, J. H. Phys. Rev. 45 : 71. 1934.

THE EMISSION OF L RADIATION IN THE DISINTEGRATION OF ThC AND RaD[1]

By B. B. Kinsey[2]

Abstract

The amount of L radiation resulting from the K conversion of γ-radiation emitted in the disintegration of ThB has been measured and found to be in general agreement with the calculations of the preceding paper. This amount, which is determined mainly by the fluorescence yield of the L_3 level, confirms the results of Küstner and Arends; selective absorption measurements confirm the calculated value for the ratio of the fluorescence yields of the L_2 and L_3 levels for the product element (bismuth). The yields of L radiation resulting from the L conversion of the low energy γ-radiation emitted in the disintegrations of ThC and of RaD have been measured and compared. In the first case the yield is too high, and in the second it is too low compared with the calculated values. Selective absorption measurements indicate that the yields of the L_1 and L_2 levels, taken together, are equal to that of the L_3 level. It is shown that the experimental result for ThC can be explained on the assumption that Auger transitions of the type $L_1 \rightarrow L_2N$ play some part in the distribution of energy in the spectrum; the result for RaD, which is consistent with the results of Stahel (1935), indicates that the low energy γ-transitions emitted by that element and converting in the L levels are excited in less than 100% of the disintegrations.

Introduction

The object of the measurements described in this paper was to determine the amount of L radiation which is emitted following the internal conversion of γ-radiation in the L levels in the heavy elements.

The yield of L radiation has been calculated in the previous paper where it was shown that a determination of this quantity is of some interest in the case of RaD. Now the determination of the fluorescence yield of L radiation from RaD requires both a measurement of the amount of L radiation emitted and a knowledge of the number of times the excited state is formed. It will be shown that there is some doubt as to the value for the latter quantity; for this reason, the amount of L radiation from RaD cannot be used as a check on the calculations of the fluorescence yield given in the previous paper. Therefore, a measurement has to be made on the yield of L radiation from a neighboring element for which the excitation of the γ-transition and the internal conversion coefficient are known with greater precision. There are very few cases among the heavy elements in which the γ-transitions have been studied in sufficient detail for this purpose. The only one suitable is the 40 kev. transition which is excited in the disintegration of ThC, for which the product nucleus, ThC″, is an isotope of thallium. ThC is very easy to prepare as a constituent of the active deposit of thoron and can be obtained as thin layers with very high specific activity. A detailed study has therefore been made of the various L radiations emitted by this deposit. A by-product of this

[1] *Manuscript received June 17, 1948.*

Contribution from the Chalk River Laboratory, Division of Atomic Energy, National Research Council. Issued as N.R.C. No. 1838.

[2] *Member of the United Kingdom Staff.*

work has been the measurement of the L radiations emitted following the K conversions produced by the disintegration of ThB, and this work has led to a confirmation of the calculation of some of the fluorescence yields discussed in the preceding paper.

Apparatus

The apparatus used in these measurements is shown in Fig. 1. The radioactive sources were supported on an aluminum slide at the position O in the figure. The radiation was detected by a counter, C, containing a mixture

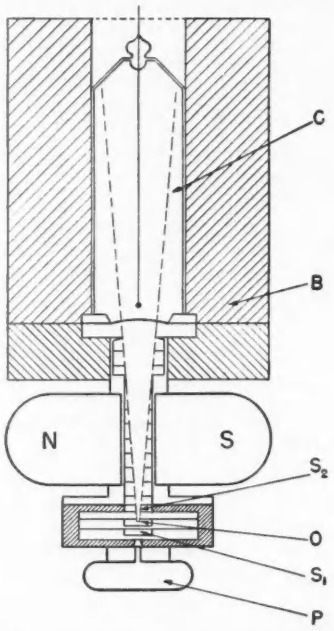

FIG. 1. *Apparatus used for the measurement of the L radiation emitted by the thorium active deposit.*

of argon, xenon, and alcohol. The electrons emitted by the source were prevented from operating the counter by the use of a small permanent magnet NS. That no electrons from the source, or Compton electrons from a filter placed at S_2, produced pulses in the counter, was verified by plotting an absorption curve of the counting rate against the thickness of a cellophane filter. After subtraction of the effect due to the hard radiations, the absorption coefficient was found to be equal to that expected of the L radiations, viz., radiations with a wave length of about one Ångstrom unit.

The beam of radiation was limited by a brass diaphragm, and the channel between the pole faces of the magnet was lined with aluminum and provided with a series of stops to trap the electrons. The radioactive material

was confined to an area bounded by a circle, $\frac{1}{8}$ in. in diameter, so that the diaphragm presented the same solid angle to all points within this circle. The beam of radiation, defined in this manner, passed through the counter from end to end without intersecting the wall of the counter. The counter wire was suspended horizontally with a small glass bead at the end where it faced the source; the area of the bead was insignificant in comparison to that of the section of the cone of radiation at this point. The end of the counter facing the source was closed with a mica window of thickness 9 mgm. per sq. cm. The counter was contained in a thick lead cylinder (B) and the whole apparatus was screened from external radiations by enclosure within thick lead walls.

To facilitate the coincidence experiments with β-particles, the source holder and the slides supporting the filters were enclosed in a steel cylinder which screened the source and its immediate vicinity from the stray magnetic field of the permanent magnet. A small hole in the far end of this steel structure allowed α- or β-particles to pass from the source through a thin window into a counter working either in the proportional region or as a Geiger–Müller counter. When coincidence measurements were made, or when the total L radiations emitted from ThB in equilibrium with its products were measured, care was taken to ensure that the activity was deposited on one side of the supporting foil only, the active surface facing downwards in Fig. 1. In this way, α- or β-particles could pass into the proportional counter at P with very little residual absorption. However, most of the other measurements were made with the active surface facing the xenon-counter; in comparing the results, therefore, a small correction has to be made to allow for the absorption of the radiations in the supporting foils and to account for the slight difference in the geometrical conditions. This correction was usually of the order of 6%.

Preliminary experiments were made with a counter filling consisting of xenon and alcohol in the usual proportions of argon–alcohol fillings. Subsequently, argon was mixed with the xenon to obtain satisfactory counting rate plateaus (7 cm. pressure of argon and 3 cm. of xenon). To ensure that the content of xenon and argon was known with sufficient accuracy, the alcohol and xenon were admitted first and successively frozen into a side tube on the counter with a freezing mixture of solid carbon dioxide and acetone and with liquid air; finally the argon was introduced and the counter sealed off. Filled in this way, and operated continuously day and night, the counter was found to have stable and reproducible characteristics over a period of several months.

Method of Measurement for Thoron Deposits

The active deposit was prepared on thin foils of aluminum and platinum. A few hours after removal from the emanating apparatus, the deposit of ThB is in equilibrium with its daughter products, all of which will then decay with the period of the parent. The number of atoms disintegrating per second can then be calculated for each member of the series in terms of the rate of disintegration of one of them. There will be a strong emission of L radiation

which follows the K conversion of the γ-rays emitted in the transition ThB–C; another powerful emission will result from L conversion in the α-decay of ThC, and a much weaker one will accompany the K conversion of the γ-radiation emitted from ThC″–D. The branch of the decay of ThC which produces the nucleus ThC′ will not be expected to produce a measurable amount of L radiation, because the intensity of the γ-radiation emitted in this process is very low and it is only weakly converted. The general decay scheme of these elements with their periods is shown in Fig. 2. The total amount of

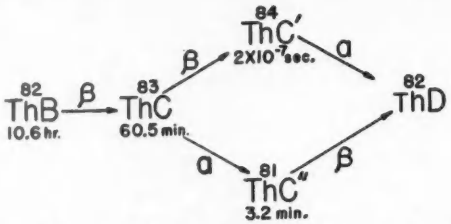

FIG. 2. *Decay scheme for elements of the thorium active deposit.*

L radiation is measured by a determination of the soft radiation emitted by ThB in equilibrium with its products; the amount produced by ThC–C″ and by ThC″–D is obtained by a study of the radiation produced by separated sources of ThC and ThC″. The difference between the first two results gives a measure of the radiation produced by ThB–C. In this case, since most of the radiation follows the emission of the K radiation of the product nucleus, viz., ThC, the measurement is in effect a check on the experimental values of the fluorescence yield of the L_3 level of bismuth (ThC) as determined by Küstner and Arends (24). The measurement of the quantity of the L radiation of ThC–C″ should test the validity of the figures given in the preceding paper for thallium. Finally, selective absorption measurements will give information on the relative values of the fluorescence yields.

The counting rate of the counter is in three parts, the first due to the hard radiations emitted by the source, the second due to cosmic rays, and the third due to L radiation. The last is distinguished from the first two by subtracting from the total counting rate the amount which is observed when a filter (containing about 30 mgm. of nickel per sq. cm.) is placed in the position S_2 in Fig. 1. For a source of ThB in equilibrium with its products, the absorption curve of the total radiation in nickel is given in Fig. 3, Curve A. Curve B (plotted in logarithmic ordinates) shows the result of subtracting the hard component of the radiations. This soft component, represented by Curve B, has the absorption coefficient corresponding to L radiations. A nickel filter of 30 mgm. per sq. cm. reduces this radiation to about 3% of its original intensity.

Except for the L radiation emitted by ThC″, which was measured in a separate experiment, the experimentally determined quantities are the ratios of the counting rates due to L radiation to the number of atoms of ThC disintegrating per second. This ratio is a counting efficiency, which will be called ϵ_1

for a source of Th (B + C) in equilibrium with its products and ϵ_2 for a source of ThC in equilibrium with ThC″. The quantities required are the efficiencies per atom disintegrating per second for each of the constituents of the active

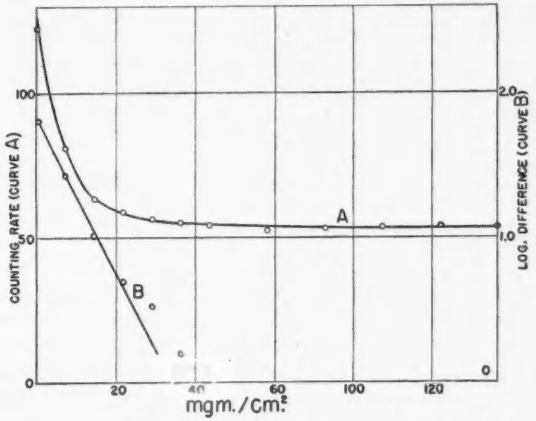

FIG. 3. *The absorption in nickel of the radiation emitted by Th(B + C). Ordinates: Curve A, counting rate, including hard radiations; Curve B, logarithm of the difference between the counting rate and that of the constant ordinate of Curve A.*

sources; these efficiencies will be denoted by ϵ_B, ϵ_C etc. They may be determined for ThB from the measurements of ϵ_1 and ϵ_2 and they will be compared with the calculations after account is taken of the absorption of the radiation in the air, in the mica window of the counter and in the filling gas. Let N_B, N_C, and $N_{C''}$ be the number of atoms of ThB, ThC and ThC″ disintegrating per second. Then, the observed quantities are related to the required quantities by the following equations, if sufficient time* is allowed to elapse after the preparation of the sources to ensure the establishment of a transient equilibrium in each case:—

$$\begin{aligned} N_C\epsilon_1 &= N_B\epsilon_B + N_C\epsilon_C + N_{C''}\epsilon_{C''} \\ N_C\epsilon_2 &= N_C\epsilon_C + N_{C''}\epsilon_{C''} \ . \end{aligned} \qquad (1)$$

These equations neglect any L radiations emitted in the disintegration ThC–ThC′–ThD; this neglect is justified by coincidence measurements to be described later. The difference between these expressions gives the efficiency for the detection of the radiation emitted by ThB–C:—

$$\epsilon_B = N_C/N_B(\epsilon_1 - \epsilon_2).$$

In transient equilibrium, N_B and N_C are related by the equation:

$$N_C/N_B = \frac{\lambda_C}{\lambda_C - \lambda_B} = 1.11,$$

* *Three or four hours is a sufficient time for ThB and 10 min. for ThC.*

where λ_C and λ_B are the disintegration constants of these atoms ($\lambda_C = 0.69$ hr.$^{-1}$ and $\lambda_B = 0.065$ hr.$^{-1}$). Thus:—

$$\epsilon_B = 1.11(\epsilon_1 - \epsilon_2). \tag{2}$$

The efficiency for ThC is obtained by subtracting from ϵ_2 a quantity proportional to the efficiency for ThC″, which is measured in a separate determination. The fraction of atoms of ThC disintegrating by α-decay is 0.34, so that the relation between the numbers of atoms of ThC″ and ThC disintegrating per second is given by:

$$N_{C''} = 0.34\, N_C \frac{\lambda_{C''}}{\lambda_{C''} - \lambda_C} = 0.365\, N_C, \tag{3}$$

the disintegration constant of ThC″ being 13.0 hr.$^{-1}$. Substitution of (3) in (1) gives:—

$$\epsilon_C = \epsilon_2 - 0.365\, \epsilon_{C''}.$$

There are two methods of measuring the efficiency for ThC which should give the same result. In the first, which will be called the direct method, the strength of the sources was determined in a separate measurement by counting the total number of α-particles collected in a known solid angle; the ratio of the counting rate of L radiation to the strength of the sources, in disintegrations of ThC per unit time, gives the quantities ϵ_1 and ϵ_2. In the second, or coincidence method, coincidences were observed between the α-particles and the pulses in the xenon counter; the ratio of the coincidence counting rate to the counting rate for α-particles gives a measure of the efficiency. The difference in the two coincidence ratios that are measured with and without a nickel filter of 30 mgm. per sq. cm. is the efficiency for detection of L radiation for the transition ThC–C″, viz., ϵ_C*. A similar coincidence method was also used to measure the efficiency for the L radiation of ThB–C; the result is more complicated in its interpretation and will be dealt with later.

Measurements by Direct Methods

(*a*) *The efficiency for ThB–C*

The first step in the determination of ϵ_B is the measurement of ϵ_2, the efficiency for detection of the radiation emitted by ThC in equilibrium with its products. In the preliminary measurements, sources of ThC were prepared by deposition on one side of a nickel foil from warm, dilute hydrochloric acid solution. The results for the efficiency of detection of L radiation soon showed a discrepancy when compared with the measurement of the efficiency determined by the coincidence method. This discrepancy was found to be due to the absorption of the L radiation within the nickel foil, and the subsequent reradiation of a considerable fraction of it as the K radiation of nickel, with a wave length of about 1.65 Å. Later, thinner layers of nickel were used, deposited electrolytically on a very thin layer of gold sputtered on aluminum

* *The use of the coincidence method is justified by the recoil experiments of Ellis (11), which show that the lifetime of the 40 kev. state is less than 10^{-7} sec.*

foil 2.0 mgm. per sq. cm. in thickness. Finally, pure ThC was prepared by electrolytic deposition on platinum in dilute hydrochloric acid solution using a method described by Hevesey and Paneth (22); the deposit was dissolved in nitric acid, the solution was concentrated by evaporation, and a drop of it was allowed to dry on a thin cellophane foil. This last method gave a result, which, when the contribution of the disintegration ThC″–D was subtracted from it, is consistent with the coincidence measurement of ϵ_C.

The results are collected in Table I, *A*; the observed results are given in the third column; a correcting factor for the nickel *K* radiation is given in the fourth column*, and the corrected result is given in the fifth column. The errors given are the statistical errors involved in the mean of the measurements; they are relatively high because of difficulties in obtaining ThC sources of sufficient strength, and because it was necessary to count for short periods so that the corrections for the decay of the source should not be too large. The purity of the source was tested by allowing it to decay for 24 hr.: the remaining α-activity is due to the generation of ThC by ThB, and is a measure of the ThB content; in practice, the impurity of ThB amounted to less than 1% of the initial ThC content. The initial strength of the source was measured in each case by counting the number of α-particles passing through a hole in a brass plate into a proportional counter filled with argon at low pressure. The dead time of the counters used in these measurements was negligible.

The measurements with sources of Th(B + C) were made with the active surface facing the proportional counter. In this case a small correction for the slightly differing solid angle (2%) and for the absorption in the support of the source is applied before comparing the results with those obtained for ThC. The sources on aluminum foil were prepared by exposing to the emanator a sandwich of two aluminum foils stuck together with grease, dissolving away the grease in ether, and separating the foils. In this way a source was obtained deposited on one side of the foil only. This foil, cut to the right size, was supported on a thin cellophane foil, 3.6 mgm. per sq. cm. in thickness. Other sources were prepared by deposition from the emanation on platinum

* *The correcting factor for the reradiation of the nickel K radiation was calculated in the following manner. Neglecting the absorption of the nickel K radiation in the nickel foil, to a first approximation the fraction of the total number of L quanta absorbed by a foil of thickness m gm. per sq. cm. and mass absorption coefficient, μ/ρ, is readily shown to be:*

$$q = \frac{1}{2}\left\{1 - \int_0^{\pi/2} e^{-m \cdot \mu/\rho \cdot \tan\theta} \cdot \sin\theta d\theta \right\}$$

when the activity is deposited on one side of it only. Of this, a fraction 0.89 is absorbed in the K shell of nickel, the remainder gives rise to the L radiation of nickel, which is strongly absorbed in the air and in the mica covering the window of the counter and is therefore not detected. Of that fraction, the proportion which gives rise to K emission is given by the fluorescence yield for nickel —0.364 according to Arends (2). The transmission of the 1.65 Å radiation through the air between the source and window is 0.89 times that of thallium L radiation, and through the mica window 0.67 times. Further, the nickel radiation is absorbed in the counter to an extent, 2.15 times greater than thallium L radiation. The efficiency of detection, therefore, has been increased by the fraction:

$$q.\ 0.89 \times 0.364 \times 0.89 \times 0.67 \times 2.15 = 0.42\ q.$$

Therefore, the observed results must be corrected by the factor $1/(1 + 0.42\ q)$. This correction neglects the absorption of the nickel K radiation in nickel. The error involved in making this approximation is very small.

TABLE I

SUMMARY OF THE RESULTS OF MEASUREMENTS ON THE EFFICIENCY OF DETECTION OF L RADIATION FROM SOURCES OF ThC AND Th(B + C), IN UNITS OF 10^{-5}

Support	Number of measurements	Uncorrected	Correction factor	Corrected
A: measurement of ϵ_2				
Nickel, 7.4 mgm./sq. cm.	4	5.00 ± 0.05	0.86	4.30 ± 0.05
" 0.5 " " "	2	4.23 ± 0.10	0.95	4.03 ± 0.10
Cellophane	3	3.85 ± 0.15	—	3.85 ± 0.15
			Mean	4.06 ± 0.10
B: measurement of ϵ_1				
Aluminum and cellophane	4	9.02 ± 0.10	1.06	9.60 ± 0.10
Cellophane	2	9.20 ± 0.10	1.03	9.50 ± 0.10
			Mean	9.55 ± 0.08

with subsequent dissolution in nitric acid concentration, and evaporation on thin cellophane foils of the same thickness. The results are given in Table 1, *B*. The difference between the mean values given in Table I, using Equation (2), gives ϵ_B :

$$\epsilon_B = 6.10 \pm 0.15 \times 10^{-5}.$$

(*b*) *The L radiation emitted by ThC″–D*

The L radiation in this case was measured with reference to the emission of hard γ-radiation instead of α-particles as a standard. For this purpose, a Geiger counter was set up near the source, and when encased in a cylinder of lead $\frac{1}{4}$ in. in thickness, the counting rate registered by it is a measure of the content of ThC″. Sources of ThC″ were prepared free from ThB and ThC by recoil from a source of Th(B + C) under reduced pressure. Both counters were operated simultaneously during two equal consecutive periods, long compared with the half-life of ThC″ (3.2 min.). Let c_1 and c_2 be the number of counts registered by the xenon counter in the two periods, and let c_1' and c_2' be the corresponding quantities recorded by the lead-screened counter; then the differences in the ratios $(c_1 - c_2)/(c_1' - c_2')$ measured without and with a nickel filter, after correction for dead time, determines the amount of L radiation in terms of the hard γ-radiation emitted by the source. With a source of ThC, it was sufficient to determine only the differences in the ratios of the counting rates in the two counters, correcting for the background, the dead time, and the decay of the source.

The ratio for ThC″ was found to be one-tenth of that obtained with a source of ThC in equilibrium with its products. The statistical error in this result was about 100%. Since the response of the lead-screened counter was a measure of the activity of ThC″ in the two sources, the contribution to the efficiency ϵ_2 due to ThC″–D must be about 10%. Subtracting 10% from the figure for the mean value of ϵ_2 given in Table I, *A*, the following value for the efficiency for ThC is obtained:

$$\epsilon_C = (3.7 \pm 0.4) \times 10^{-5}.$$

Taking the ratio of the number of atoms of ThC″ disintegrating per unit time to the number of atoms of ThC disintegrating per unit time as 0.365, the ratio of $\epsilon_{C''}$ to ϵ_C is found to be about 0.3. Thus,

$$\epsilon_{C''} \simeq (1 \pm 1) \times 10^{-5}$$

Coincidence Measurements

For measurements on ThC, a source of Th (B + C) was deposited on one side of a thin layer of aluminum as described in a previous paragraph. The active surface faced a proportional counter, the α-particles passing into it through a thin window; the total stopping power of the air between the window and the source, and the window itself, was equivalent to that of 2.0 cm. of air. That all the α-particles could be detected in the counter without reduction in number by absorption was verified by plotting absorption curves. The pulses produced by the proportional counter were passed into a fast amplifier with a band width of about 2 Mc., the pulses from the xenon counter were also amplified, and both were connected to a mixing unit. The size of the pulses from the xenon counter, and the size of those produced by the fast amplifier for the most energetic α-particles, were each made about 60 v.; these pulses both operated a multivibrator in each channel of the mixing unit, for which the threshold voltage was maintained constant at about 3 v. A minimum delay was therefore ensured between the coincident times of detection in the counters and the instants at which they operated the circuits of the mixing unit. However, the large diameter of the xenon counter might be expected to produce an appreciable delay in that counter.* To determine the minimum resolving time at which the full coincidence counting rate would be expected to be developed, a subsidiary experiment was made to measure the coincidence counting rate between β- and γ-rays from a source of Co^{60} with the aid of another thin walled counter of much smaller dimensions. The coincidence rate in this experiment was found to rise rapidly as resolving times were increased to 1 μsec. and remain constant above this amount. The minimum resolving time used in subsequent work, therefore, was 1 μsec.

* *Cf. Hartog, Miller and Verster, ref. (21). The proportional counter was filled with argon with 2% of carbon dioxide.*

For coincidence measurements on the L radiation emitted by ThB–C the proportional counter was removed and a Geiger counter with a thin window of about 1.5 cm. air equivalent was used in its place. The source was prepared in the same way as for the measurements with ThC.

Coincidence Measurements with α-Particles

The coincidence measurements with α-particles fall into three categories:

1. The measurement of the efficiency, when both the long and the short range α-particles are recorded, and no filter is used in front of the xenon counter.

2. Coincidence counting with both groups of α-particles with a filter of nickel, 30 mgm. per sq. cm. in thickness, placed between the source and the xenon counter.

3. Coincidence measurements with sufficient absorption in the path of the α-particles, so that those due to ThC–C″, the shorter range group, are completely absorbed, and without a filter before the xenon counter.

The difference between the efficiency as measured by Methods (1) and (2) gives the efficiency for detection of L radiation for ThC–C″, viz., ϵ_C per atom of ThC. Method (3) gives the efficiency for detection of all types of radiation for atoms of ThC disintegrating along the branch ThC–C′–D. If this result is multiplied by 0.65, the fraction of ThC atoms disintegrating in this manner, it should give the same value as Method (2) (provided no L radiation is emitted in this branch), since the hard radiations emitted by ThC–C″ are of very low intensity compared with those emitted by ThC–C′.

Since the coincidence counting rate was very low, a procedure was adopted in which the total number of coincidences was measured in a time comparable with the lifetime of the source (half period, 10.6 hr.). For this purpose the mean value of the background counting rate, due to cosmic rays (q_0) of the xenon counter, was determined before and after a run. The initial counting rate (q_γ) of the xenon counter was determined, together with the initial counting rate (q_α) for the α-particles. If Q_c is the total number of genuine coincidences recorded in the time of duration of the run, t, the efficiency for detection per α-particle is:

$$\epsilon = \frac{Q_c}{q_\alpha} \cdot \frac{\lambda_B}{1 - e^{-\lambda_B \cdot t}}$$

The efficiency of the detection of L radiation is then given by the differences between these expressions obtained with and without a nickel filter. In each case, from the observed number of coincidences (Q_0), the number due to random coincidences must be subtracted. This number is calculated from the resolving time (τ) and the initial counting rates, using the formula:

$$Q_r = \frac{2\tau q_\alpha}{\lambda_B} \cdot [\tfrac{1}{2} q_\gamma (1 - e^{-2\lambda_B \cdot t}) + q_0 (1 - e^{-\lambda_B \cdot t})] .$$

The statistical error in the measurement of an efficiency contains significantly statistical errors in Q_c and Q_r only, because both the initial counting rates can be determined with high accuracy. It was found that the resolving time, measured with random coincidences, could be trusted to remain constant to about 1% over a period of continuous operation of several weeks, and could be measured to that order of accuracy. The error in ϵ is therefore given by $\sqrt{(Q_0 + Q_r)}/(Q_0 - Q_r)$. The results obtained are plotted in Fig. 4 as a func-

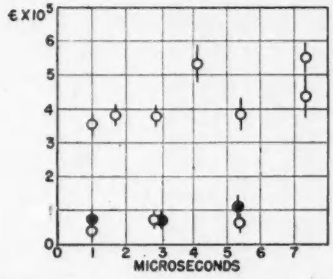

FIG. 4. *The efficiency for the detection of radiation emitted by ThC in units of 10^{-5} plotted against the coincidence resolving time, in microseconds. Open circles: results of Methods (1) and (2). Full circles: Method (3).*

tion of the resolving time. The values obtained at the higher resolving times are very inaccurate, owing to the large correction for random coincidences. At the lower resolving times this correction amounted to about 10%, but at the higher values for the resolving time, the correction could amount to 50% of Q_0.

The mean results of these measurements are given in Table II together with the measurement of ϵ_C obtained by the direct method. It will be seen that the two results agree within the experimental error of 10%. The equality

TABLE II

EFFICIENCY BY COINCIDENCE METHODS, IN UNITS OF 10^{-5}

All coincidence results corrected by 6% to allow for absorption in aluminum and cellophane and for slightly different geometry

Method	Number of measurements	Mean corrected result
(1) No filter, both ThC and ThC′ α-particles	6	4.16 ± 0.2
(2) Ditto, with filter	3	0.52 ± 0.2
(3) No filter, ThC′ α-particles only	3	0.80 ± 0.3
Difference, (1) minus (2)	—	$\epsilon_C = 3.6 \pm 0.3$
By direct method	—	$\epsilon_C = 3.7 \pm 0.4$

of the results obtained by Methods (2) and (3) in the second and third rows of the table shows that no appreciable L radiation is emitted in the ThC–ThC′–ThD branch of the disintegration (in the latter case, the measured efficiency has been multiplied by 0.65).

Coincidence Measurements with β-Particles

The greater part of the L radiation emitted by ThB–C is the result of the secondary process following the emission of K radiation after K conversion. A coincidence measurement of the efficiency for production of this L radiation should serve as a check on the validity of the method as applied to ThC.

Since the greater part of the β-emission from ThB is of low energy, the residual absorption between the source and the interior of the Geiger counter was made as low as possible. The coincidence counting rate depends, then, not only on the coincidences between the L radiation and the β-emission of ThB, but also on the coincidences between the α-particles and the L radiation of ThC–C″ (since the α-particles will also be registered by the counter), on L radiation coincidences with the β-particles emitted by ThC″–D, and on coincidences between the various hard radiations and the α- and β-particles. The efficiency is measured as the ratio of the total number of genuine coincidences to the initial counting rate of the counter, and the portion due to L radiation is measured by the difference between the efficiencies obtained without and with a nickel filter.

Let h_r be the single counting rate in the Geiger counter of particles of type r and if these particles contribute to the L radiation detected in the xenon counter with an efficiency ϵ_r, the total efficiency for L radiation measured by the difference method is given by ϵ_3:

$$\epsilon_3 = \frac{Q_c}{q_0} \cdot \frac{\lambda_B}{1 - e^{-\lambda_\beta \cdot t}} \cdot \frac{1}{f} = \sum_r (h_r \epsilon_r),$$

where q_0 is the initial counting rate in the Geiger counter, f a correction factor of the order of unity to correct for the dead time of that counter, t the duration of the measurements, and the other symbols have their previous significance. If τ_0 is the dead time of the counter, the correction factor f is given by:

$$f = 1 + q_0 \tau_0 \left[1 - \frac{1}{2} \left\{ \frac{1 - e^{-2\lambda_\beta \cdot t}}{1 - e^{-\lambda_\beta \cdot t}} \right\} \right].$$

To determine the efficiency for ThB–C, then, the efficiency due to the L radiations of ThC–C″ and ThC″–C must be subtracted from the result for ϵ_3. After making these corrections, the efficiency due to ThB–C will consist of two terms, one representing the coincidence rate between the L radiation and the nuclear β-particles emitted by ThB, and the other representing the coincidence counting rate which arises from coincidences with the conversion electrons emitted in this transition. If both could be detected without any absorption between the source and the counter, the efficiency for detection

would be the same in both cases, so that the net efficiency would be just double that detected by the direct method. The absorption, however, reduces the numbers of primary β-particles more rapidly than the conversion electrons owing to the preponderance of low energy β-particles in the former. If ϵ' is the efficiency remaining after subtraction of the irrelevant terms, and if the fractions of the primary and conversion electrons remaining after absorption are y_p and y_e respectively,

$$\epsilon' = \epsilon_B(y_p + y_e).$$

y_e may be computed from the absorption curves given by Eddy (10) for those conversion electrons, and y_p may be calculated from the absorption curve of the β-particles emitted from ThB after subtraction of the contribution of the conversion electrons.

To determine the values of the fractions denoted by h, absorption curves were made for the β-particles emitted by Th(B + C) and ThC. Two such curves are shown in Fig. 5; the ordinate of each curve is equal to the ratio

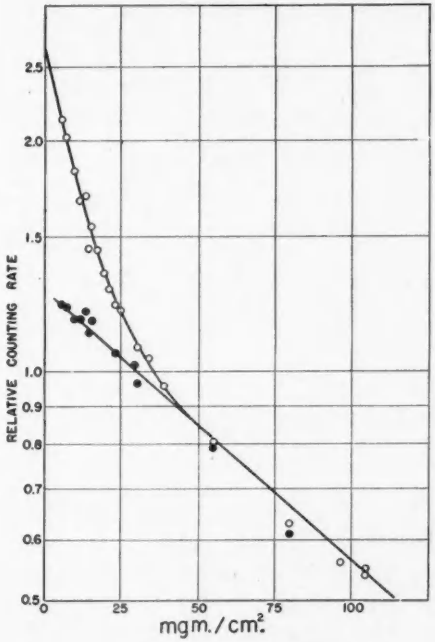

FIG. 5. *Absorption of electrons. Upper curve: from Th(B + C); lower curve: from ThC. The ordinates are the ratio of the number of electrons emitted per unit time to the number of α-particles emitted by the source in the same geometrical conditions. The abscissae are the total amount of absorption in aluminum in the path of the electrons.*

of the number of β-particles to the number of α-particles emitted by each source under the same geometrical conditions. The latter quantity was obtained by removing the absorbing material, lowering the potential on the counter until it operated in the proportional region, and connecting it to an amplifier and discriminator. Both α- and β-particle counts were corrected for the decay of the source and, when the counter was operated in the Geiger region, for the dead time of the counter. The number of primary β-particles from ThC in transient equilibrium with its products should exceed the number of α-particles emitted by about 2%; it will be seen that the excess is actually about 20%. This is due, no doubt, to scattering at the walls of the hole defining the beam of particles entering the counter. The difference between the two curves represents the number of β-particles due to ThB. It was found very difficult to measure this difference with high accuracy because the curve is very sensitive to the thickness of the aluminum absorbers. Only a few measurements have been made, therefore, in the region of very small absorptions.

The results are collected in Table III. In this table the differences between the efficiencies, without and with a filter, have been corrected by 6% to allow for the absorption in the supporting foil and for the slightly different geometry.

TABLE III

RESULTS OF COINCIDENCE MEASUREMENTS WITH THB

Efficiencies are given in units of 10^{-5}

Absorption	ϵ_3	h_α	$h_\alpha\epsilon_c$	$h_{c''}\epsilon_{c''}$	h_B	$h_B\epsilon'$	y_p+y_e	ϵ_B
5 mgm./cm.^{2}	4.40 ± 0.28	0.32	1.18	0.3	0.30	2.9 ± 0.3	1.7	5.8 ± 1.0
7 "	2.70 ± 0.25	0	0	0.4	0.31	2.3 ± 0.3	1.6	4.8 ± 0.8
13 "	2.91 ± 0.40	0	0	0.4	0.32	2.5 ± 0.3	1.1	7.1 ± 1.1

Mean result $\epsilon_B = 5.9 \pm 0.8$

h_B is the fraction of the counting rate in the Geiger counter due to the electrons from ThB and is obtained from the difference between the two curves; the contribution due to the small amount of L radiation emitted by ThC″–D is roughly estimated from previous information and the fraction of the counting rate due to ThC in equilibrium with its products. The value for y_e is taken from Eddy's measurements, and y_p is estimated by subtracting from the difference curve the number of electrons due to the conversion of the F, E, and H γ-rays, which (in the absence of absorbing material) is taken to be 0.35 electrons per disintegration of ThB. The final result is given in the last column of the table; it is inaccurate because of the large statistical error involved in the measurements, and the difficulty in estimating the fractions denoted by y. It will be seen that the mean result agrees quite well with that obtained by the direct method.

The Counter Efficiency

The experimental efficiencies must now be compared with the calculated values. The first step in this direction is the calculation of the counter efficiencies. Let Ω be the solid angle defined by the brass diaphragm of Fig. 1, z_L the number of L conversions per disintegration. Then if q represents the number of quanta emitted from an L level, E the efficiency with which they are detected in the counter, and R the mean value by which the efficiency is increased by absorption and re-radiation at the end of the counter, the efficiency of detection of L radiation per disintegration is given by:

$$\epsilon = \frac{\Omega}{4\pi} \cdot z_L \cdot \sum_{1,2,3} (qE) \cdot R . \tag{4}$$

The quantities denoted by q have been calculated in the preceding paper (Table VIII). The efficiency E is given by the formula:

$$E = \sum_{\lambda} [C_\lambda T_\lambda (1 - e^{-k\lambda})] , \tag{5}$$

where C_λ is the fraction of the radiation width concerned with the emission of a radiation of wave length λ (Table III of the preceding paper), T_λ is the transmission coefficient in the air between the source and counter, the mica window of the counter, and the dead space in the latter before the active region, and k_λ is a quantity depending on the absorption within the counter. If d is the effective length of the counter, and if m and μ/ρ are the superficial densities and mass absorption coefficients of the constituent gases, k is given by:

$$k = d \sum (m \cdot \mu/\rho) .$$

The greater part of the absorption in the counter is due to the xenon content. For this element, the following mass absorption coefficient* has been used:

$$\mu/\rho = 103\lambda^{2.73} \text{ sq. cm. per gm.},$$

where the wave length λ is measured in Ångstrom units. For argon, Colvert's (5) result has been used:

$$\mu/\rho = 33.4\lambda^{2.7} + 0.67\lambda^{0.94} \text{ sq. cm. per gm.}$$

The transmission of the mica window has been calculated from data given by Williams (44).

To measure the effective length of the counter, the counting rate of the counter was plotted against its position (along the axis) when a sheet of hard γ-radiation, defined by a channel in a lead block, was allowed to traverse the counter symmetrically in a plane perpendicular to the axis. The results are shown in Fig. 6. The distance between the positions at which the counting rate is reduced to one-half represents the effective length. The mean result for different fillings was 13.7 cm.

* *This result has been obtained from an extrapolation of the results of Schultz (36) for tellurium and the results of Laubert (26) for tin. The figures obtained are in close agreement, but appreciably higher than the result obtained by White (43), using xenon itself (93 sq. cm. per gm.).*

The absorption of the radiation and its re-radiation in the form of the characteristic X-rays of the material forming the end of the counter produces an increase in the efficiency which is represented by the factor R in Equation (4).

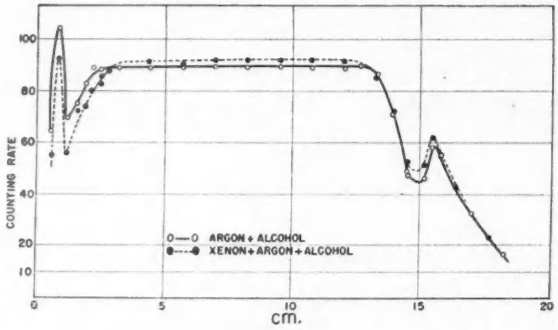

FIG. 6. *Measurement of the effective length of the counter. The ordinates represent the counting rate of the counter; the abscissae, the distance along the axis of the counter in centimeters. The peaks at the end of the curves are due to scattering of γ-radiation into the active region of the counter by the flange supporting the mica window and the junction of the counter wall with the conical endpiece.*

An elementary calculation shows that the effect is only a few per cent in the case of xenon fillings and three or four times larger for a brass-ended counter filled with argon. The result should be negligible with an aluminum endpiece. To test this, the counting rates of L radiation were measured with RaD sources with both brass and aluminum endpieces, and with xenon–argon and with argon fillings. As anticipated, with the argon fillings the counting rates with the brass endpiece were some 10% higher than with the aluminum end. The mean results of several measurements with the different fillings are listed in Table IV, in which H is the counting rate and H/E is the counting rate divided by the efficiency calculated * from Equation (5); a correction of

TABLE IV

COMPARISON OF THE COUNTING RATES OF RaD SOURCES WITH DIFFERENT FILLINGS AND WITH DIFFERENT ENDPIECES

Endpiece	Filling	Source No. 1		Source No. 3	
		H	H/E	H	H/E
Brass	Xe + A	5.70 ± 0.05	20.1	1.57 ± 0.10	5.5
	A	2.58 ± 0.04	20.3	0.67 ± 0.02	4.3
Aluminum	Xe + A	5.97 ± 0.05	21.1	1.43 ± 0.04	5.1
	A	2.35 ± 0.04	20.6	0.55 ± 0.03	4.8

* *This efficiency was calculated on the basis of an energy distribution in the L spectrum obtained in selective absorption measurements described in a later paragraph.*

10% has been applied only in the case of the argon filling and the brass endpiece. The agreement in the figures for this ratio show that the mass absorption coefficients of xenon and argon which have been used are mutually consistent. For the xenon fillings, therefore, R is equated to unity.

Calculation of the Efficiency for ThC–C″

The efficiency for the detection of the L converted radiations of this disintegration is given by Equation (4). The value of z_L, the number of L conversions per disintegration, may be obtained directly from measurements on the electrons ejected from the L levels, or it may be calculated from the excitation of the 40 kev. state, experimental information on the γ-emission from that state, and the fraction of the electrons which are converted in the L levels.

In measurements on the conversion electrons, Gurney (20) found 0.18 L electrons and Arnoult (3) 0.23 L electrons per α-disintegration of ThC. Flammersfeld (14), however, has shown that these figures are too low*; he obtained 0.59 L electrons per disintegration using a special method of preparing the source. His figure must be corrected for the electrons due to the K conversion of the γ-ray denoted by E by Ellis, which have not been detected separately from the L_1 conversion of the 40 kev. transition of ThC. This K conversion should amount to about 0.10 electron per α-disintegration of ThC (see Table V). Flammersfeld's figure for the number of L electrons must therefore be reduced to 0.49 electron per α-disintegration of ThC, and since the efficiencies measured experimentally are reckoned in terms of the total disintegration rate of ThC, ε_L becomes 0.17.

Lewis and Bowden (28) found that the 40 kev. state is excited directly in 70% of the α-disintegrations of ThC. The total excitation of this state, by α-emission from ThC and by γ-ray emission from higher states, probably amounts to about 72%. If the γ-ray emission** (about 13 ± 8% per α-disintegration) is subtracted from this figure, the total number of conversion electrons should be about 0.59 ± 0.05 per α-disintegration, which is in agreement with a result obtained by Richardson and Leigh-Smith (35). Flammersfeld gives 0.82 and Arnoult gives 0.72 for the fraction of these electrons which are converted in the L levels. These figures include, however, the electrons due to the E γ-ray; for purposes of calculation, the fraction will be assumed to be 0.75, which may be accurate to 5 to 10%. z_L is therefore $0.59 \times 0.35 \times 0.75 = 0.15$ electron per disintegration of ThC.

Both methods of computation of z_L involve errors which are difficult to assess. Taking the mean of the two, viz., $z_L = 0.16$, the counter efficiencies,

*This consisted in concentrating a solution of ThB in equilibrium with its products and evaporating a drop of it on to a very thin foil of lacquer. Previous workers had obtained lower results by using a source deposited directly from the emanation, a procedure which causes some of the ThB atoms to be driven into the surface by α-recoil from ThA.

** From measurements by the author, hitherto unpublished.

E, for the radiations of the L_1, L_2, and L_3 levels are respectively 0.270, 0.276, and 0.351. Using the figures for the q's given in the preceding paper, and $\Omega/4\pi = 1.62 \times 10^{-3}$, the efficiency is found to be:

$$\epsilon_C \text{ (from calculation)} = 2.5 \times 10^{-5}$$

$$\epsilon_C \text{ (from observation (Table II))} = 3.7 \times 10^{-5}$$

The experimental result is thus appreciably higher than that calculated. The significance of this will be discussed after the measurements on RaD have been described.

Calculation of the Efficiency for ThB–C

In this case, most of the L radiation follows the K conversion; to a smaller extent L radiation is also produced by L conversion and by Auger transitions between the K and L levels.

The uncorrected results of Duane and Stenstrom (9) correspond to transition probabilities for the emission of the $K\alpha_1$ and $K\alpha_2$ lines in tungsten which are respectively 0.51 and 0.26 of the total radiation probability of the K level. Massey and Burhop's (30) figures give 0.53 and 0.26 for both gold and uranium and these are adopted in the present calculations. If f_K is the fluorescence yield of the K level, the excitation of the L_3 and L_2 levels by K conversion is therefore 0.53 and 0.26 of $z_K f_K$.

The amount of L radiation arising from L conversion is given in Table VIII of the preceding paper.

The Auger electrons arising from transitions from the K level producing ionizations in the L levels were detected by Ellis (12) by a photographic method. His values for the intensities of these electrons is equivalent to about 8.0% of the intensity of the F-line; if the intensity of this line is taken to be 0.28 electron per disintegration, the number of Auger transitions corresponds to 6.6% of the number of times the K level is excited. Flammersfeld's (14) results for this quantity are probably more accurate, and are equivalent to 2.4% of the K excitation. The fluorescence yield, f_K, therefore, must be very near 0.97. The greater part of the remaining 3% lead to double ionizations in the L levels; counting each ionization of the L_1 level as an excitation of the L_3 level, by the Coster–Kronig process, the excitation of the L_3 level by Auger transitions is therefore 3% per K conversion. The ionization of the L_1 level will be taken to be 3% and that of L_2, 1% per K conversion. Thus, the total number of quanta emitted by the three levels per disintegration is given by the equations:

$$\begin{aligned} Q_1 &= 0.09\, z_L + 0.03\, z_K f_1 \\ Q_2 &= 0.04\, z_L + z_K f_2(0.26 f_K + 0.01) \\ Q_3 &= 0.19\, z_L + z_K f_3(0.53 f_K + 0.03). \end{aligned} \tag{6}$$

The number of conversion electrons which are emitted in the disintegration ThB–C are listed in Table V below, which is compiled from Flammersfeld's

(14) results. The number of K conversion electrons of the E γ-ray is computed from his figure for the number of the L conversions, using his value (5.5) for the ratio of the intensities of the K to the L conversion of the F γ-ray.

TABLE V

CONVERSION OF THE γ-RAYS OF THB–C, ACCORDING TO FLAMMERSFELD (14), IN ELECTRONS PER DISINTEGRATION OF THB

γ-ray	z_K	z_L
F	0.284	0.0513
E	(0.035)	0.0063
H	0.011	0.002
D	0.0016	
Total	0.332	0.060

Using the figures given in Table IV of the preceding paper, Equation (6) gives: $Q_1 = 0.007$, $Q_2 = 0.040$, $Q_3 = 0.065$. The counter efficiencies, E, (Equation (5)) for bismuth radiations, were found to be 0.234, 0.246, and 0.327 for the radiations of the L_1, L_2 and L_3 levels respectively. The efficiency for the detection of the L radiation, ϵ_B, is found to be:

From calculation	5.4	($\times 10^{-5}$)
From direct observation	6.1 ± 0.2	
From coincidence measurements	5.9 ± 0.8	

It will be seen that there is a fair agreement.

Calculation of the Efficiency for ThC″–D

The efficiency for the production of L radiation from ThC″–D may be calculated in a similar manner. In this case the product element, ThD, is an isotope of lead, and in view of the inaccuracy of the measurement of the efficiency it is sufficient to assume that the sensitivity of the counter is the same as for bismuth. The efficiency required is therefore given by the efficiency for ThB–C reduced in the ratio of the numbers of K conversion electrons emitted by the two nuclei. From Flammersfeld's results, the total number of electrons resulting from K conversion attributable to ThC″–D is 0.0228 electron* per disintegration of ThC, when ThC″ is in equilibrium with it. Since the total number of K conversion electrons emitted by ThB–C is 0.33 electron per disintegration of ThB, to a sufficient accuracy,

$$\epsilon_{C''} = \frac{0.0228 \times 5.4 \times 10^{-5}}{0.37 \times 0.33} = 1.0 \times 10^{-5}$$

which is in agreement with the observed efficiency.

* *This quantity is the sum of the numbers of K conversion electrons, per disintegration of ThC, for the γ-rays, G, L, M, P, and X, after a correction has been made for the superposition of the K conversion electrons of the ray M on the L_1 conversion of the ray L.*

Selective Absorption Measurements

The ratio of the number of quanta emitted by the L_1 and L_2 levels (taken together) to the number emitted by the L_3 level can be estimated by the method of selective absorption. If an absorbing material is used for which the K absorption limit lies at a wave length above those of the lines of the L spectrum to be examined, the absorption will be strong; if below, the absorption will be relatively weak. When the absorption limit lies in the middle of the L spectrum the intermediate value of the absorption coefficient can be used to measure the relative intensities of the radiations with wave lengths below and above the limit. Fig. 7 shows the distribution of the lines of the L series for thallium

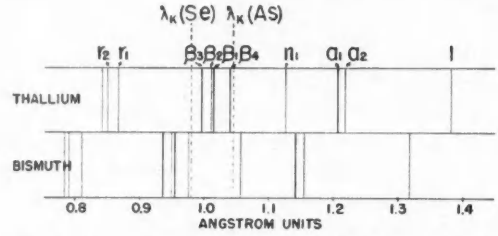

FIG. 7. *Distribution in wave length of the lines of the L spectrum of thallium (81) and bismuth (83) with reference to the wave lengths of the absorption limits of selenium and arsenic.*

and bismuth and the position of the K absorption limits of selenium and arsenic. It will be seen that, except for the line $L\beta_2$ and some very weak lines, all the more intense radiations of the L spectrum can be grouped into two categories, the lines originating in the L_3 level with wave lengths above that of the absorption limit and the lines characteristic of the L_1 and L_2 levels with wave lengths less than that limit. For thallium, arsenic, and for bismuth, both selenium and arsenic are suitable absorbing materials.

Let P be the counting rate, P_0 a constant representing the counting rate in the absence of the absorber, a and $(1-a)$ the proportions of the counting rate (in the absence of absorption) due to the L_1 and L_2 levels and due to the L_3 level, respectively, n the number of absorbing foils, and k a quantity representing the absorption per foil, i.e., the sum of the products of the superficial densities of the constituents with their mass absorption coefficients. Let k' refer to the mean value of this quantity for wave lengths lying below that of the absorption limit, and k'' to wave lengths above the limit. Then:

$$P/P_0 = ae^{-nk'} + (1 - a)e^{-nk''}$$

and

$$\bar{k} = -\frac{1}{P_0}\left(\frac{dP}{dn}\right)_{n=0} = ak' + (1 - a)k''.$$

The absorbers were made by evaporating selenium *in vacuo* on to thin foils of aluminum (2.0 mgm. per sq. cm.); the arsenic absorbers were prepared by evaporation of arsenious oxide on aluminum foils of the same thickness.

A small correction must be made for the absorption in these foils; if k_0 refers to the absorption in the aluminum of the foil and, in the case of the arsenic foils, to the oxygen in chemical combination with it, the above equation must be replaced by

$$\bar{k} = ak' + (1 - a)k'' + k_0 ,$$

whence

$$a = \frac{\bar{k} - k'' - k_0}{k' - k''} .$$

Since the radiations from L_1 and L_2 are concentrated about the group of lines, $L\beta_3$, $L\beta_2$, $L\beta_1$, and $L\beta_4$, it is sufficient to ignore the γ-group and to use the mean wave length of the β-group of lines to calculate k'. Similarly, k'' is computed for the wave length of the line $L\alpha_1$.

Now the counting rate, a, includes that due to the line $L\beta_2$ which arises from the excitation of the L_3 level, and a correction must be made to allow for the fact that this line lies below the K absorption limit. The radiation width corresponding to this line is about 13% of the total radiation width of the L_3 level. If then, Q_{12} is the number of quanta emitted by both the levels, L_1 and L_2, Q_3 that emitted by the level L_3, the Q's are related to a by the expression:

$$\frac{a}{1 - a} = \frac{Q_{12} + 0.13Q_3}{0.87 \times Q_3} \cdot \frac{\text{Probability of detection of } L_1 \text{ and } L_2 \text{ radiations}}{\text{Probability of detection of } L_3 \text{ radiations}}$$

Selective Absorption Measurements with ThB–C

In this case the admixture of L_1 radiations due to L conversions is very small; the measurement of the ratio of Q_{12} to Q_3 is therefore a check on the ratio of the fluorescence yields f_2 and f_3 which have been calculated in the preceding paper. Since these radiations arise from bismuth, both selenium and arsenic are appropriate absorbing materials. The absorption curves for selenium are given in Fig. 8. A is the absorption curve of a source of ThC in equilibrium with its products, the source being deposited in a pure state on a thin film of cellophane with the active surface facing the xenon counter; B is the absorption curve of a source of Th(B + C) deposited on a cellophane surface in a similar way. The ordinates of the curves are adjusted so that, in the absence of an absorber, the counting rates are in the ratio of the mean values of ϵ_1 and ϵ_2 which are given in Table I. The difference in the ordinates of these two curves is the absorption for the L radiation due to ThB–C, and is represented by the curve C in the figure.

The values for the k's were obtained by an interpolation of the figures given by Schultz (36). With selenium, the mass absorption coefficient is 158 for the β-group of radiations; for $L\alpha_1$, it is 36 sq. cm. per gram; for arsenic, the corresponding figures are 145 and 33 sq. cm. per gram. The results are given in the first two rows of Table VI; both materials give $Q_{12}/Q_3 = 0.71$. From a previous paragraph, the sum of the number of quanta from L_1

and L_2 is 0.047, and from L_3, 0.065 per disintegration of ThB; the ratio of these two values is 0.73. This is good agreement and confirms the calculations which have been made for f_2.

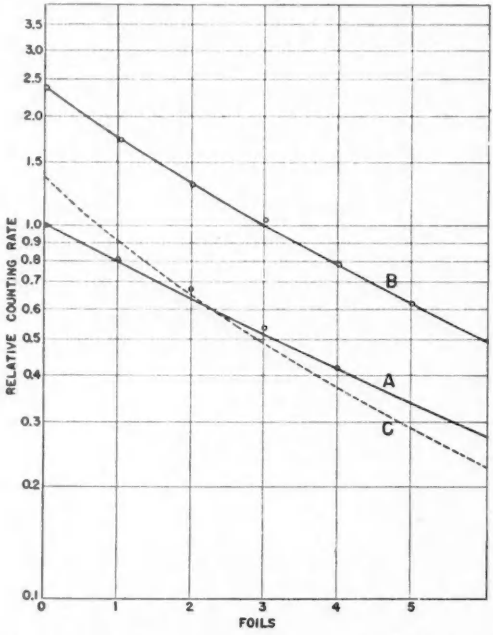

FIG. 8. *The absorption of L radiation in selenium. Curve A: ThC. Curve B: Th(B + C). The ordinates are chosen so that both sources contain equal numbers of atoms of ThC disintegrating per second. Curve C is obtained by subtracting Curve A from Curve B.*

TABLE VI

RESULTS OF SELECTIVE ABSORPTION MEASUREMENTS WITH THB AND THC

Absorber	Amount of absorber per foil	$\bar{k}$ per foil	k_0 per foil	a	Q_{12}/Q_3
		For ThB–C			
Se	4.5 mgm./sq.cm.	0.430	0.036	0.42	0.71
As	2.36 mgm./sq.cm. (as metal)	0.231	0.039	0.42	0.71
		For ThC–C″			
As	2.36 mgm./sq.cm.	0.290	0.043	0.48	0.91
As	1.50 mgm./sq.cm.	0.210	0.042	0.54	1.18
				Mean	1.04

Selective Absorption Measurements with ThC–C″

The measurements on the absorption of the L radiation from a source of ThC are given in the lower part of Table VI. Except for a small amount (about 10%) due to the conversions associated with the disintegration of ThC″–D ,this L radiation is due to thallium, and therefore arsenic is the only absorbing material which can give a selective effect. The values of k' and k'' were calculated for the radiations of thallium from an interpolation of Schultz' results. The mean value found for Q_{12}/Q_3 is about unity. The calculated intensities are 0.12 quanta per L conversion from the L_1 and L_2 levels, and 0.165 quanta per L conversion from the L_3 level. This gives $Q_{12}/Q_3 = 0.73$. The discrepancy is appreciable.

The absorption of the ThC radiation in selenium (Fig. 8) gives a mass absorption coefficient of about 36 sq. cm. per gm. which is approximately the value to be expected for the α- and β-groups of radiations for which the wave lengths lie just above that of the K absorption limit of selenium.

The Radiations from RaD

For many years it has been supposed that the emission of a very low energy primary β-particle from RaD leads to the excitation of the RaE nucleus at 47 kev. above its ground state. Recent experiments have shown that all the disintegrations of RaD do not follow this simple procedure and that some serious discrepancies exist. The evidence for this will now be reviewed.

The energy of the secondary electrons from RaD has been measured by Curtiss (7) who showed that the difference between their energies is consistent with the energies of the X-ray levels of RaE, which is an isotope of bismuth. The number of these secondaries per disintegration is still uncertain. Using a cloud chamber method Kikuchi (23) (1927) concluded that the rate of production of the secondaries is slightly less than the disintegration rate of RaD. The accuracy of his figure was limited by special difficulties involved in his cloud chamber technique. The number of secondaries was studied by Stahel (37) in 1931 using a counter method. He obtained 0.83 electron per disintegration; this figure should be an upper limit to the number of secondaries because the effects of scattering and reflection tend to increase it. More recently, very much lower figures for the number of secondaries have been given by Lee and Libby (27) (1939) and by Ouang Te-Tchao and collaborators (31) (1943). In these experiments, the influence of absorption on the number of secondaries is not clear and it is difficult, therefore, to assess the value of the results.

The distribution in energy of the secondaries has been studied in cloud chambers by Feather (13) (1929), Petrová (32) (1929) and by Richardson (33) (1931). The general shape of the energy distribution obtained by these workers is in agreement with that obtained by Curtiss using a β-spectrograph. The energy distribution, however, has been studied by a more accurate method by Richardson and Leigh-Smith (34) (1937) who introduced RaD

into a cloud chamber in vapor form. They were able to identify the electrons due to internal conversion, the Auger electrons, and the primary nuclear electrons of RaD, and showed that 60% of the latter must have a range of less than 0.05 cm. of air at N.T.P. corresponding to an energy of 5 kev. Since only a fraction of the primary β-particles were observable, these authors were unable to measure the relative numbers of conversion electrons to primaries.

According to the measurements of Curtiss, the energy of the γ-ray associated with the disintegration of RaD is 46.7 kev. The absolute intensity of this radiation has been studied by a number of experimenters: by Gray and O'Leary (19) (1929), by Stahel and Sizoo (39) (1930) and by Gray (18) (1932). Recent results are probably more accurate and give three or four quanta emitted per 100 disintegrations of RaD. Von Droste (8) found 3.5%; Bramson (4) 3.1%; Gray (18) 4%; and Stahel (38) (1935) 3.8%. Recently, using the method of crystalline diffraction, Frilley (15) has shown that the 47 kev. radiation is accompanied by weaker radiations with energies at 43, 37, and 32 kev.; the 47 kev. radiation appears to contribute about 80% of the energy of the γ-radiation in this range. Further, using a strong source of RaD, Tsien and Marty (41, 42) have found two softer radiations with energies of 7.3 and 23 kev.

The yield of L radiation from RaD was measured by Stahel (38) in 1935. He found 0.25 L quanta are emitted per disintegration, in approximate agreement with an earlier determination by Gray (18). The spectrum of this radiation was examined by Frilley and Tsien (17) (1945) using a Cauchois spectrograph. These authors concluded that the emission of radiation from the L_1 level relative to that of the L_2 level was less frequent than was to be expected. In another paper, Frilley, Surugue, and Tsien (16) have pointed out that this discrepancy might be due to the presence of Auger transitions of the Coster–Kronig type.

The L Radiations from RaD

It will now be shown that the measurements of Stahel on the L radiation of RaD are not consistent with the assumption that the 47 kev. radiation and the weaker radiations with energies of about 40 kev. are excited in 100% of the disintegrations.

Stahel used his measurement of the L radiation to calculate the conversion coefficient of the 47 kev. radiation. The yield of L radiation is equal to the product of the excitation of the excited state corresponding to that radiation (which he assumed to be 100%) with the fluorescence yield and the fraction of the ejected electrons which are produced by conversion in the L levels. For the fluorescence yield he used Lay's result (25); for the fraction, that of Curtiss (7) (60%). From these figures he concluded that the γ-radiation was 97% converted.

Curtiss's value for the fraction is probably too low, because he used the photographic method of detection which, in this energy range, enhances the effect of the more energetic electrons from the M and N levels. The cloud chamber results of Richardson and Leigh-Smith (34) are free from this objection; they found 0.84 for this fraction with a statistical error of 10%. It has been shown that the fraction appropriate to the 40 kev. transition of ThC–C″ is about 0.75 and there is no theoretical reason to show that this fraction should vary appreciably with atomic number. Using this value, and a total fluorescence yield of 0.47*, the total number of conversions obtained from Stahel's result is 0.71 per disintegration. Now the number of γ-quanta which are capable of converting in the L levels is only 0.04 per disintegration; the rate of production of L converting excited states in RaE is therefore appreciably less than the disintegration rate of RaD. This conclusion is confirmed by the new measurements described below.

Measurements on the L Radiations of RaD

Sources of RaD were prepared from the nitric acid solution of the contents of some old radon tubes. After evaporation and solution in dilute hydrochloric acid, the polonium was first removed by rotation of a silver foil in the solution for 24 hr.; the RaE was then removed by cathodic deposition on platinum, the method of Hevesey and Paneth (22, p. 217); finally, the RaD was removed using a higher current. After solution in nitric acid, the pure RaD was concentrated and allowed to evaporate on two cellophane foils; these sources are called No. 2 and No. 3 in the measurements which follow. The strength of these sources was determined by following the growth of polonium in them, the measurements being made with a proportional counter with a fixed geometry in a manner similar to that used for the measurement of the strength of sources containing ThC. After a time t, the ratio of the number Q_α of α-particles emitted per second by a source of initially pure RaD, to the number Q_D of disintegrations of that source per second, is given to a first approximation by the equation:

$$Q_\alpha/Q_D = 1 - \lambda_D t - \frac{\lambda_E}{\lambda_E - \lambda_{Po}} \cdot e^{-\lambda_{Po} \cdot t} + \frac{\lambda_D}{\lambda_{Po}} (1 - e^{-\lambda_{Po} \cdot t}) + \frac{\lambda_{Po}}{\lambda_E - \lambda_{Po}} \cdot e^{-\lambda_E \cdot t}$$

where the λ's refer to the disintegration constants of RaD, RaE, and Po. With numerical values for these constants, the equation reduces to:

$$Q_\alpha/Q_D = 1.033 - \lambda_D t - 1.069\, e^{-\lambda_{Po} \cdot t} + 0.036\, e^{-\lambda_E t} \qquad (7)$$

The emission of α-particles from the source was followed for a period of about 90 days; the results are plotted in Fig. 9 after subtraction of a small amount representing contamination of the source by polonium not entirely extracted by silver. The amount subtracted was of the form $Ce^{-\lambda_{Po} t}$, the constant C being determined in each case by making the points fit the curve (7).

* *This figure is obtained from the calculated value for bismuth given in Table VIII of the preceding paper, multiplied by the ratio of the experimental and calculated efficiencies for the L radiations of ThC–C″.*

The initial value of this correction was only about 3% of the strength of the RaD sources. The source strengths determined in this way are given in Table VII together with the mean counting rates measured in the counter

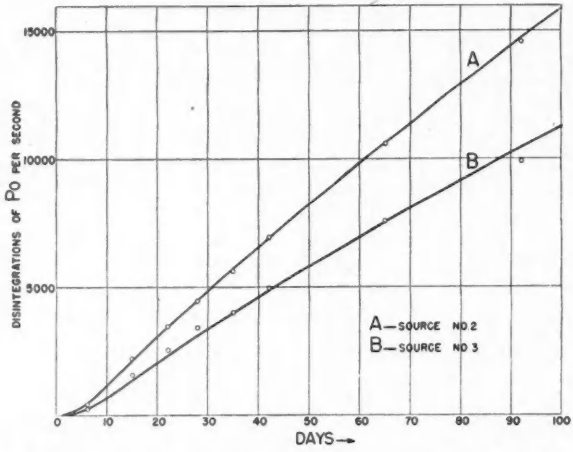

FIG. 9. *Growth of polonium in sources of RaD. Ordinates: number of α-particles emitted per sec., less* $Ce^{-\lambda_{Po}t}$, *where C = 1200 disintegrations per sec. for source No. 2, and C = 1000 for source No. 3. Abscissae: time in days after preparation of the sources. Curve A: calculated from Equation (7) to fit points of source No. 2; Curve B: calculated to fit source No. 3.*

filled with the same xenon mixture used in the ThC and ThB measurements. These rates were obtained as the difference between the counting rates measured without and with a filter of nickel, 30 mgm. per sq. cm. in thickness. An absorption curve of the radiation in nickel showed that about 5% of the counting rate without the nickel filter was due to the γ-radiations, and that, with this filter, about 3% of the L radiations is transmitted through it. The counting rates in Table VII have therefore been increased by 3% to account for this effect.

TABLE VII

EFFICIENCIES FOR DETECTION OF L RADIATION FROM RaD

	Source No. 2	Source No. 3
Mean counting rate per sec.	4.38 ± 0.08	3.30 ± 0.10
Disintegrations of RaD per sec.	4.20×10^4	2.97×10^4
Efficiency, ϵ_D	$10.4 \pm 0.2 \times 10^{-5}$	$11.1 \pm 0.3 \times 10^{-5}$
Mean efficiency	$10.7 \pm 0.2 \times 10^{-5}$	

The efficiency was calculated from the figures given in Table VIII of the preceding paper. In this case (bismuth), $q_1 = 0.090$, $q_2 = 0.041$, and $q_3 = 0.192$ quanta per L conversion. Assuming, for the moment, that the total

conversion is 97% of the disintegration rate of RaD, and that the fraction of the conversion electrons ejected from the L levels is 0.75, the comparison of observed and calculated efficiencies is:

From calculation: 11.0×10^{-5}

From observation: 10.7×10^{-5}.

This agreement is accidental because the calculated values of the fluorescence yields are certainly too low.

Selective Absorption Measurements on RaD

Selective absorption measurements have been made on the source No. 2 similar to those made with sources of ThC and Th(B + C). The results are given in Table VIII. By comparison with the results of Table VI it will be seen that the mean results for the ratio Q_{12}/Q_3 are very similar in the two cases and both are greater than the calculated result, which, for bismuth, is 0.68.

TABLE VIII

RESULTS OF SELECTIVE ABSORPTION MEASUREMENTS WITH SOURCES OF RaD

Absorber	Amount of absorber per foil	$\bar{k}$ per foil	k_0 per foil	a	Q_{12}/Q_3
Se	3.6 mgm. per sq. cm.	0.386	0.036	0.50	1.05
As	2.36 mgm. per sq. cm. (as metal)	0.257	0.039	0.51	1.10
				Mean	1.07

Comparison of the Results for ThC and RaD

If the ratio of the number of conversions in the L levels to the total number of conversions is assumed to be the same for ThC and RaD, the ratio of the experimental values for the efficiencies should be nearly equal to the ratio of the total number of conversions, because the counter efficiencies (Equation (5)) are very nearly equal. Using the figures given in the preceding paper, the ratio of the counter efficiency for ThC to RaD is 1.03. Although the calculated efficiencies are too low, this ratio is unlikely to be in error. The total number of conversion electrons is about 0.60 electron per α-disintegration of ThC; assuming, then, that 0.97 conversion electron is produced by RaD per disintegration, the ratio of the efficiencies (ϵ_C/ϵ_D) should be:

From calculation 0.23

From experiment 0.35.

The discrepancy is clearly outside the errors of computation and measurement. It seems certain that the L radiation emitted by ThC, although excessive by comparison with the calculated values, cannot be anomalous;

for if the 40 kev. state could decay in any way other than conversion or γ-emission with the full energy, this process would have been detected in a more complex structure in the groups of α-particles emitted by ThC. The discrepancy can be explained if it is assumed that the γ-rays emitted by RaD are not excited in every disintegration, and this conclusion is in general agreement with the analysis of the measurements of Stahel already discussed.

This explanation, however, leads to serious difficulties, for the deficit in the number of γ-transitions must be made up by β-transitions to the ground state of RaE, and the maximum energy of these β-particles must exceed 47 kev. The continuous spectrum of these β-particles would not have been detected by the earlier observers. In the cloud chamber such β-particles would appear unaccompanied by secondary tracks. If it is assumed that 80% of the disintegrations produce L and M conversion electrons, about 40% of these disintegrations will produce tracks in the cloud chamber which are single or accompanied by a very short range nuclear β-particle corresponding to the normal mode of disintegrations. Half of the observed single tracks, then, should belong to the continuous distribution; the work of Richardson and Leigh-Smith (34) shows no evidence of this.

Discussion of the Fluorescence Yield

The findings of the present measurements will now be reviewed.

(1) The selective absorption measurements in the case of ThB sources show that the fluorescence yields of the L_2 and L_3 levels, viz., f_2 and f_3, calculated in the preceding paper, are in the correct ratio. The measurements on the total yield of radiation show that there is agreement between the experimental and calculated values of these fluorescence yields. The results, however, are consistent with the conclusion of the preceding paper, that the radiation widths calculated from Massey and Burhop's (30) figures are too low by 10%.

(2) The selective absorption measurements on the radiations emitted by ThC and RaD show clearly that these radiations are essentially of the same type. There is no reason to suppose therefore that the energy distribution is anomalous, as has been suggested by Frilley and Tsien (17), unless the anomaly is common to both disintegrations. However, the total yield of the L_1 and L_2 levels, relative to the L_3 level, is greater than anticipated, and the predicted ratio of 2 to 1 for the yields of the L_1 and L_2 levels is not apparent in the intensity measurements of Frilley and Tsien. An elementary calculation on the basis of the intensities given by these authors for the lines $L\beta_4$ and $L\beta_1$ shows that the yields of the L_1 and L_2 levels are approximately equal. This discrepancy cannot be explained in terms of an error in the values for the fluorescence yields which have been used in the calculation, for it has already been shown that the ratio of f_2 to f_3 is correct; and if f_1 were too great, the correction necessary is not substantiated by the X-ray evidence.

(3) An enhancement of the L_2 lines could be obtained if it is assumed that Auger transitions of the type $L_1 \rightarrow L_2N$ occur. The value of the coefficient A_{12} required to make the total yield of the L_1 and L_2 levels together equal to

that of the L_3 level is 0.12 for bismuth and thallium, corresponding to a partial width in the L_1 level of about a volt. These transitions will increase the total fluorescence yield of the L levels by an amount which will give a fair agreement between the calculated and experimental efficiencies of detection for the radiation of ThC although the result for RaD—on the basis of 97% conversion—will be much too great. Taking this effect into account and increasing all the fluorescence yields by 10%, the total fluorescence yield in thallium is increased from 0.29 to 0.36, and in bismuth from 0.32 to 0.41. The comparison of the efficiencies therefore becomes:

	ThC–C″	RaD–E
From calculation	3.2×10^{-5}	14.1×10^{-5}
From observation	$3.7 \pm 0.4 \times 10^{-5}$	$10.7 \pm 0.2 \times 10^{-5}$

L Radiation Accompanying α-Particle Emission

On general theoretical grounds a feeble emission of X-rays might be expected to accompany the production of α-particles. A feeble emission of L radiation associated with the disintegration of polonium has been reported by Curie and Joliot (6); more recently, a strong emission of L radiation associated with the disintegration of U^{234} has been observed by Macklin and Knight (29). The observation of the latter authors is difficult to understand except in so far as it results from internal conversion in an excited state which has hitherto escaped detection. The equipment used in the present work was not very sensitive but sufficient information was obtained to show that for polonium and for ThC′ the emission of L radiation is very weak. A measurement of short duration with a pure polonium source revealed no L radiation; from the statistical errors of the measurement it was concluded that this radiation must be equivalent to less than one quantum emitted per 200 disintegrations, in agreement with the work of Curie and Joliot. The maximum yield of L radiation from ThC′ may be computed from the statistical errors of the coincidence measurements, (2) and (3), of Table II. The efficiency is less than 0.5×10^{-5} per disintegration of ThC′, which is equivalent to less than one quantum per 100 disintegrations.

Acknowledgments

This work was rendered possible by the gift of some old radon tubes by Dr. J. A. Gray, of Queen's University, Kingston, Ont. The author is indebted also to Mr. J. S. Foster, jr., for assistance in the construction of some of the apparatus, and to Mr. G. Hanna, of this laboratory, for the measurement of the α-emission of the RaD sources.

References

1. ALLEN, S. J. M. Phys. Rev. 24 : 1. 1924.
2. ARENDS, E. Ann. Physik, 22 : 281. 1935.
3. ARNOULT, R. Ann. phys. 12 : 240. 1939.
4. BRAMSON, S. Z. Physik, 66 : 721. 1930.
5. COLVERT, W. W. Phys. Rev. 36 : 1619. 1930.

6. CURIE, I. and JOLIOT, F. J. phys. radium, 2 : 20. 1931.
7. CURTISS, L. F. Phys. Rev. 27 : 257. 1926.
8. DROSTE, G. VON. Z. Physik, 84 : 17. 1933.
9. DUANE, W. and STENSTRÖM, W. Proc. Natl. Acad. Sci. U.S. 6 : 477. 1920.
10. EDDY, C. F. Proc. Cambridge Phil. Soc. 25 : 50. 1929.
11. ELLIS, C. D. Proc. Roy. Soc. London, A, 136 : 396. 1933.
12. ELLIS, C. D. Proc. Roy. Soc. London, A, 139 : 336. 1933.
13. FEATHER, N. Proc. Cambridge Phil. Soc. 25 : 522. 1929.
14. FLAMMERSFELD, A. F. Z. Physik, 114 : 227. 1939.
15. FRILLEY, M. Compt. rend. 218 : 505. 1944.
16. FRILLEY, M., SURUGUE, J., and TSIEN, S.-T. J. phys. radium, 7 : 350. 1946.
17. FRILLEY, M. and TSIEN, S.-T. Compt. rend. 220 : 144. 1945.
18. GRAY, J. A. Nature, 130 : 738. 1932.
19. GRAY, J. A. and O'LEARY, A. J. Nature, 123 : 568. 1929.
20. GURNEY, R. W. Proc. Roy. Soc. London, A, 112 : 380. 1926.
21. HARTOG, H. DER, MILLER, F. A., and VERSTER, N. F. Physica, 13 : 251. 1947.
22. HEVESEY, G. VON, and PANETH, F. A. A manual of radioactivity. 2nd ed. Oxford University Press, London, New York, Toronto. 1938.
23. KIKUCHI, S. Proc. Phys.-Math. Soc. Japan, 4 : 143. 1927.
24. KÜSTNER, H. and ARENDS, E. Ann. Physik, 22 : 443. 1935.
25. LAY, H. Z. Physik, 91 : 533. 1934.
26. LAUBERT, S. Ann. Physik, 40 : 553. 1941.
27. LEE, D. D. and LIBBY, W. F. Phys. Rev. 55 : 252. 1939.
28. LEWIS, W. B. and BOWDEN, B. V. Proc. Roy. Soc. London, A, 145 : 235. 1934.
29. MACKLIN, R. L. and KNIGHT, G. B. Phys. Rev. 72 : 435. 1947.
30. MASSEY, H. W. S. and BURHOP, E. H. S. Proc. Cambridge Phil. Soc. 32 : 461. 1936.
31. OUANG, T.-T., SURUGUE, J., and TSIEN, S.-T. Compt. rend. 217 : 535. 1943.
32. PETROVÁ, J. Z. Physik, 55 : 628. 1929.
33. RICHARDSON, H. O. W. Proc. Roy. Soc. London, A, 133 : 367. 1931.
34. RICHARDSON, H. O. W. and LEIGH-SMITH, A. Proc. Roy. Soc. London, A, 160 : 454. 1937.
35. RICHARDSON, H. O. W. and LEIGH-SMITH, A. Proc. Roy. Soc. London, A, 162 : 391. 1937.
36. SCHULTZ, K. Ann. Physik, 27 : 1. 1936.
37. STAHEL, E. Z. Physik, 68 : 1. 1931.
38. STAHEL, E. Helv. Phys. Acta, 8 : 651. 1935.
39. STAHEL, E. and SIZOO, G. J. Z. Physik, 66 : 741. 1930.
40. TSIEN, S.-T. Phys. Rev. 69 : 38. 1946.
41. TSIEN, S.-T. and MARTY, C. Compt. rend. 220 : 688. 1945.
42. TSIEN, S.-T. and MARTY, C. Compt. rend. 221 : 177. 1945.
43. WHITE, T. N. Phys. Rev. 46 : 865. 1934.
44. WILLIAMS, J. H. Phys. Rev. 44 : 146. 1933.

CANADIAN JOURNAL OF RESEARCH

Notes on the Preparation of Copy

GENERAL:—Manuscripts should be typewritten, double spaced, and the **original and one extra copy** submitted. Style, arrangement, spelling, and abbreviations should conform to the usage of this Journal. Names of all simple compounds, rather than their formulae, should be used in the text. Greek letters or unusual signs should be written plainly or explained by marginal notes. Superscripts and subscripts must be legible and carefully placed. Manuscripts should be carefully checked before being submitted, to reduce the need for changes after the type has been set. If authors require changes to be made after the type is set, they will be charged for changes that are considered to be excessive. **All pages, whether text, figures, or tables, should be numbered.**

ABSTRACT:—**An abstract of not more than about 200 words, indicating the scope of the work and the principal findings, is required.**

ILLUSTRATIONS:

(i) *Line Drawings:*—All lines should be of sufficient thickness to reproduce well. Drawings should be carefully made with India ink on white drawing paper, blue tracing linen, or co-ordinate paper **ruled in blue only**; any co-ordinate lines that are to appear in the reproduction should be ruled in black ink. Paper ruled in **green, yellow, or red should not be used** unless it is desired to have all the co-ordinate lines show. Lettering and numerals should be neatly done in India ink preferably with a stencil (**do not use typewriting**) and be of such size that they will be legible and not less than one millimeter in height when reproduced in a cut three inches wide. All experimental points should be carefully drawn with instruments. Illustrations need not be more than two or three times the size of the desired reproduction, but the ratio of height to width should conform with that of the type page. **The original drawings and one set of small but clear photographic copies are to be submitted.**

(ii) *Photographs:*—Prints should be made on glossy paper, with strong contrasts; they should be trimmed to remove all extraneous material so that essential features only are shown. Photographs should be submitted **in duplicate**; if they are to be reproduced in groups, one set should be so arranged and mounted on cardboard with rubber cement; the duplicate set should be unmounted.

(iii) *General:*—**The author's name, title of paper, and figure number should be written in the lower left-hand corner (outside the illustration proper) of the sheets on which the illustrations appear.** Captions should not be written on the illustrations, but typed on a separate page of the manuscript. All figures (including each figure of the plates) should be numbered consecutively from 1 up (arabic numerals). **Each figure should be referred to in the text.** If authors desire to alter a cut, they will be charged for the new cut.

TABLES:—Titles should be given for all tables, which should be numbered in Roman numerals. Column heads should be brief and textual matter in tables confined to a minimum. **Each table should be referred to in the text.**

REFERENCES:—**These should be listed alphabetically by authors' names, numbered in that order, and placed at the end of the paper.** The form of literature citation should be that used in the respective sections of this Journal. **Titles of papers should not be given in references listed in Sections A, B, E, and F, but must be given in references listed in Sections C and D.** The first page only of the references cited in papers appearing in Sections A, B, and E should be given. **All citations should be checked with the original articles.** Each citation should be referred to in the text by means of the key number; in Sections C and D the author's name and the date of publication may be included with the key number if desired.

The *Canadian Journal of Research* conforms in general with the practice outlined in the *Canadian Government Editorial Style Manual*, published by the Department of Public Printing and Stationery, Ottawa.

Reprints

Fifty reprints of each paper without covers are supplied free. Additional reprints, if required, will be supplied according to a prescribed schedule of charges. On request, covers can be furnished at cost.